

MINISTRY OF EDUCATION AND SCIENCE OF UKRAINE

National aerospace university  
«KharkivAviation Institute»

Faculty of AircraftEngines

Aircraft Engines Design Department

## Explanatory note graduation project

**O**

(type of qualification work)

**of bachelor**

(educational degree)

topi  
c

«*Gas Generator of Turbofan with Take-off Thrust 239kN* »

XAI.203.240F.22S.134. \_\_\_\_\_ EN

Made by: Mudassir student year, group 24  
of 4th № OF

Branch of  
knowledge

*13 Mechanical engineering*

(code and name)

Specialty

*134 Aerospace Engineering*

(code and name)

Educational  
program

*Operational Diagnostics, Maintenance and  
Repair of Aircraft Engines and Power Plants*

(name)

Supervisor:

*Mudassir Saiyed Mohammad*

(student's surname and initials)

Reviewer:

*Prof. Sergiy Bezugly*

(surname and initials)

*Prof. Fesenko K.V.*

(surname and initials)

Kharkiv – 2022

## **ACKNOWLEDGEMENT**

I would like to express my deepest appreciation, gratitude and respect to the head of department Professor Yepifanov S.V. and my academic advisor, Prof. BezuglyiS. V. for their invaluable guidance and generous support throughout my bachelor project and my study in the NationalAerospace University.

I appreciate Department of Aviation Engine Design (203) and Department of Aviation Engine Theory (201) for providing me the information, the technical data, the technical manuals, and the drawings, posters of prototype engine and its accessory units. In addition, I am thankful to Prof. O.D. Degterov and Prof. K.V. Fesenko for providing knowledge and information on calculation of thermo-gas dynamics, impeller machines calculation.

Special thanks to Department of Manufacturing Technology (204), particularly Prof. Knyazyev who has helped me with the technological section of my bachelorthesis. He is always helpful and insightful throughout the submission of my technological work.

Last but not least, I extend my gratitudeto Prof. Martensuik, Prof. Garkusha and Prof. Sukhovii S.I. (from aviation engine design department)for their help and guidance on my courseproject. I also would like to thank my friends and colleagues for their insightfulreview and suggestions on my research work.

## INITIAL DATA

Fulfillment of the engine turbine geometric parameters calculation and turbineblade profiling for 3-shaft turbofan engine with parameters:

$$P = 239000 \text{ N}$$

$$m = 5.60$$

$$\pi_c^* = 26.2$$

$$T_{ch}^* = 1615 \text{ K}$$

The prototype engine D – 18 has the following main parameters:

$$P = 230000 \text{ N}$$

$$m = 5.60$$

$$\pi_c^* = 25.0$$

$$T_{ch}^* = 1600 \text{ K}$$

$$G = 765.0 \text{ kg / s}$$

Design regime is characterized by the following conditions:

$$P_0 = 101325 \text{ Pa}$$

$$T_0 = 288.15 \text{ K}$$

$$H = 0$$

$$M_H = 0$$

## **ABSTRACT**

The main objective in this bachelor thesis is to perform and carry out the research and development of a turbofan engine with high by-pass ratio for heavy cargo aircraft. The research and development include various stages.

In the first stage, the theoretical estimation of the gas path and profiling of the blades of the engine will be determined by using gas dynamic calculations and parameter matching of the compressor and turbine.

In the second stage, the various parts of the engine such as the blades, blade lock, and disc will be subjected to strength analysis, further, the blades will be subjected to bending oscillation analysis by giving several operating conditions for the blade that simulates the various operating conditions of the engine. The safety factors of these parts will be determined and studied to see the structural airworthiness of the parts.

In the third stage, the technological aspect of the thesis will be covered by performing the planning and machining of the part, further the cutting conditions of a the part will be determined, namely turning, drilling and milling, which includes the choosing of tools, machines and cutting fluids, etc. The gear shaft is an aviation part belongs to the drive of an auxiliary power unit. Hence the planning and determining the machining routes will be under aviation standards.

The fourth and last stage consists of the economic viability of the engine and its cost effectiveness. Various expenses of the company such as labor charge, utility expenses and expense of principal investments will be considered to find out the cost of the engine, further a profit margin would be assigned in order to gain profit per unit sold.

## TABLE OF CONTENTS

ACKNOWLEDGEMENT .....	4
INITIAL DATA .....	5
ABSTRACT .....	6
1. THEORETICAL PART .....	8
1.1 Engine thermo-gas-dynamic calculation .....	9
1.2 Thermo gas dynamic calculation computation .....	13
1.3 The compressor and turbine parameters matching .....	15
1.4 Compressor gas dynamic calculation .....	19
1.5 Compressor rotor blades profiling.....	31
1.6 Conclusion.....	43
2. DESIGNING PART .....	45
2.1 General information about prototype .....	46
2.2 Compressor blade strength analysis .....	47
2.3 Strength analysis of the compressor blade lock.....	54
2.4 Strength analysis of the compressor disc.....	59
2.5 Compressor blade oscillation analysis.....	66
2.6 Conclusion.....	<b>Error! Bookmark not defined.</b>
3. TECHNOLOGICAL PART .....	72
3.1 Calculations of cutting conditions for turning operation .....	73
3.2 Calculations of cutting conditions for drilling operation .....	83
3.3 Calculations of cutting conditions for milling operation .....	91
3.4 Drawing of part .....	97
3.5 Drawinf of th blank.....	99
ANNEX .....	<b>Error! Bookmark not defined.</b>

# **1. THEORETICAL PART**

## 1.1 Engine thermo-gas-dynamic calculation

Modern gas turbine engines (GTE) are characterized by many schemes. This is explained by the variety of areas of application of gas turbine technology. Gas turbine engines are used in aviation, energy, sea and land transport, gas transmission and gas production sectors.

The first step in the design of a gas turbine engine is the choice of the scheme and parameters of the GTE cycle. The scheme of designed 3-shaft turbofan engine is represented in the graphical part of a given course project.

The purpose of thermo-gas-dynamic calculation is to determine the specific parameters of gas turbine engines – specific thrust  $P_{sp}$  and specific fuel consumption  $c_{sp}$ . By these specific parameters, it is possible to assess the level of perfection of the designed gas turbine engine by comparing it with existing and prospective GTE and also determine the required mass flow rate  $G_{En}$ . Its value allows us to estimate the diameter of the designed gas turbine engine.

Thermo-gas-dynamic calculation also determines the total temperature  $T^*$  and pressure  $P^*$  in the characteristic sections of the engine flow path and the main parameters characterizing the operation of the engine units.

### 1.1.1 Choice and justification of the design regime parameters

The parameters of the engine cycle ( $\pi_c^*$  and  $T_{Ch}^*$  (TIT)) are set on the basis of technical and economic requirements for the engine.

The development of materials science and manufacturing technology of gas turbine engines, also the improvement of cooling systems for turbine blades have significantly increased permissible values of  $T_{Ch}^*$ . The upward trend is explained, first of all, by the fact that this makes it possible to increase significantly the specific thrust, which entails a decrease in the overall dimensions of the engine and its mass.

Despite the favorable effect of the increase of  $\pi_c^*$  on the specific parameters of the engine, the use of large values of  $\pi_c^*$  is limited because of the engine design complexity, the increase in mass and size of the engine.

A choice of the main engine parameters influences strongly the efficiency of its work. The main requirement for a designed engine is high efficiency (low values of fuel consumption) and high specific thrust [1].

For thermos-gas-dynamic calculation of a gas turbine engine, it is necessary to know the losses in its units. Accounting for losses can be carried out using various coefficients: efficiency ( $\eta$ ), total pressure recovery coefficients ( $\sigma$ ), velocity coefficients ( $\varphi$ ), combustion efficiency ( $\eta_b$ ).

Since at the stage of the preliminary thermos-gas-dynamic calculation the geometry of the flow path and the flow velocity are still unknown, the choice of the coefficients taking into account the losses is carried out approximately. As the geometry of the flow path and the flow parameters are refined, these coefficients are refined as well and then used in the design of gas turbine engine units and their elements.

### 1.1.2 Efficiency of the compressor and the turbine

The compressor efficiency can be represented as the product:

$$\eta = \eta_c^* \cdot \eta_m^* \quad (1.1)$$

Here  $\eta_m^*$  is mechanical compressor efficiency which takes into account losses outside the flow path (due to friction of the disks of the rotor blades and shaft against the gas medium and friction in the compressor bearings). It is usually  $\eta_m^* = 0.985...0.995$ . Accepted  $\eta_m^* = 0.995$ .

The value of multistage compressor isentropic efficiency in the parameters of stagnation depends on compressor pressure ratio and the efficiency of its stages:

$$\eta_c^* = \frac{\pi_c^{*\frac{\kappa-1}{\kappa}} - 1}{\pi_c^{*\frac{\kappa\eta_{st}^*}{\kappa-1}} - 1} \quad (1.2)$$

Where  $\eta_{st}^*$  – the compressor stages average efficiency.

For the design regime the stage average efficiency in multistage axial compressors of modern aircraft engines lies within the limits  $\eta_{st}^* = 0.88...0.9$ . Accepted  $\eta_{st}^* = 0.89$ .

Thus, we obtain:

$$\eta_c^* = 0.833. \quad (1.3)$$

The fan efficiency calculation is performed similarly, but fan stage average efficiency is accepted  $\eta_{st}^* = 0.89$ . And fan efficiency equals

$$\eta_f^* = 0.8896 \quad (1.4)$$

The values of the efficiency of uncooled aircraft turbines in the parameters of the stagnated flow usually lie within  $\eta_{tuncooled}^* = 0.9...0.92$ . Greater turbine inlet temperature ( $T_{Ch}^*$ ) corresponds to smaller efficiency value. Accepted  $\eta_{tuncooled}^* = 0.915$ .

Turbine cooling reduces turbine efficiency. A larger amount of bleed air for cooling the turbine blades corresponds to a greater decrease in turbine efficiency.

Thus, as the gas temperature at the combustion chamber exit is greater than 1250 K turbine blade cooling is required, the turbine efficiency can be calculated by the formula:

$$\eta_t^* = \eta_{tuncooled}^* - 0.000125 \times (T_{ch}^* - 1250) \quad (1.5)$$

$$\eta_t^* = 0.915 - 0.00013 (1615 - 1300) = 0.874. \quad (1.6)$$

### 1.1.3 Losses in the engine units

The total pressure recovery factor for the subsonic air inlet ducts is  $\sigma_{inl} = 0.97 \dots 0.995$ . Greater bypass ratios correspond to greater  $\sigma_{inl}$ . Accepted  $\sigma_{inl} = 0.995$ .

The total pressure losses in the main combustion chambers are caused by hydraulic and thermal resistance. The hydraulic resistance is mainly determined by the losses in the diffuser, flame tube head, the stream mixing and the flow rotation ( $\sigma_{hydr} = 0.93 \dots 0.97$ ). Accepted  $\sigma_{hydr} = 0.97$ .

The thermal resistance is the result of a heat supply to the moving gas. For the main combustion chambers  $\sigma_{therm} = 0.97 \dots 0.98$ . Accepted  $\sigma_{therm} = 0.98$ .

The overall total pressure losses in the main combustion chamber are calculated by the formula:

$$\sigma_{ch} = \sigma_{hydr} \cdot \sigma_{therm} = 0.97 \cdot 0.98 = 0.951 \quad (1.7)$$

The heat losses in the combustion chambers are mainly related to incomplete fuel combustion and estimated by combustion efficiency  $\eta_b$ . For the design regime this factor is  $\eta_b = 0.97 \dots 0.995$ . Accepted  $\eta_b = 0.995$ .

The total pressure losses in the transition channel from the fan exit to the high pressure compressor entrance is  $\sigma_{tc} = 0.98 \dots 0.995$ . Accepted  $\sigma_{tc} = 0.995$ .

The total pressure losses in the outer flow path are characterized by pressure recovery factor in the range  $\sigma_{II} = 0.975 \dots 0.995$ . Accepted  $\sigma_{II} = 0.995$ .

To describe the power losses in the engine bearings and the engine power takeoff to drive auxiliary units, serving the engine and aircraft, the mechanical efficiency  $\eta_m$  is used. These values  $\eta_m$  usually equals to 0.98 ... 0.995. Larger values of mechanical efficiency correspond to the larger engines. Accepted  $\eta_m = 0.985$  (for high pressure rotor) and  $\eta_m = 0.995$  (for fan rotor).

Losses in the nozzles of jet engines are evaluated by velocity coefficient  $\varphi_n$ . These losses are relatively small:  $\varphi_n = 0.975 \dots 0.985$ . Accepted  $\varphi_n = 0.992$ .

For turbojet engines output devices in the form of nozzles are used. Convergent or convergent-divergent nozzles are used.

In convergent nozzles, the regimes of full expansion ( $P_{Nz} = P_{En}$ ) are realized at subsonic gas outflow from the nozzle and the regimes of under-expansion ( $P_{Nz} = P_{cr} > P_{En}$ ) at the sound speed of gas outflow from the nozzle.

In convergent-divergent nozzles, full expansion regimes ( $P_{Nz} = P_{En}$ ), under-expansion regimes ( $P_{Nz} > P_{En}$ ) and over-expansion regimes ( $P_{Nz} < P_{En}$ ) are realized depending on the total gas pressure before the nozzle and the ratio of the exit cross-sectional area  $F_{Nz}$  and the critical section area  $F_{cr}$ .

Nozzle operating conditions are characterized by an available nozzle pressure decrease ratio  $\pi_{Nz} = P_{T(Aft)}/P_{Nz}$ . For convergent nozzles, always specify  $\pi_{Nz} = 1$ . For convergent-divergent nozzles  $\pi_{Nz} = 0.1 \dots 0.3$ . Accepted  $\pi_{Nz} = 1$ .

Typically, when designing a compressor, there is an intention to maintain a constant flow work along the height of the blade. However, for stages with a large relative blade height, this condition requires an unacceptably large curvature of the profiles in the hub sections of the fan. Therefore, in a turbofan engine with a high bypass ratio, the fan work in the inner flow channel is less than in the outer one. The distribution of fan work between the channels is estimated by the coefficient

$\overline{L}_f = L_{fI}/L_{fII}$ . For turbofan engines with a small bypass ratio  $\overline{L}_f = 1$  and for turbofan engines with a bypass ratio of the order of 5 ... 6  $\overline{L}_f = 0.35 \dots 0.7$ . Accepted  $\overline{L}_f = 0.7$ .

The value of the relative bypassed mass flow rate  $\Delta G_b$  for cooling the hot elements of the engine and for the needs of the aircraft can be up to 20% of the total mass flow rate. Accepted  $\Delta G_b = 0.132$ .

## 1.2 Thermo gas dynamic calculation computation

Based on the received in paragraph 1.1 and predefined input data, the source file for the computing has been completed (Table 1.1). Table 1.2 shows the results of thermo-gas-dynamic calculation.

**Table 1.1– Initial data**

Исходные данные			
Число значений $m$ :	<input type="button" value="1"/>	Число значений $Tg^*$ :	<input type="button" value="1"/>
Число значений $Pk1^*$ :	<input type="button" value="1"/>	Число значений $Pw2$ :	<input type="button" value="1"/>
Суммарный расход воздуха $G_{вс}$ (Кг/С)	1		
Высота прлета $H$ (Км)	0		
Скорость полета $Mn$	0		
КПД вентилятора первого контура $\eta_{в1}$	0.885		
КПД вентилятора второго контура $\eta_{в2}$	0.885		
КПД турбины вентилятора $\eta_{тв}^*$	0.92		
Чдальная работа вентилятора относительная $L_{в0}$	.7		
Величина относительного отбора воздуха $\Delta B_{отб}$	0.132		
Коэффициент восстановления полного давления во входном устройстве $\sigma_{вх0}$	0.995		
Коэффициент восстановления полного давления перед компрессором $\sigma_{вк}$	0.995		
Коэффициент восстановления полного давления в камере горения $\sigma_{кс}$	0.95		
Коэффициент восстановления полного давления во втором контуре $\sigma_2$	0.995		
Коэффициент восстановления полного давления в камере смешения $\sigma_{см}$	1		
Коэффициент восстановления полного давления в форсажной камере горения $\sigma_{Ф}$	1		
Коэффициент гидравлических потерь в форсажной камере горения $\sigma_{гидрФ}$	1		
Коэффициент полноты горения $\eta_g$	0.995		
Коэффициент полноты горения в форсажной камере горения $\eta_{Ф}$	1		
Механический КПД ротора высокого давления $\eta_{мвд}$	0.985		
Механический КПД ротора вентилятора $\eta_{тв}$	0.995		
Коэффициент скорости реактивного сопла первого контура $\sigma_{с1}$	0.992		
Коэффициент скорости реактивного сопла второго контура $\sigma_{с2}$	0.992		
Относительная степень расширения в сопле внутреннего контура $\sigma_{с01}$	1		
Относительная степень расширения в сопле внешнего контура $\sigma_{с02}$	1		
Степень двухконтурности $m$	5.6		
Температура газов перед турбиной $Tg^*$ (К)	1615		
КПД турбины компрессора высокого давления $\eta_{твд}^*$	0.874		
Степень повышения давления в компрессоре $Pk^*$	26.2		
КПД компрессора $\eta_k^*$	0.829		
Относительная степень повышения давления в вентиляторе наружного контура $Pw2$	0.96		

**Table 1.2 – Thermo-gas-dynamic calculation results**

Данные для согласования:							
312.4	312.4	0.03769	0.03769	1.698	1.455	18.09	
5.60000	26.2	0.843	0.885	0.885	0.874	0.92	
3.702e+04	5.288e+04	4.889e+05	5.718e+05	3.348e+05			
288.2	324.6	340.8	787.8	1615	1161	894.9	
1.008e+05	1.467e+05	1.712e+05	2.641e+06	2.509e+06	4.584e+05	1.308e+05	
819.7	1045	1.379	287	1.46e+05	0.132	0.96	
894.9	1259	1.296	287.5	5.474	3.504	0.995	
*****							

Исходные данные:

Дата: 15.04.2021

т = 5.60

Tг\* = 1615.0

КПДт\* = 0.8740

Пк\* = 26.20

КПДк\* = 0.8290

Pво = 0.960

### Термогазодинамический расчет ТРДД

Исходные данные:	Gв = 1.00	Tф = 1800.0	Готб = 0.1320
H = 0.00	MН = 0.00	NВ1 = 0.8850	NВ2 = 0.8850 LВ0 = 0.700
КПДтв = 0.9200	Пс01 = 1.000	Sв0 = 0.995	Sвк = 0.995 Skс = 0.950
S2 = 0.995	Sсм = 1.000	Sф = 1.000	Sфн = 1.000 Nr = 0.995
Nф = 1.000	КПДтвд = 0.9850	КПДтв = 0.9950	Fi1 = 0.992 Fi2 = 0.992
Пс02 = 1.000	Sвх = 0.995	TH = 288.15	TH* = 288.15 RH = 101325.0
РН* = 101325.0	PВ* = 100818.4	VH = 0.00	

Схема печати:	RY	R	CY	QT	AKC	FK2	RY2	CC2
	GT	PIC2	SC2	LC2	РФН2	PC2	Срг	Кг
	RO	TKB1	TK2	TK	TTВД	PT	PK2	P2
	КПДквд	КПДтвд	РКВ1	РВВД	РК	РГ	РТВД	РТ
	Пів2	Пів1	Піквд	Лв2	Лв1	Lквд	Lтвд	Lтв
	Птвд	Птв	Пто	Пс1	Sc1	Fкр1	RY1	Сс1
	Lс1	PC01	PC1	PC2	FC1	FC2		

m = 5.60	Tг = 1615.0	Пк = 26.20	П2опт = 1.769	Pво = 0.960	КПДк = 0.8290		
312.38	312.3848	0.037686	0.021583	2.717328	0.002302	304.8674	304.8674
11.773	1.681082	0.991128	0.902456	170335.6	168824.4	1259.044	1.295974
1.0000	324.6237	340.7764	787.7963	1160.8300	894.8812	171191.6	170335.6
0.8430	0.874000	146712.6	145979.0	2641441.4	2509369.4	458398.3	130812.7
1.6980	1.455217	18.094662	52883.64	37018.54	488894.5	571819.8	334841.1
5.4742	3.504234	19.182919	1.291021	0.995819	0.001021	354.4822	354.4822
0.6577	130265.8	101325.0	101325.0	0.001021	0.002302		

As a result of the thermo-gas-dynamic calculation specific thrust  $P_{sp} = 312.38$  N·s/kg and specific fuel consumption  $C_{sp} = 0.037686$  kg/N·h are obtained. Specific thrust of newly designed engine is more than specific thrust of the prototype engine ( $P_{sp\ prot} = 300.654$  N·s/kg) and specific fuel consumption of newly designed engine is less than specific fuel consumption of the prototype engine ( $C_{sp\ prot} = 0.0377$  kg/N·h). These values meet current standards of turbofan engines parameters.

### 1.3 The compressor and turbine parameters matching

Matching the engine turbine and compressor is the most important stage of engine designing. The purposes of matching are the distribution of work between the spools of the compressor and the turbine and the definition of the engine main geometrical parameters. In the course of the matching calculation it is essential to observe the basic conditions which ensure reliable and efficient engine operation.

Among them are the relative blades height of the compressor last stages and the first turbine stage; the relative hub diameter at the compressor exit, the load on the compressor and turbine stages.

#### 1.3.1 Parameters choice

The initial data for this calculation are the values of the total parameters of the working fluid (air and combustion products) in the characteristic sections of the flow path, the basic geometric relationships of the cascades of the impeller machines and the accepted values of the aerodynamic loading coefficients of the compressor and turbine stages.

##### Initial data for calculation:

- 1) Thrust value:  $P = 239000$  N.
- 2) The ratio of work to increase the total pressure in low pressure compressor (LPC) stages to total work of both compressors of the internal channel:  $L_{lpc}/L_c = 0.32$ .
- 3) Efficiency of LPC:  $\eta_{lpc}^* = 0.88$ .
- 4) The total pressure recovery factor in the transition channel from fan stages of internal channel to LPC:  $\sigma_{f\_lpc} = 0.995$ .

##### ***Parameters of the high-pressure compressor(HPC):***

- 5) HPC work distribution between axial part of the HPC and its centrifugal stage:  $L_{ac}/L_{hpc} = 1$ .
- 6) HPC efficiency:  $\eta_{hpc}^* = 1$ .
- 7) The total pressure recovery factor in the transition channel from an axial part of the HPC to centrifugal:  $\sigma_{tc} = 1$ .
- 8) Identifier of the flow path shape:  $k_{s\_hpc} = 1$ .
- 9) The number of HPC stages:  $Z_{hpc} = 7$ .
- 10) The relative hub diameter at the entrance to HPC:  $D_{ha}/D_{ta} = 0.81$ .
- 11) The ratio of the outer diameter at the entrance of centrifugal stage to the outer diameter at the outlet of the HPC:  $D_{lcs}/D_{ta} = 1$ .
- 12) The ratio of the outer diameter of the impeller of centrifugal stage to the outer diameter of HPC at the entrance:  $D_2/D_{ta} = 1$ .
- 13) The ratio of the exit diameter of centrifugal stage to the outer diameter of the impeller of centrifugal stage:  $D_4/D_2 = 1$ .
- 14) The flow (axial) velocity at the entrance to the axial part of HPC:  $C_{ea} = 194$  m/s.
- 15) The flow (axial) velocity at the discharge of HPC:  $C_{da} = 125$  m/s.
- 16) The circular velocity at the outer diameter of the HPC first stage:  $U_{hpc} = 415$  m/s.

**Parameters of the high-pressure turbine (HPT):**

- 17) Identifier of the flow path shape:  $k_{s\_hpt} = 3$ .
- 18) The number of HPT stages:  $Z_{hpt} = 1$ .
- 19) The ratio of the average diameter of the HPT at the entrance to the outer diameter of the HPC at the entrance:  $D_{mhpt}/D_{ta} = 1.153$ .

20) Flow gas-dynamical function at the entrance to the HPT:  $q(l_{ch}) = 0.30$ .

21) Flow (axial) velocity at the HPT discharge:  $C_{dhpt} = 185$  m/s.

**Parameters of the low-pressure compressor (LPC):**

22) Identifier of the flow path shape:  $k_{s\_lpc} = 2$ .

23) The number of LPC stages:  $Z_{lpc} = 7$ .

24) The relative hub diameter at the entrance to LPC:  $D_{hla}/D_{ila} = 0.67$ .

25) The flow (axial) velocity at the entrance to LPC:  $C_{elpc} = 180$  m/s.

26) The flow (axial) velocity at the discharge of LPC:  $C_{dlpc} = 175$  m/s.

27) The circular velocity at the outer diameter of LPC first stage:  $U_{lpc} = 335$  m/s.

**Parameters of the low-pressure turbine (LPT):**

28) Identifier of the flow path shape:  $k_{s\_lpt} = 3$ .

29) The number of LPT stages:  $Z_{lpt} = 1$ .

- 30) The ratio of the average diameter of LPT at the entrance to the outer diameter of LPC at the entrance:  $D_{mlpt}/D_{tlpc} = 0.98$ .

31) Flow (axial) velocity at the LPT entrance:  $C_{elpt} = 170$  m/s.

32) Flow (axial) velocity at the LPT discharge:  $C_{dlpt} = 185$  m/s.

- 33) The total pressure recovery factor in the transition channel between HPT and LPT:  $\sigma_{tct} = 0.99$ .

**Fan parameters:**

34) Identifier of the flow path shape:  $k_{s\_f} = 2$ .

35) The number of fan stages:  $Z_f = 1$ .

36) The relative hub diameter at the entrance to the fan:  $D_{hf}/D_{tf} = 0.292$ .

- 37) Flow (axial) velocity at the entrance and the discharge of the fan:  $C_{ef} = 210$  m/s,  $C_{df} = 175$  m/s.

38) The circular velocity at the outer diameter of the fan first stage:  $U_f = 470$  m/s.

**Fan turbine parameters:**

39) Identifier of flow path shape:  $k_{s\_ft} = 2$ .

40) The number of fan turbine stages:  $Z_{ft} = 4$ .

- 41) The ratio of the average diameter of the fan turbine at the entrance to the outer diameter of the fan at the entrance:  $D_{mft}/D_{tf} = 0.452$ .

- 42) Flow (axial) velocity at the entrance and the discharge of the fan turbine:  $C_{eft} = 185$  m/s,  $C_{dft} = 240$  m/s.

- 43) The total pressure recovery factor in the transition channel between HPT and fan turbine:  $\sigma_{tct} = 1$ .

**Other parameters:**

- 44) The relative length of the passages: fan – LPC ( $sp(1) = 0.25$ ), LPC – HPC ( $sp(2) = 0.3$ ), the HPT – the LPT ( $sp(3) = 0.1$ ), the LPT – fan turbine ( $sp(4) = 0$ ).
- 45) The values of coefficients  $K_{vf} = 0.55$ ,  $K_{vb} = 2$  and  $K_{vhpc} = 2$  ( $K_v = 0$  – no inlet guide vanes,  $K_v = 1$  – with inlet guide vanes,  $K_v = 2$  – both inlet guide vanes and double exit guide vanes,  $K_v = 3$  – no inlet guide vanes, but with double exit guide vanes).
- 46) The values of coefficients  $K_{chpt} = 1.25$  and  $K_{cft} = 1$  ( $K_c = 1.25$  means cooled turbine,  $K_c = 1$  – uncooled turbine).

### 1.3.2 The calculation results and the engine conceptual design

Graphical representation of turbofan gas generator flow path corresponding to the calculation results (Table 2.1) is shown on Figure 2.1.

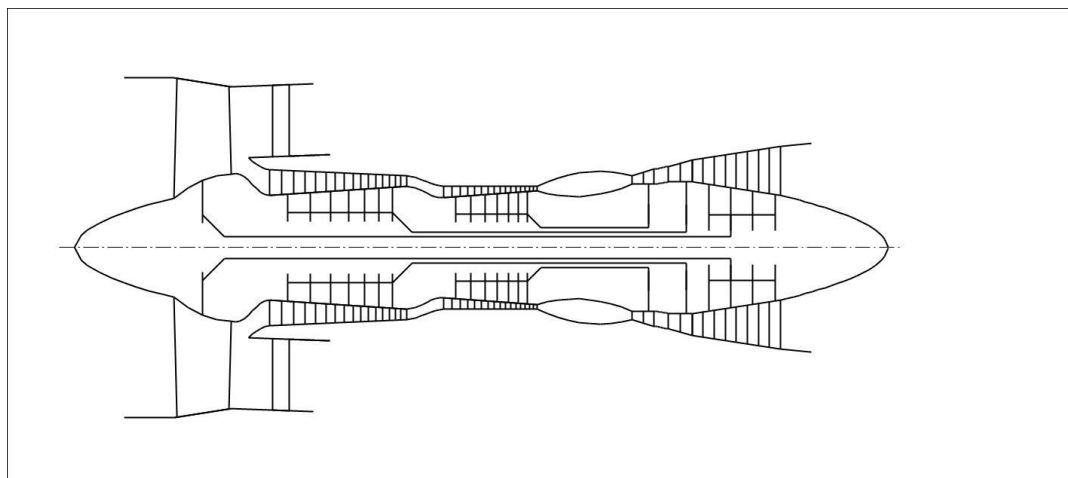


**Figure 1.1** – Schematic of the engine flow path

**Table 1.3 – The matching calculation results**

Формирование облика ГГ и ТВК ТРДД-3 ( КВД – ОК или ОЦК )  
31.12.2001

**Исходные данные:**

Руд = 312.4	Суд = 0.0377	КПДк = 0.8430	КПДТк = 0.8740
Лк = 488900	Лтк* = 571800	Лтв* = 334800	КПДТв = 0.9200
Лв2 = 52880	Лв1 = 37020	КПД2 = 0.8850	КПД1 = 0.8850
Срг = 1259.0	Кг = 1.2960	Срв = 1045.0	Кв = 1.3790
Р = 239000	Гбо = 765.04	Гв1 = 115.916	ркс = 0
do = 0.292	Дсртв/Дк = 0.452		
дов = 0.670	Дсртн/Дкн = 0.980		
дово = 0.810	D1цс/Дкко = 1.000	D2цс/Дко = 1.000	
D4цс/D2цс = 1.000	Dствд/Дко = 1.153		
Лкн/Лк = 0.320	КПДкн* = 0.880	Сркнв = 0.995	
Лок/Лкв = 1.000	КПДок* = 0.875	Сркоц = 1.000	
Сркв = 0.995	Сртвн = 0.990	Сртнв = 0.990	
Ук = 470.0	Укнд = 335.0	Уквд = 335.0	

**Результаты расчета:**

*ВЕНТ*,	Кф = 2	Zк = 1	
Лк* = 52880.0	Пік* = 1.698	КПД* = 0.8850	Ук = 470.0
Дк = 2.2552	dob = 0.2920	dok = 0.4549	Hзс = 0.2523
пв = 3980.2			
*КНД*,	Кф = 2	Zк = 7	
Лк* = 154883.5	Пік* = 3.418	КПД* = 0.8800	Ук = 335.0
Дк = 1.0394	dob = 0.6700	dok = 0.8516	Hзс = 0.2147
пнд = 6155.6			
*ОК ВД*,	Кф = 1	Zк = 7	
Лк = 329127.5	Пік* = 5.320	КПД* = 0.8753	Ук = 415.0
Дк = 0.8185	dob = 0.8100	dok = 0.9194	Hзс = 0.2730
пвд = 9683.8			
*ТВД*	Кф = 3	Zт = 1	
Лт* = 388824.0	Піт* = 3.023	КПД* = 0.8565	(h/D)г = 0.0618
Уср = 467.5	Mz = 1.7791	Dср = 0.9437	(h/D)т = 0.1050
Sp = 229.4	Tw* = 1393.0		
*ТНД*	Кф = 3	Zт = 1	
Лт* = 182976.0	Піт* = 1.793	КПД* = 0.8916	(h/D)г = 0.1075
Уср = 321.3	Mz = 1.7727	Dср = 1.0186	(h/D)т = 0.1457
Sp = 150.3	Tw* = 1202.0		
*ТВ*	Кф = 2	Zт = 4	
Лт* = 334800.0	Піт* = 3.504	КПД* = 0.9200	(h/D)г = 0.1454
Уср = 212.4	Mz = 7.4184	Dср = 1.0194	(h/D)т = 0.3176
Sp = 143.3	Tw* = 912.8		

**Сечение/параметр**

	T*	P*	C	C/акр	F
	К	Па	м/с	---	кв.м
В – В	288.2	100800	210.0	0.6782	3.6540
К В1 – К В1	324.6	146700	175.0	0.5216	2.8489
В КНД – В КНД	324.6	146000	180.0	0.5477	0.4676
К КНД – К КНД	472.8	498985	175.0	0.4412	0.1957
В КВД – В КВД	472.8	496490	194.0	0.4891	0.1809
К – К	787.8	2641000	125.0	0.2442	0.0814
Г – Г	1615.0	2509000	138.4	0.1912	0.1574
Т ТВД – Т ТВД	1306.2	830000	185.0	0.2841	0.2937
Г ТНД – Г ТНД	1306.2	821700	170.0	0.2611	0.3210
Т ТНД – Т ТНД	1161.0	458400	185.0	0.3014	0.4748
Г ТВ – Г ТВ	1161.0	458400	185.0	0.3014	0.4748
Т – Т	894.9	130800	240.0	0.4453	1.0369

	Дн1	Дср1	Двт1	Дн2	Дср2	Двт2	Зст
ВЕНТ	2.2552	1.6613	0.6585	2.1386	1.6613	0.9727	1
КНД	1.0394	0.8847	0.6964	0.9525	0.8847	0.8112	7
ОК ВД	0.8185	0.7448	0.6630	0.8185	0.7862	0.7525	7
ТВД	0.9560	0.9003	0.8446	1.0428	0.9437	0.8446	1
ТНД	1.0798	0.9750	0.8702	1.1670	1.0186	0.8702	1
ТВ	1.1676	1.0194	0.8711	1.3432	1.0194	0.6956	4

The formation of the conceptual design (flow path) of a gas turbine engine is one of the most important initial stages in the design of a gas turbine engine, immediately following the thermo-gas-dynamical calculation and the previous gas-dynamic calculations of the flow part units (spools of compressors and turbines). When performing calculations on the formation of the engine conceptual design, the following features are determined: the shape of the flow path, the rotational speeds and the number of stages of the spools of impeller machines.

Three-shaft turbofan engine conceptual design was formed.

The fan with  $D_{mid} = \text{const}$ , middle – loaded ( $H_z = 0.2523$ ) consists of a single stage and has a value of efficiency  $f^* = 0.885$ .

The low-pressure compressor with  $D_{mid} = \text{const}$ , low – loaded ( $H_z = 0.2147$ ) consists of seven stages and has a value of efficiency  $l_{pc}^* = 0.88$ .

The high-pressure compressor with  $D_{tip} = \text{const}$ , high – loaded ( $H_z = 0.273$ ) consists of seven stages and has a value of efficiency  $h_{pc}^* = 0.8753$ .

The hub relative diameter at the discharge from the last stage of the HPC  $d_h = 0.9194$  does not exceed the permissible value  $d_h = 0.92$ .

The single-stage high-pressure turbine with  $D_{hub} = \text{const}$ , high – loaded ( $t = 1.7791$ ) has a value of efficiency  $h_{pt}^* = 0.8565$ .

The single-stage low-pressure turbine with  $D_{hub} = \text{const}$ , high – loaded ( $t = 1.7727$ ) has a value of efficiency  $l_{pt}^* = 0.8916$ .

The four-stage fan turbine with  $D_{mid} = \text{const}$ , high – loaded ( $t = 1.8546$  per stage) has a value of efficiency  $f_{ft}^* = 0.92$ .

The factor which characterize relative blades height of the turbine stages  $h/D$  should be in the range 0.065...0.32. For the high-pressure turbine it equals to 0.0618 and for the fan turbine – 0.3176.

## 1.4 Compressor gas dynamic calculation

Compressor calculation is a very important step in the designing of a gas turbine engine. The combustion chamber and turbine design depends on the compressor parameters. Compressor often forms the main part of the engine length. So the compressor has the great influence to the general dimensions of the engine and its weight.

### 3.1 Parameters choice

Designed turbofan engine compressor is axial two-spool (the first spool belongs to the low-pressure compressor and the second one – to the high-pressure compressor). The main part of the gas-dynamic calculation of the axial compressor is the final determination of the geometric dimensions and the number of stages. It is necessary to divide correctly the work between the compressor stages.

The gas-dynamic calculation of the axial compressor is a sequential calculation of all his stages on the average radius. The distribution of the parameters is made in accordance with the recommendations in [3].

Flow velocity component decreases from the inlet to the outlet to have a moderate value at the combustor inlet. To avoid falling efficiency decrease of  $C_a$  within the stages should not exceed 10...15 m/s [3].

Initial data for the gas-dynamic compressor calculation have the following values:

$G_A = 115.916 \text{ kg/s}$  – working fluid (air) mass flow rate through the compressor;

$T_{En}^* = 324.6 \text{ K}$  – the total temperature at the compressor inlet;

$P_{En}^* = 146000 \text{ Pa}$  – the total pressure at the compressor inlet;

$k = 1.379$  and  $R = 287.2 \text{ J/(kgK)}$  – the physical constants of the working fluid;

$\pi_c^* = 18.093$  – the total pressure ratio in the compressor;

$U_{k\ lpc} = 335 \text{ m/s}$  – the circular velocity on the rotortipdiameter of the low-pressure compressor first stage;

$U_{k\ hpc} = 415 \text{ m/s}$  – the circular velocity on the rotortipdiameter of the high-pressure compressor first stage;

$C_c = 125 \text{ m/s}$  – the axial velocity at the compressor exit;

$Z_1 = 7, Z_{\text{total}} = 14$  – the number of compressors stages;

$k_{s\_lpc} = 2, k_{s\_hpc} = 1$  – identifiers of the flow path shape;

$= 0.6700$  – the relative hub diameter at the first stage rotor entrance;

$= 0.842$  – the ratio of the average diameter of the compressor second spool first stage to the average diameter of the compressor first spool last stage;

$K_{G1} = 1.02$  – factor that takes into account the clutter of cross-sectional area of flow path by blades bodies;

$\sigma_{GV} = 0.995$  – the total pressure recovery factor of the compressor guide vanes;

$\sigma_{IGV} = 0.990$  – the total pressure recovery factor of the compressor inlet guide vanes;

$\sigma_{TCh} = 0.995$  – the total pressure recovery factor of the transition channel between compressor spools.

The follow values are given like the arrays of values for all stages:

$C_a$  – axial velocity at the inlet of the stage rotor, m/s;

$H_z$  – the stage work, kJ/kg;

$\eta_s^*$  – the stage isentropic efficiency by total parameters;

$\kappa$  – kinematic reactivity coefficient;

$i$  – incidence angle of the stage rotor blades on the average radius, degree;

#### 1.4.2 The calculation results

Initial data for the calculation are shown in Table 1.4, The results are presented in Table 1.5.

**Table 1.4** – Initial data

<b>N<sub>k</sub></b>	2	<b>K<sub>Φ1</sub></b>	2	<b>K<sub>Φ2</sub></b>	1	<b>Z<sub>1</sub></b>	7	<b>Z<sub>k</sub></b>	14	<b>K<sub>r</sub></b>	1	<b>T<sub>b*</sub></b>	324.6	<b>P<sub>b*</sub></b>	146000	<b>K</b>	1.379	<b>R</b>	287.2
<b>G<sub>b</sub></b>	115.916	<b>П<sub>ik*</sub></b>	18.093	<b>П<sub>i1*</sub></b>	3.418	<b>U<sub>k1</sub></b>	335	<b>U<sub>k2</sub></b>	415	<b>C<sub>k</sub></b>	125	<b>d<sub>вт1/D<sub>k1</sub></sub></b>	0.67	<b>D<sub>срв2/D<sub>срк1</sub></sub></b>	0.842	<b>S<sub>вна</sub></b>	0.99	<b>S<sub>на</sub></b>	0.995
<b>S<sub>нв</sub></b>	0.995	<b>K<sub>g</sub></b>	1.02	<b>m</b>	0														
<b>C<sub>1ai</sub></b>	180	179.286	178.572	177.858	177.144	176.43	175.716	194	190	186									
	180	172	162	148															
<b>H<sub>zi</sub></b>	22.5	23	23.5	23.5	22.384	21	19	45.5	47	47.8									
	48.528	47.8	47.	45.5															
<b>N<sub>cti</sub></b>	0.88	0.89	0.895	0.897	0.895	0.89	0.88	0.88	0.890	0.895									
	0.897	0.895	0.89	0.88															
<b>r<sub>ki</sub></b>	0.55	0.55	0.55	0.55	0.55	0.55	0.55	0.55	0.55	0.55									
	0.55	0.55	0.55	0.55															
<b>i<sub>рki</sub></b>	0	0	0	0	0	0	0	0	0	0									
	0	0	0	0															
<b>D<sub>коi</sub></b>	1	1	1	1	1	1	1	1	1	1									
	1	1	1	1															

Next step in compressor calculation is obtaining the graphical representation of the schematic of the compressor air flow path; dependences of the change in temperature, pressure and velocity along compressor flow path. The results are shown on Figures 1.2 and 1.3.

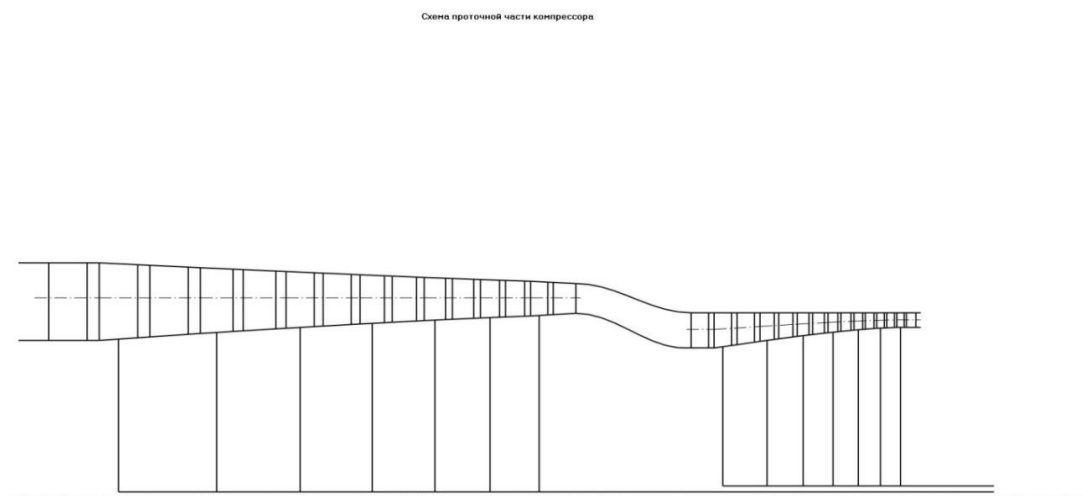


**Figure 1.2 – Schematic of the turbine**

**Table 1.5 – The results of gas-dynamic calculation of the compressor**

ГДР МОК Дата: 27.04.2021

Исходные данные:  
 Нк = 2 Кф1 = 2 Кф2 = 1 z1 = 7 zK = 14 Кг = 1  
 Пк = 18.093 Пк1 = 3.418 G = 115.92 n1 = 5965.9 n2 = 9382.8  
 k = 1.38 R = 287.20 Tв = 324.60 Pv = 146000.0 P10 = 144540.0  
 Svna = 0.990 Sna = 0.995 Shv = 0.995 m = 0.00

Результаты расчета:

№ст	Dк	Dср	Dвт	Дот	КПД	Mw1	Mс2
1	1.072	0.9128	0.7185	0.67	0.8849	0.7668	0.6945
2	1.05	0.9128	0.7503	0.7143	0.8951	0.7424	0.6728
3	1.033	0.9128	0.7742	0.7495	0.9003	0.7199	0.6529
4	1.018	0.9128	0.7935	0.7794	0.9026	0.6975	0.6331
5	1.006	0.9128	0.8089	0.8042	0.9012	0.6732	0.6119
6	0.9962	0.9128	0.8209	0.824	0.8969	0.6587	0.5923
7	0.9885	0.9128	0.8301	0.8398	0.8879	0.6286	0.5816
8	0.8447	0.7685	0.684	0.8097	0.8857	0.796	0.7804
9	0.8447	0.7822	0.7142	0.8455	0.896	0.7639	0.6725
10	0.8447	0.7927	0.7371	0.8726	0.9014	0.7317	0.643
11	0.8447	0.8005	0.7537	0.8923	0.9038	0.6995	0.6132
12	0.8447	0.8061	0.7656	0.9064	0.9024	0.6644	0.5806
13	0.8447	0.81	0.7738	0.9161	0.898	0.6306	0.548
14	0.8447	0.8121	0.7781	0.9212	0.8888	0.5947	0.511
№ст	C1a	C2a	C1u	C2u	C1	C2	УК
1	180	179.6	88.38	168.2	200.5	246.1	335
2	179.3	178.9	86.99	169.6	199.3	246.6	328.1
3	178.6	178.2	85.56	171.1	198	247	322.7
4	177.9	177.5	85.02	171.6	197.1	246.9	318.1
5	177.1	176.8	86.55	178.1	197.2	245.3	314.2
6	176.4	176.1	88.63	168	197.4	243.4	311.2
7	175.7	180	91.94	164.7	198.3	244	308.8
8	194	192	103.1	234.4	219.7	303	415
9	190	188	105	239.3	217.1	304.3	415
10	186	183	107.1	242.3	214.6	303.6	415
11	180	176	108.4	244.7	210.1	301.4	415
12	172	167	111.2	244.7	204.8	296.2	415
13	162	155	113.5	244.4	197.8	289.4	415
14	148	136.5	116.2	242.9	188.2	278.6	415
№ст	Hz	Rk	a11	a12	be1	be1a	be2
1	2.25e+04	0.55	63.85	46.88	42.45	42.45	56.95
2	2.3e+04	0.55	64.12	46.53	42.14	42.14	57.16
3	2.35e+04	0.55	64.4	46.17	41.82	41.82	57.38
4	2.35e+04	0.55	64.45	45.97	41.63	41.63	57.4
5	2.238e+04	0.55	63.96	46.11	41.73	41.73	56.94
6	2.1e+04	0.55	63.33	46.35	41.92	41.92	56.36
7	1.9e+04	0.55	62.38	47.55	42.29	42.29	56.21
8	4.55e+04	0.55	62	39.33	35.28	35.28	52.64
9	4.7e+04	0.55	61.07	38.15	34.22	34.22	51.87
10	4.78e+04	0.55	60.07	37.06	33.37	33.37	50.83
11	4.853e+04	0.55	58.93	35.73	32.29	32.29	49.56
12	4.78e+04	0.55	57.12	34.31	31.12	31.12	47.63
13	4.7e+04	0.55	54.99	32.38	29.66	29.66	45.17
14	4.55e+04	0.55	51.87	29.33	27.63	27.63	41.17
№ст	Пст	Нтк	Сак	Kg	Kn	U1	U2
1	1.231	0.2029	0.5373	1.02	0.988	285.1	285.1
2	1.223	0.2189	0.5464	1.022	0.976	285.1	285.1
3	1.215	0.2341	0.5534	1.024	0.964	285.1	285.1
4	1.202	0.244	0.5592	1.026	0.952	285.1	285.1
5	1.181	0.2412	0.5637	1.028	0.94	285.1	285.1
6	1.159	0.2337	0.5669	1.031	0.928	285.1	285.1
7	1.135	0.2175	0.569	1.033	0.916	285.1	285.1
8	1.33	0.2922	0.4675	1.035	0.904	377.6	380.9
9	1.314	0.3032	0.4578	1.037	0.9	384.3	386.9
10	1.294	0.3084	0.4482	1.039	0.9	389.5	391.4
11	1.275	0.3131	0.4337	1.041	0.9	393.3	394.7
12	1.25	0.3084	0.4145	1.043	0.9	396.1	397
13	1.227	0.3032	0.3904	1.046	0.9	398	398.5
14	1.203	0.2935	0.3566	1.048	0.9	399	399
№ст	T2o	T1	T2	P2o	P3o	P1	P2
1	346.1	305.4	317.1	1.806e+05	1.797e+05	1.157e+05	1.314e+05
2	368.1	327.1	339.1	2.209e+05	2.198e+05	1.463e+05	1.637e+05
3	390.6	349.4	361.4	2.684e+05	2.67e+05	1.817e+05	2.023e+05
4	413.1	372	384	3.227e+05	3.211e+05	2.236e+05	2.472e+05
5	434.5	394.5	405.7	3.81e+05	3.791e+05	2.715e+05	2.969e+05
6	454.6	415.9	426.3	4.417e+05	4.395e+05	3.232e+05	3.495e+05
7	472.8	435.8	444.3	5.015e+05	4.99e+05	3.769e+05	4.001e+05
8	516.4	449.7	472.4	6.638e+05	6.605e+05	4.138e+05	4.804e+05
9	561.3	493.8	517	8.725e+05	8.682e+05	5.614e+05	6.469e+05
10	607.1	539.3	563	1.129e+06	1.124e+06	7.504e+05	8.582e+05
11	653.5	585.9	610	1.44e+06	1.433e+06	9.877e+05	1.121e+06
12	699.3	633.4	657.3	1.8e+06	1.791e+06	1.279e+06	1.437e+06
13	742.2	680.5	704.2	2.208e+06	2.197e+06	1.622e+06	1.805e+06
14	787.8	727.3	750.6	2.655e+06	2.642e+06	2.02e+06	2.227e+06
Dкк	Dск	Dвк	Dок	Tк	Pк	Ск	
0.9782	0.9128	0.8423	0.8611	456.6	4.394e+05	184.3	
0.8447	0.8119	0.7777	0.9207	780.3	2.551e+06	125	

Пк = 18.09 КПД = 0.8523 Lк = 484012

Пк1 = 3.418 КПД1 = 0.8801 Lк1 = 154884

Пк2 = 5.32 КПД2 = 0.8753 Lк2 = 329128

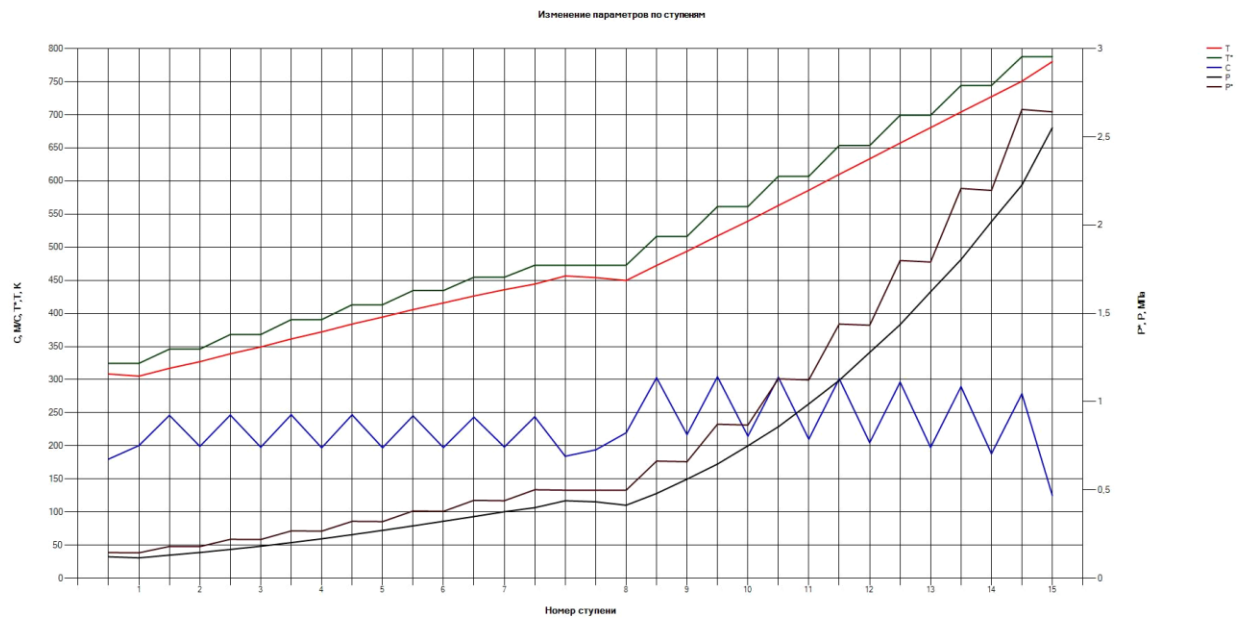


**Figure 1.3 –  $T^*$ ,  $T$ ,  $P^*$ ,  $P$  and  $C$  distribution between the compressor stages along the compressor flow path**

Efficiencies and reactivity coefficients as well as velocity and work distribution between the compressor stages are shown on Figures 1.4 and 1.5

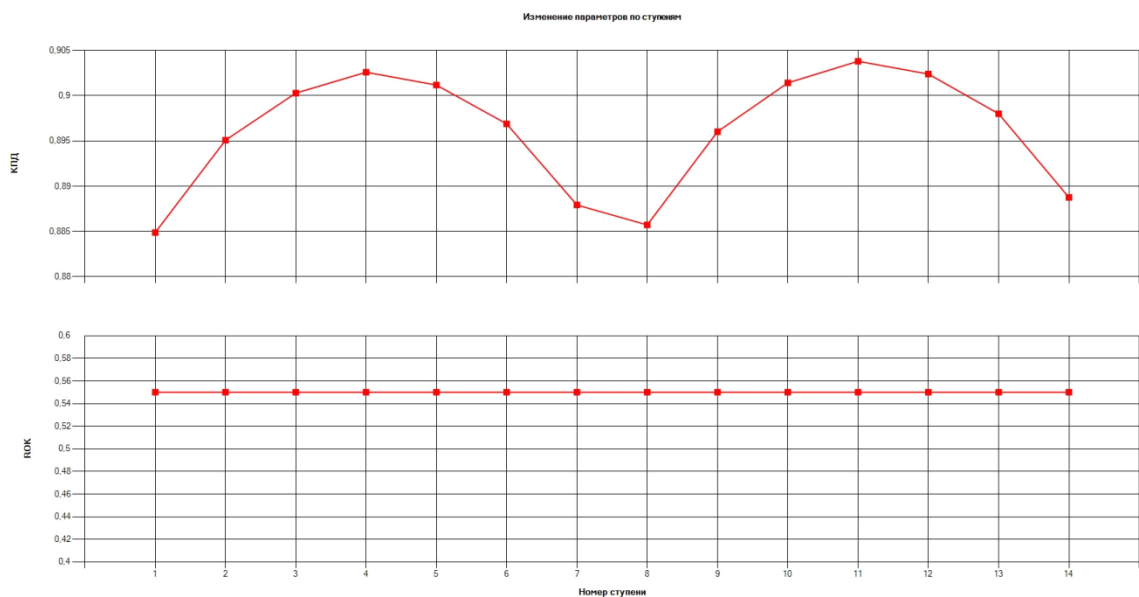


**Figure 1.4 – Efficiencies and reactivity coefficients distribution between the compressor stages**

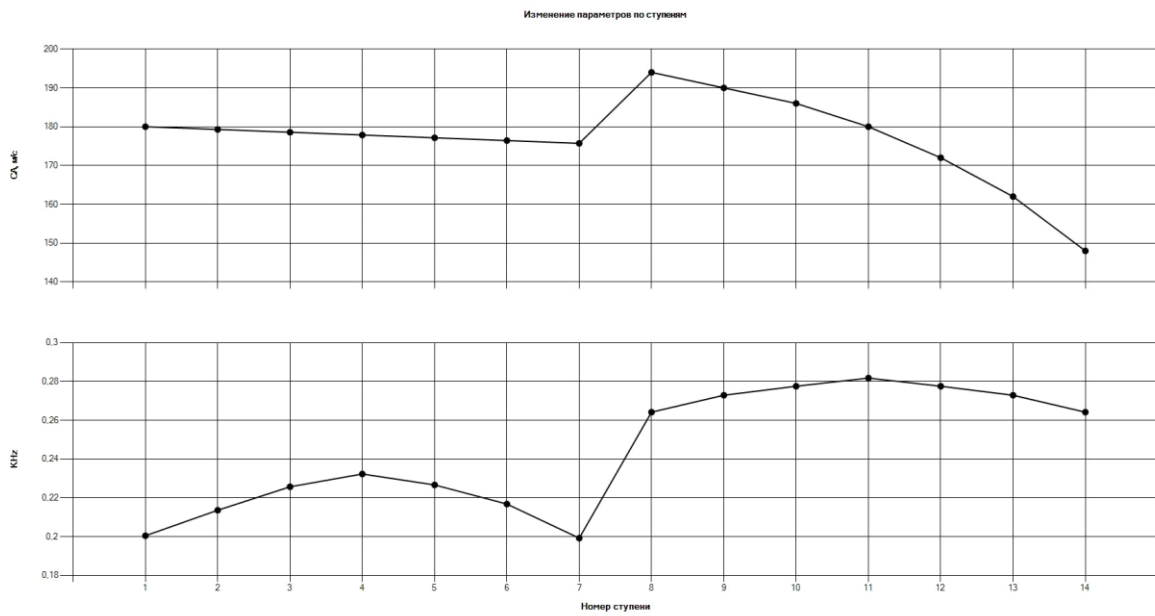


Figure 1.5 Velocity and work distribution between the compressor stages  
Velocity diagrams of the compressor stages on middle radius are represented on Figures 1.5 – 1.17.

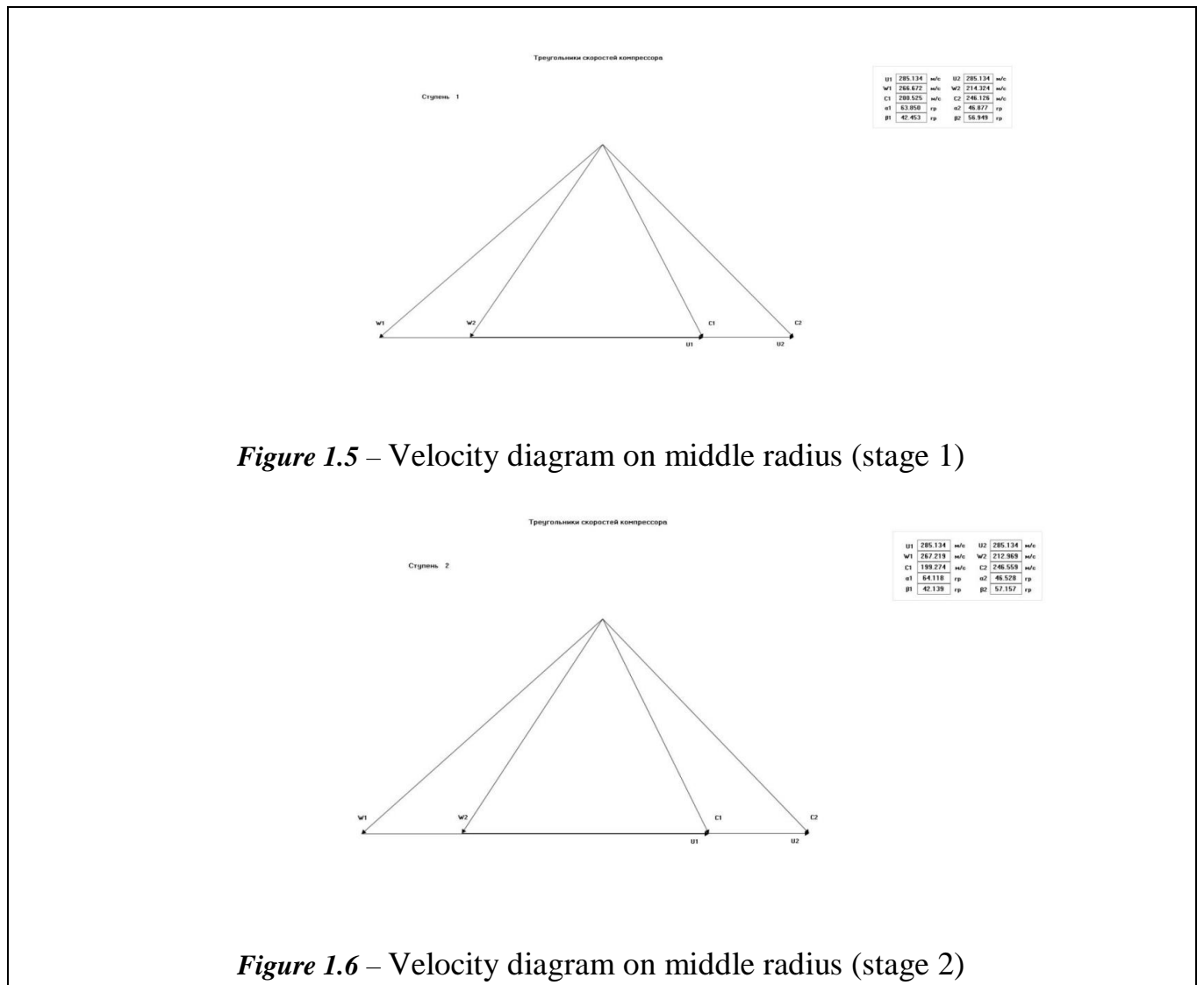
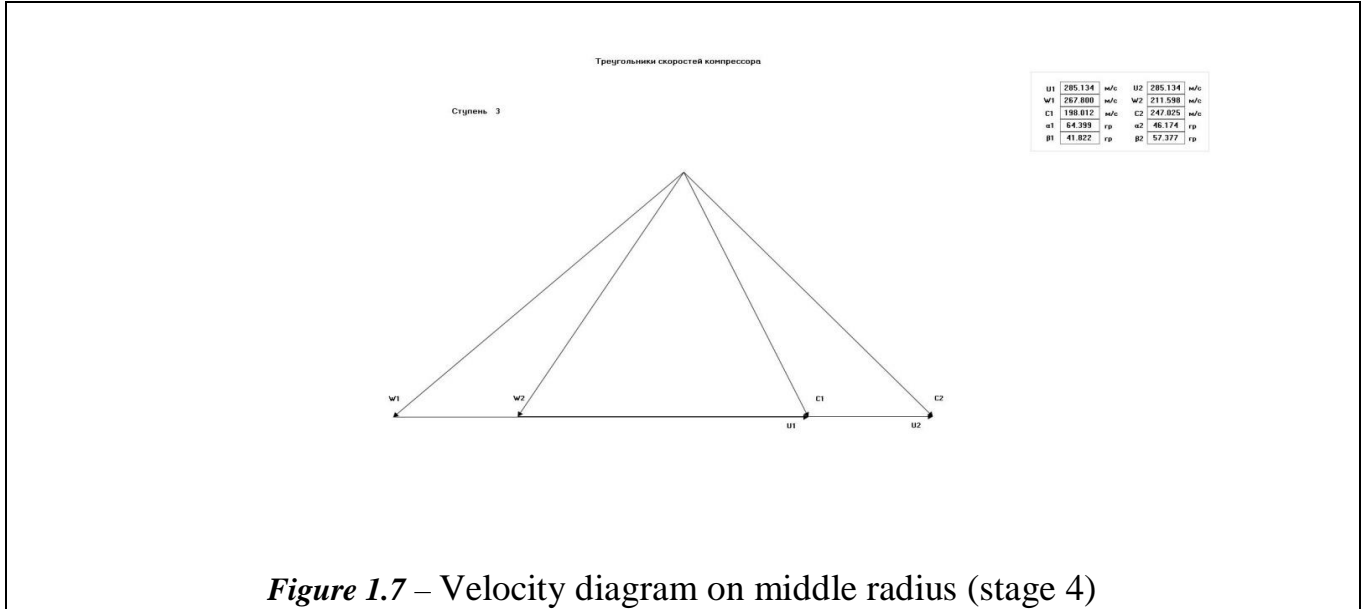


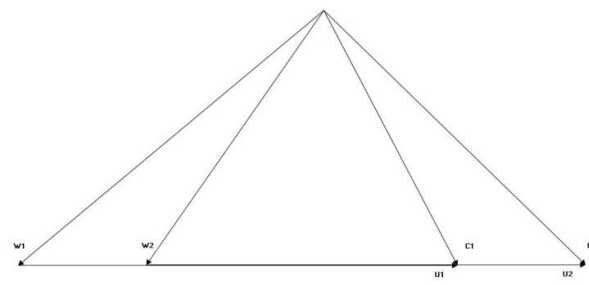
Figure 1.5 – Velocity diagram on middle radius (stage 1)

Figure 1.6 – Velocity diagram on middle radius (stage 2)



**Figure 1.7 – Velocity diagram on middle radius (stage 4)**

Треугольники скоростей компрессора					
Ступень 5					
u1	285.134	m/s	u2	285.134	m/s
w1	268.110	m/s	w2	210.936	m/s
c1	197.158	m/s	c2	246.039	m/s
a1	63.968	гр	a2	46.110	гр
p1	41.735	гр	p2	56.941	гр



**Figure 1.8 Velocity diagram on middle radius (stage 5)**

Треугольники скоростей компрессора					
Ступень 6					
u1	285.134	m/s	u2	285.134	m/s
w1	264.087	m/s	w2	211.480	m/s
c1	197.158	m/s	c2	246.039	m/s
a1	63.928	гр	a2	46.345	гр
p1	41.913	гр	p2	56.364	гр

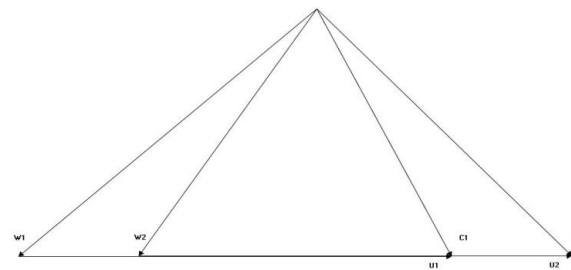


**Figure 1.9 Velocity diagram on middle radius (stage 6)**

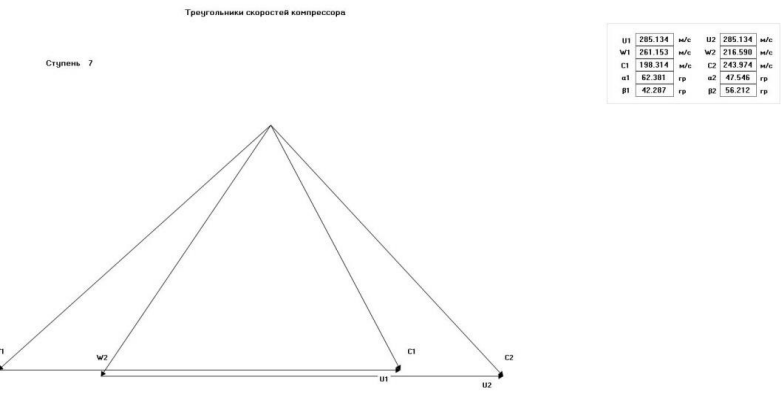


Figure 1.10 Velocity diagram on middle radius (stage 7)

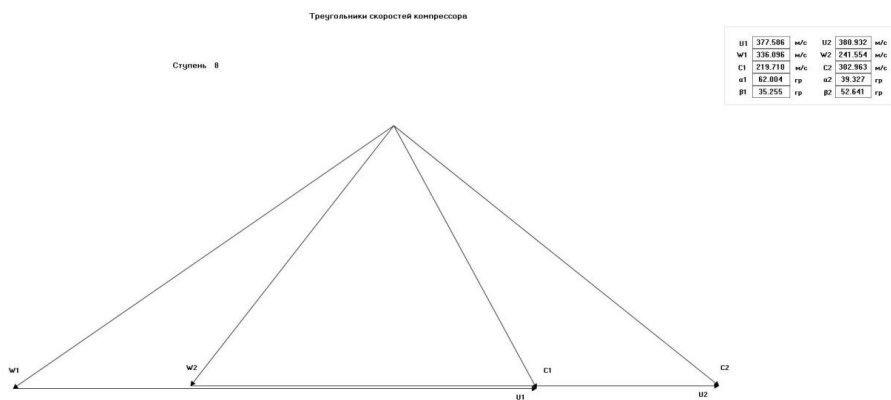


Figure 1.11 Velocity diagram on middle radius (stage 8)

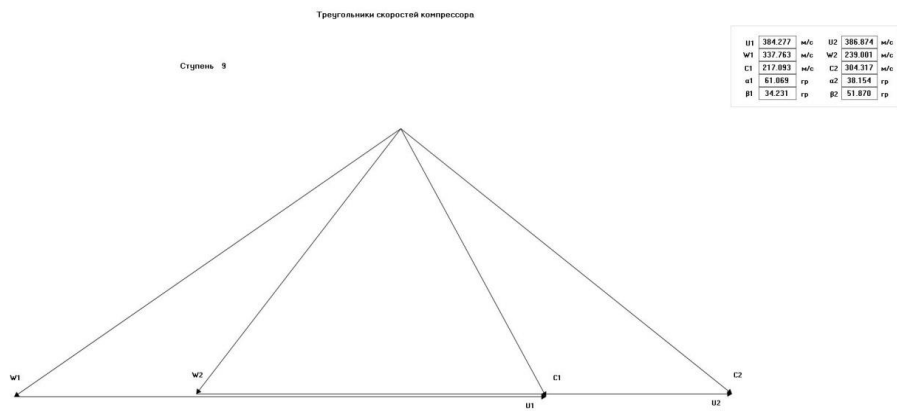


Figure 1.12 Velocity diagram on middle radius (stage 9)

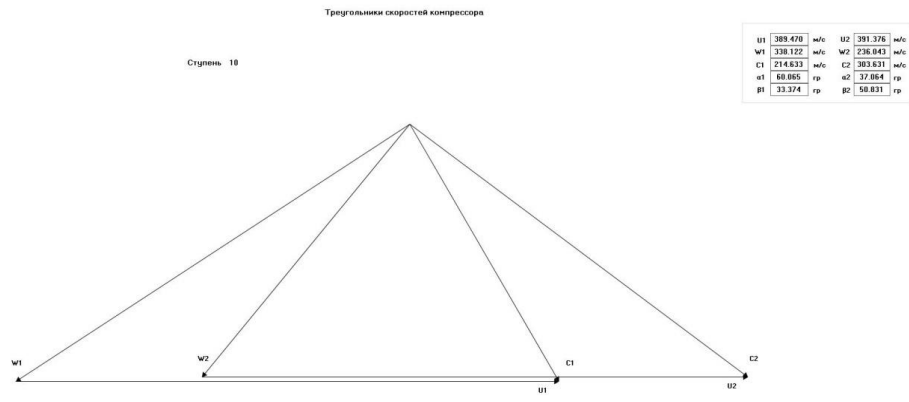


Figure 1.13 Velocity diagram on middle radius (stage 10)

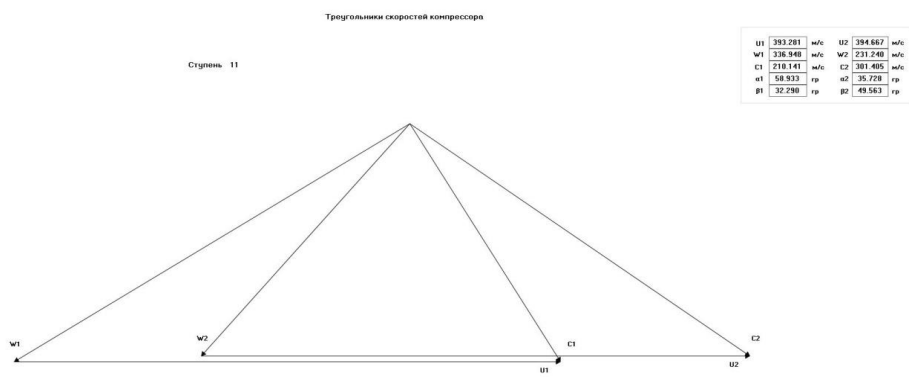


Figure 1.14 Velocity diagram on middle radius (stage 11)

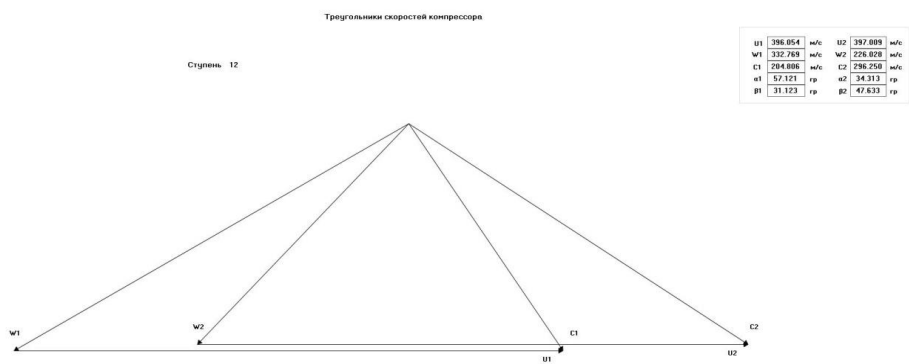


Figure 1.15 Velocity diagram on middle radius (stage 12)

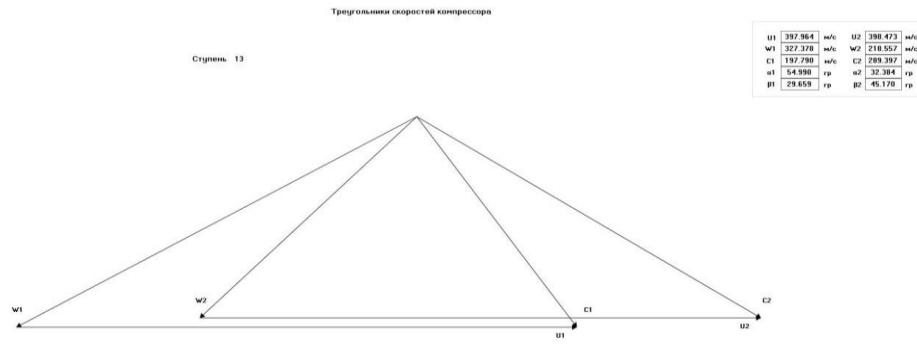


Figure 1.6 Velocity diagram on middle radius (stage 13)

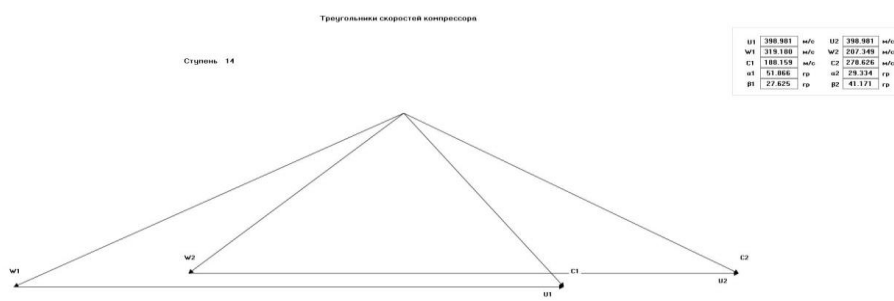


Figure 1.17 Velocity diagram on middle radius (stage 14)

As a result of the gas-dynamic calculation the compressor parameters were obtained that meet allthe requirements of modern aviation compressors designing. Distribution of the main parameters ( $C$ ,  $T^*$ ,  $T$ ,  $P^*$  and  $P$ ) along the flow path corresponds to the typical patterns of the axial multistage compressors. Work and pressure ratio of each stage were obtained as well.

From the calculation results it can be seen that the resulting axial compressor provides the initial pressure ratio and has agood value of efficiency.

Seven-stagelow-pressure compressorhas  $M_{w1}= 0.7668$  at the inlet to the first stage rotor. It has low-loaded the first, second, seventh stages and middle-loaded other stages. Efficienciesof low-pressurecompressor stages are in the range 0.8849 ... 0.9026.

Seven-stagehigh-pressure compressorhas high-loaded all stages. The values of  $M_{w1}$ at the inlet to the all HPC stage rotors do notexceed $M_{w1}<0.796$ . The relative hub

diameter of the HPClass stage = 0.9212 exceeds slightly the permissible values = 0.92.

Efficiencies of high-pressure compressor stages are in the range 0.8857 ... 0.9038.

## 1.5 Compressor blade profiling

The gas-dynamic and kinematic parameters of the profiled stage at the middle radius are the initial data for profiling the compressor rotor blade. They are obtained as a result of gas-dynamic calculation of the compressor. Next, after choosing the law of profiling all parameters in five sections along the height of the blade are calculated by the appropriate formulas.

The model flow is considered as steady-state, axisymmetric, with constant hydraulic losses along the radius. Numerical methods are commonly used to calculate the axisymmetric flow in blade rows. For simplicity, it is believed that the flow moves in axial stage according to the equation of radial equilibrium.

We choose the law of change of parameters along the radius. The criterion for choosing the optimal profiling law is providing of subsonic flow velocities and acceptable flow angles (in particular,  $M_{w1}$  and  $M_{c2} < 0.84$ ,  $\gamma_g < 25$  degrees at the periphery,  $\gamma_g < 90$  degrees at the hub. Calculations show that for subsonic stages with relative hub diameters of approximately 0.8, the laws of constancy of the reactivity coefficient and the law of the solid body are suitable.

### Parameters choice

Accept the solid body law of profiling along the radius. In practice, this law is widely used for profiling in gas turbine engines subsonic compressor first stage.

All initial data for the first part of profiling are represented in Table 1.6

**Table 1.6** – Initial data for calculation

$k = 1.38$	$H_{hub} = 0.26$	$d_{1hub} = 0.8097$	$P_1^* = 491540 \text{ (Pa)}$
$R = 287.2$	$st_i^* = 0.8857$	$d_{2hub} = 0.8276$	$C_{1umid} = 103.1 \text{ (m/s)}$
$st_i^* = 1.343$	$GV = 0.995$	$C_{1amid} = 194 \text{ (m/s)}$	$D_{1tip} = 0.8447 \text{ (m)}$
$U = 415 \text{ (m/s)}$	$d_{21} = 1$	$T_1^* = 472.8 \text{ (K)}$	$K_H = 0.904$

**Table 1.7 – Calculation results**

ГДР СТ.ОК      Дата: 03.06.2021

**ИСХОДНЫЕ ДАННЫЕ:**

$M = 1$        $KR = 3$        $K\Gamma = 1.380$        $R\Gamma = 287.20$   
 $P_{i*} = 1.343$        $U_k = 415.000$        $H_{TBT} = 0.260$        $KPD* = 0.886$        $S_{Na} = 0.995$   
 $D21 = 1.000$        $d1_{BT} = 0.810$        $d2_{BT} = 0.828$   
 $m = 0.000$        $C1a = 194.000$        $T1* = 472.80$        $P1* = 491540.0$        $C1u = 103.100$   
 $D_k = 0.845$        $K_h = 0.904$   
 $W1KC = 1.000$        $W1BC = 1.000$        $A = 0.273$        $B = 0.000$        $D = 0.000$

**ГАЗОДИНАМИЧЕСКИЙ РАСЧЕТ СТ. ОК**

$P1 = 1.337$        $P2 = 1.343$        $H21 = 46325.5$        $H22 = 47099.0$   
 $P01 = 657072.6$        $P02 = 660138.2$        $T01 = 517.22$        $T02 = 517.96$   
 $G_B = 116.925$        $ROK = 0.5442$        $HTO = 0.3025$        $WC = 9383.1$

Таблица 1

N	U	CU	CA	T0	T	P0	P
ROTH	R0	C	W	LC	LW	AL	BE
11	415.00	113.32	182.25	472.80	450.72	491540.0	413176.1
1.0000	3.1918	214.60	352.46	0.5408	0.8550	58.128	31.136
12	395.96	108.12	188.46	472.80	450.17	491540.0	411342.2
0.9541	3.1816	217.27	344.05	0.5475	0.8373	60.157	33.213
13	376.55	102.82	194.30	472.80	449.63	491540.0	409566.1
0.9073	3.1716	219.83	335.68	0.5540	0.8196	62.113	35.368
14	356.62	97.38	199.83	472.80	449.11	491540.0	407841.2
0.8593	3.1619	222.29	327.32	0.5602	0.8017	64.020	37.625
15	336.03	91.75	205.08	472.80	448.60	491540.0	406162.2
0.8097	3.1525	224.67	318.95	0.5662	0.7836	65.896	40.015
*	*	*	*	*	*	*	*
21	415.00	238.86	168.34	517.96	477.02	661117.2	490256.5
1.0000	3.5785	292.22	243.65	0.7036	0.5938	35.175	43.704
22	397.07	238.63	182.12	517.82	474.62	660537.9	481403.9
0.9568	3.5317	300.19	241.39	0.7228	0.5900	37.351	48.978
23	379.38	237.69	194.48	517.40	472.19	658802.1	472635.7
0.9142	3.4852	307.12	240.62	0.7398	0.5897	39.291	53.925
24	361.71	236.05	205.79	516.71	469.69	655916.4	463865.6
0.8716	3.4387	313.16	241.12	0.7549	0.5923	41.081	58.591
25	343.87	233.71	216.30	515.73	467.12	651891.9	455016.7
0.8286	3.3917	318.45	242.74	0.7684	0.5976	42.785	63.011
*	*	*	*	*	*	*	*
81	415.00	113.32	182.25	472.80	450.72	491540.0	413176.1
1.0000	3.1918	214.60	352.46	0.5408	0.8550	58.128	31.136
82	397.07	108.42	188.11	472.80	450.20	491540.0	411445.9
0.9568	3.1822	217.12	344.53	0.5471	0.8383	60.042	33.092
83	379.38	103.59	193.48	472.80	449.71	491540.0	409819.2
0.9142	3.1730	219.46	336.89	0.5531	0.8222	61.835	35.051
84	361.71	98.77	198.46	472.80	449.24	491540.0	408272.4
0.8716	3.1644	221.68	329.43	0.5586	0.8063	63.542	37.044
85	343.87	93.89	203.13	472.80	448.79	491540.0	406789.2
0.8286	3.1560	223.78	322.10	0.5639	0.7905	65.192	39.098

Received graphical dependences of flow parameters along the rotor blade height of a given compressor stage are shown on Figures 1.18 – 1.20:

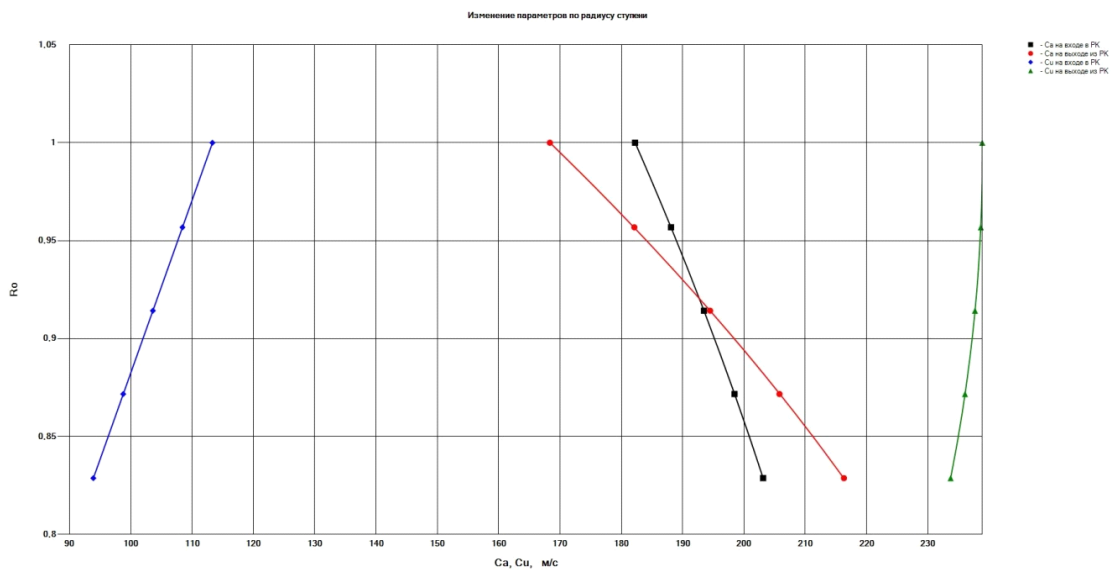


Figure 1.18  $Ca$  and  $Cu$  distribution along the blade height at the inlet and the outlet of the rotor blade

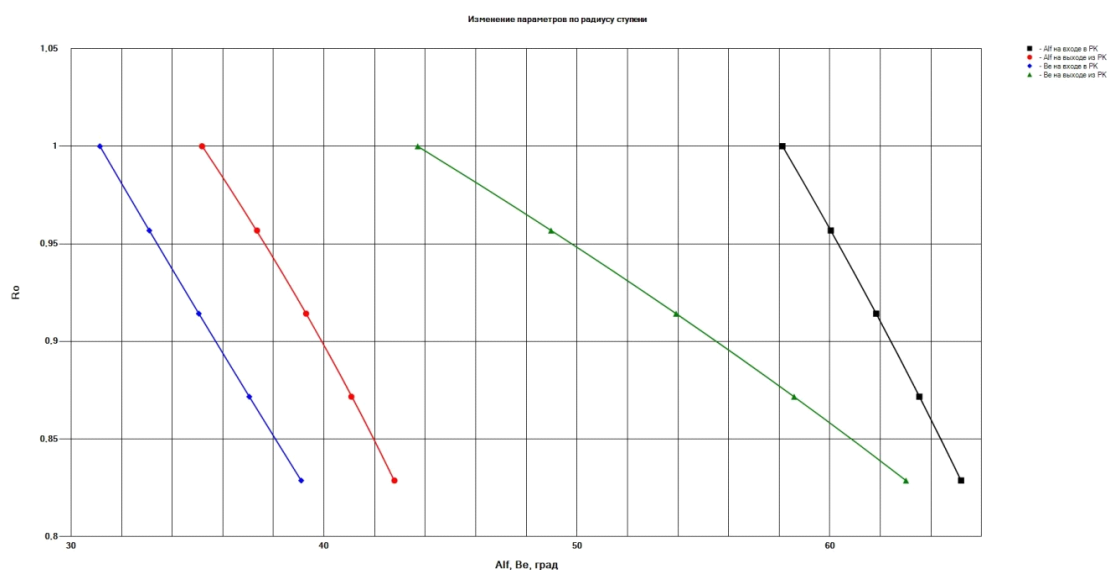


Figure 1.19  $\alpha$  and  $\beta$  distribution along the blade height at the inlet and the outlet of the rotor blade

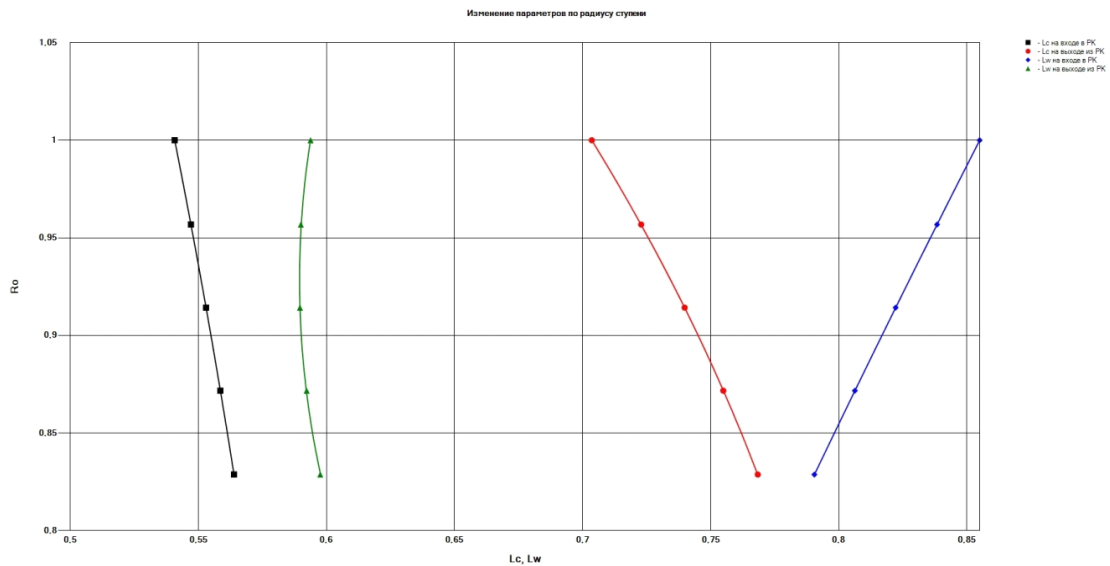


Figure 1.20  $c$  and  $w$  distribution along the blade height at the inlet and the outlet of the rotor blade

The resulting velocity diagrams along the blade height are shown on Figures 1.21 – 1.25:

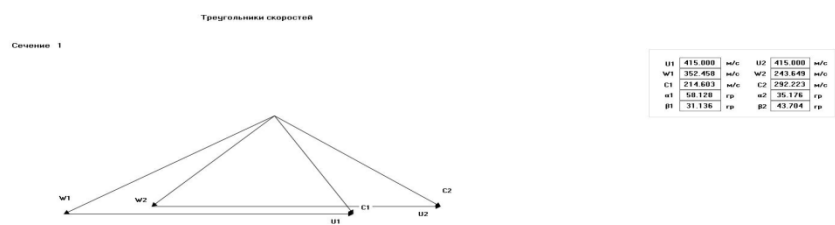


Figure 1.21 Velocity diagram in section 1 (tip)

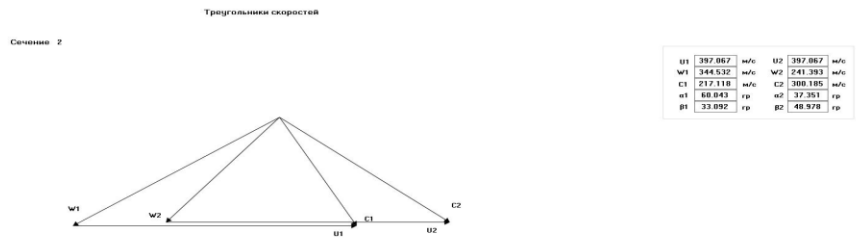


Figure 1.22 Velocity diagram in section 2

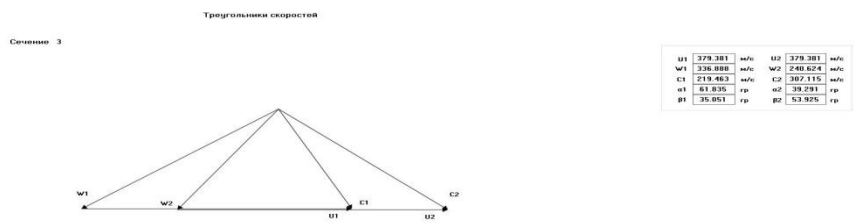


Figure 1.23 Velocity diagram in section 3 (middle)

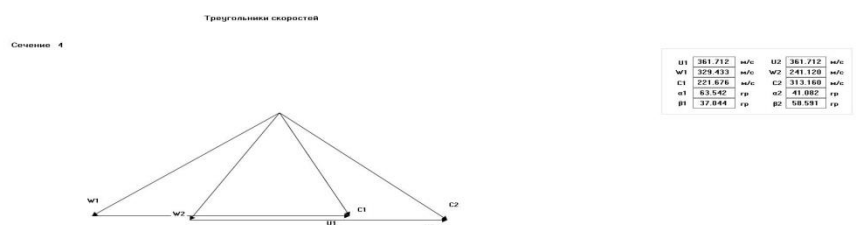


Figure 1.24 Velocity diagram in section 4

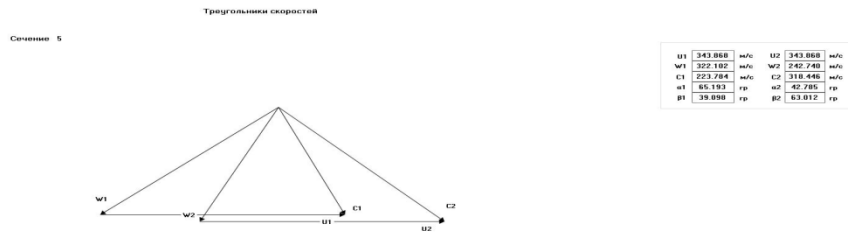


Figure 1.25 Velocity diagram in section 5 (hub)

### Parameters choice for rotor blades profiling

The blade aspect ratio is the ratio of the length of the blade to the chord on the middle radius  $\overline{h_b} = \frac{h_{bl}}{b_{mid}}$ . If you increase the blade aspect ratio, the longitudinal dimensions of the stage and its mass will decrease, and the gas-dynamic stability boundary of the compressor stage will shift toward higher mass flow rates. This leads to a decrease in stability margin and an increase in vibrations from dynamic stresses in the rotor blades, especially in the first stages.

The main priority when choosing blade aspect ratio is to ensure a sufficient stability margin for the stage. According to the recommendations for the blade aspect ratio, it is selected in the range of 3.0 ... 4.5 in the group of first stages and up to 1.5 ... 2.5 in the group of last stages. For the first stages of high-pressure compressor this range is 2.5...3. Accepted  $\overline{h_b} = 3$ .

To a large extent, the aerodynamic loading of the blade cascade determines such a parameter as the cascade solidity  $\frac{b}{t}$  ( $b$  – the profile chord,  $t$  – cascade space). If there has been a decrease in the cascade solidity in comparison with the optimum, then this means underloading the stage, and with increasing cascade solidity, the efficiency decreases.

Determination of the cascade solidity of the rotor blades is performed at the design regime, which is characterized by continuous flow around the cascade without stalls in the absence of an increase in losses.

The ratio of the calculated flow turning angle  $\Delta\beta$  to the angle on the designed regime  $\Delta\beta^*$  determines the stability margin for stall the compressor cascade.

The value of  $\Delta\beta/\Delta\beta^*$  is taken equal to 0.8 ... 1 for the first stages of the compressor. Accepted  $\Delta\beta/\Delta\beta^* = 1$ , whereas  $\Delta\beta = \beta_2 - \beta_I = 53.925 - 35.051 = 18.874$ (degrees).

According to the graph in Figure 1.26, the flow turning angle when  $\frac{b}{t} = 1 \Delta\beta_{\frac{b}{t}=1}$  is found depending on the exit flow angle from the cascade  $\beta_2$ . In our case  $\beta_2 = 53.925$  degrees,  $\Delta\beta_{\frac{b}{t}=1} = 18.43$  degrees. The required cascade solidity is determined according to the graph in Figure 1.27, depending on the parameter E:

$$E = \frac{\Delta\beta}{\Delta\beta_{\frac{b}{t}=1} \frac{\Delta\beta}{\Delta\beta^*}} = \frac{18.874}{18.43} = 1.024; \quad \frac{b}{t} = 1.03.$$

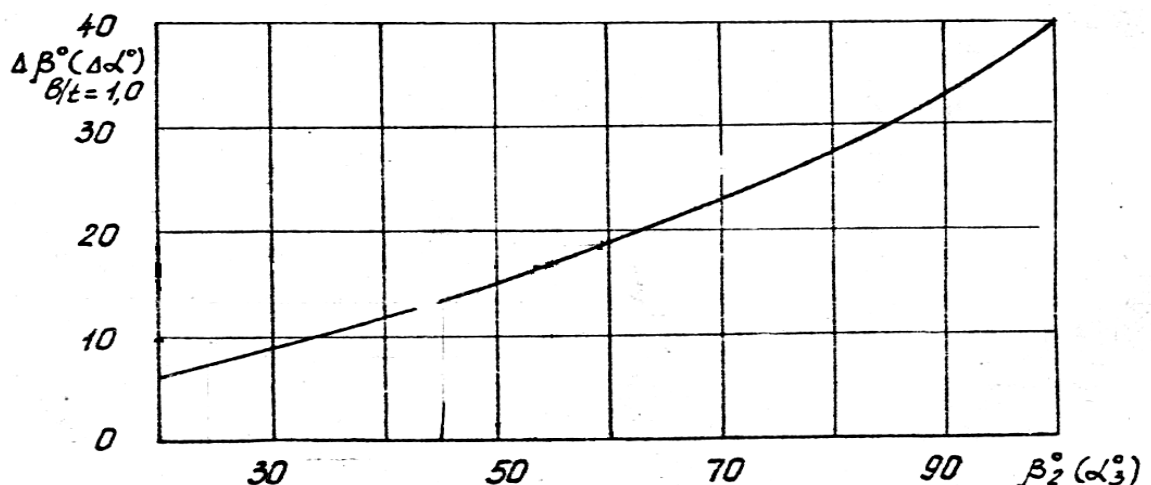


Figure 1.26 Dependency graph  $\Delta\beta_{\frac{b}{t}=1}$  from  $\beta_2$

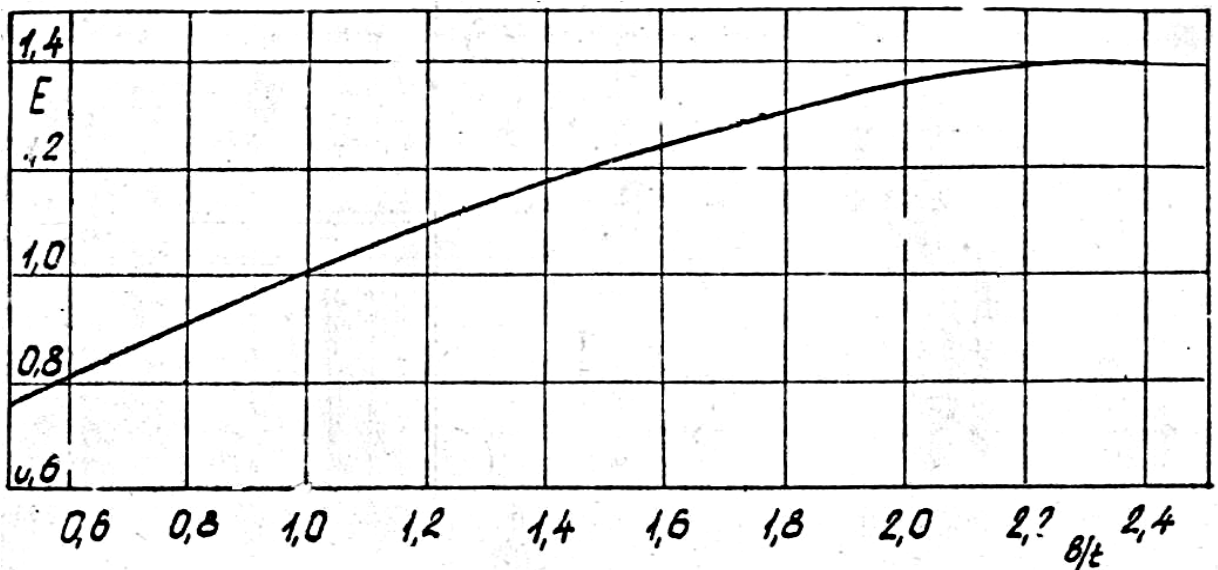


Figure 1.27 Dependency graph E from  $\frac{b}{t}$

The graphs are taken from the manual [4]. The required values of the cascade solidity on the hub and the periphery of the blade can be adjusted for design and technological reasons. The cascade solidity on the hub and the periphery may be changed due to the choice of a variable chord along the radius.

With the selected cascade solidity on the middle radius, the preliminary value of the cascade space is found by the formula:

$$t'_{mid} = \frac{b'_{mid}}{\left(\frac{b}{t}\right)_{mid}}$$

Preliminarily find the value of the chord on the middle radius:

$$h_{bl} = \frac{D_{tip} - D_{hub}}{2} = \frac{0.8447 - 0.684}{2} = 0.08035 \text{ (m)};$$

$$b'_{mid} = h/\bar{h}_b = \frac{0.08035}{3} = 0.02678 \text{ (m)};$$

$$t'_{mid} = \frac{b'_{mid}}{\left(\frac{b}{t}\right)_{mid}} = \frac{0.02678}{1.03} = 0.026007 \text{ (m)}.$$

Then the preliminary number of blades will be equal:

$$Z' = \frac{\pi \cdot D_{mid}}{t'_{mid}} = \frac{3.14 \cdot 0.7685}{0.026007} = 92.83.$$

Accepted  $Z = 93$  rotor blades.

The results of profiling of high-pressure compressor first stage rotor blades are

presented in Table 1.8.

Table 1.8 – Profiling results

Таблица 2

Профилирование лопатки РК по радиусу

Параметр	Сечение по высоте лопатки				
	1(пер)	2	3(ср)	4	5(вт)
<i>r<sub>0</sub></i>	<b>1.0000</b>	<b>0.9568</b>	<b>0.9142</b>	<b>0.8716</b>	<b>0.8286</b>
<i>b</i>	<b>24.13</b>	<b>24.13</b>	<b>24.13</b>	<b>24.13</b>	<b>24.13</b>
<i>t</i>	<b>28.53</b>	<b>27.30</b>	<b>26.09</b>	<b>24.87</b>	<b>23.64</b>
<i>b/t</i>	<b>0.8456</b>	<b>0.8838</b>	<b>0.9250</b>	<b>0.9702</b>	<b>1.0206</b>
<i>c<sub>m</sub></i>	<b>0.0300</b>	<b>0.0350</b>	<b>0.0400</b>	<b>0.0450</b>	<b>0.0500</b>
<i>i</i>	<b>0.0000</b>	<b>0.0000</b>	<b>0.0000</b>	<b>0.0000</b>	<b>0.0000</b>
<i>del</i>	<b>6.791</b>	<b>7.892</b>	<b>8.645</b>	<b>9.115</b>	<b>9.351</b>
<i>dbe</i>	<b>12.567</b>	<b>15.886</b>	<b>18.874</b>	<b>21.547</b>	<b>23.913</b>
<i>tet</i>	<b>19.358</b>	<b>23.778</b>	<b>27.519</b>	<b>30.662</b>	<b>33.264</b>
<i>be11</i>	<b>31.14</b>	<b>33.09</b>	<b>35.05</b>	<b>37.04</b>	<b>39.10</b>
<i>be21</i>	<b>50.49</b>	<b>56.87</b>	<b>62.57</b>	<b>67.71</b>	<b>72.36</b>

Число рабочих лопаток – 93 шт

The resulting rotor blade airfoil cascades are shown on Figures 1.28 – 1.33:

Решетка профилей РК компрессора  
Сечение  $\bar{x} = 1.000$

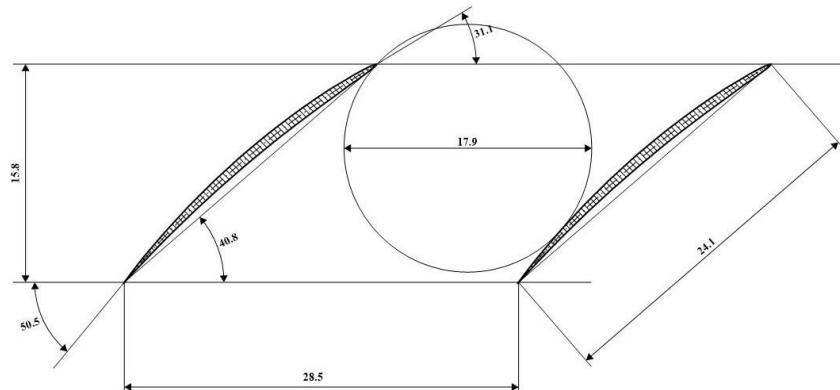


Figure 1.28 Rotor blade airfoil cascade in section 1 (tip)

Сечение  $\bar{r} = 0.957$

Решетка профилей РК компрессора

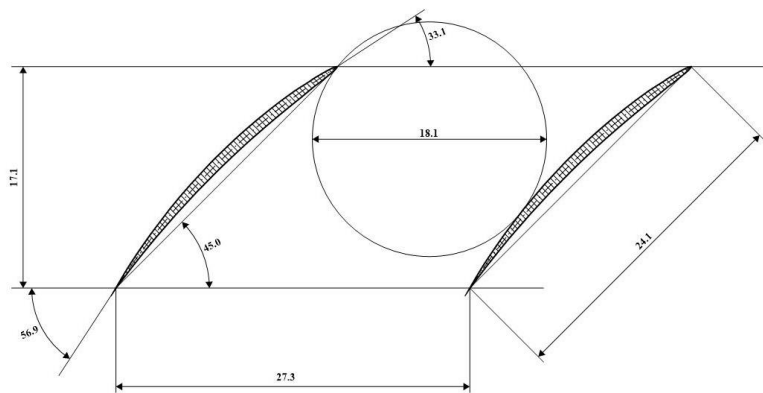


Figure 1.29 Rotor blade airfoil cascade in section 2

Сечение  $\bar{r} = 0.914$

Решетка профилей РК компрессора

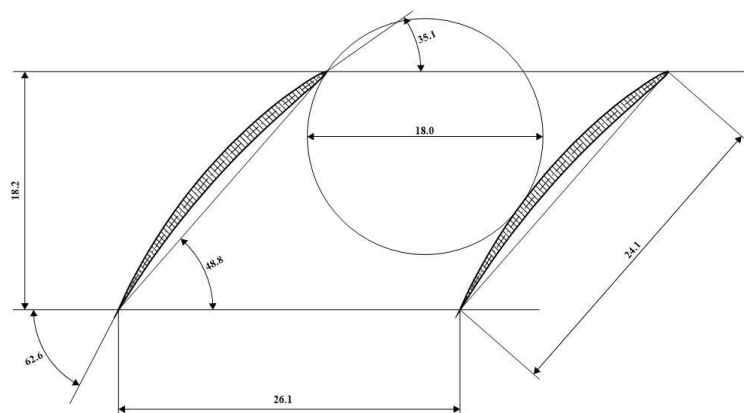


Figure 1.30 Rotor blade airfoil cascade in section 3 (middle)

Решетка профилей РК компрессора  
Сечение  $\bar{r} = 0.872$

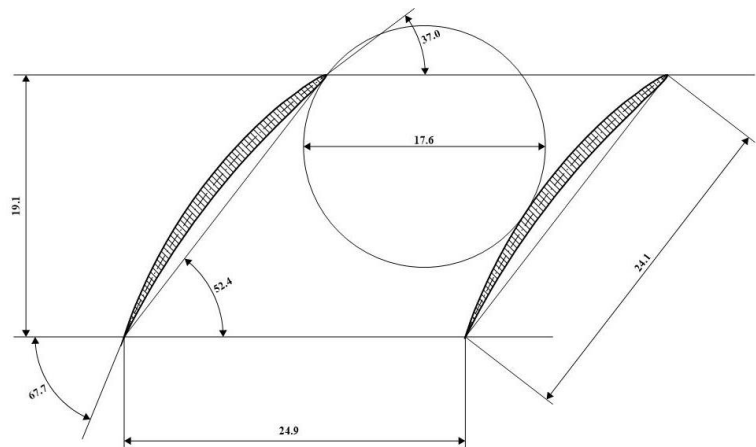


Figure 1.31 Rotor blade airfoil cascade in section 4

Решетка профилей РК компрессора  
Сечение  $\bar{r} = 0.829$

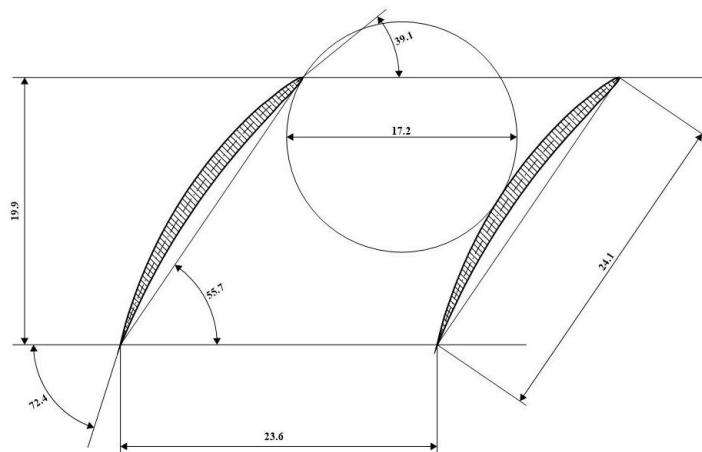


Figure 1.32 Rotor blade airfoil cascade in section 5 (hub)

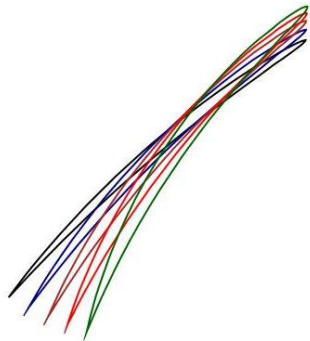


Figure 1.33 Rotor blade airfoils (all sections)

The results obtained and the designed rotor blades cascade of the first stage of the high-pressure compressor satisfy the established requirements and can provide the required parameters.

## Conclusion

After completing this course project, a modification of 3-shaft turbofan engine with increased specific thrust and reduced specific fuel consumption based on the prototype engine D – 18 was developed.

As a result of the thermo-gas-dynamic calculation specific thrust

$P_{sp} = 312.38 \text{ N}\cdot\text{s}/\text{kg}$  and specific fuel consumption  $C_{sp} = 0.037686 \text{ kg}/\text{N}\cdot\text{h}$  are obtained. Specific thrust of newly designed engine is more than specific thrust of the prototype engine ( $P_{sp\ prot} = 300.654 \text{ N}\cdot\text{s}/\text{kg}$ ) and specific fuel consumption of newly designed engine is less than specific fuel consumption of the prototype engine ( $C_{sp\ prot} = 0.0377 \text{ kg}/\text{N}\cdot\text{h}$ ). These values meet current standards of turbofan engines parameters.

The engine compressor and turbine parameters matching calculation formed 3-shaft turbofan engine conceptual design. When performing calculations on the formation of the engine conceptual design, the following features are determined: the shape of the flow path, the rotational speeds and the number of stages of the spools of impeller machines.

The fan with  $D_{mid} = \text{const}$ , middle – loaded ( $\bar{H}_z = 0.2523$ ) consists of a single stage and has a value of efficiency  $\eta_f^* = 0.885$ .

The low-pressure compressor with  $D_{mid} = \text{const}$ , low – loaded ( $\bar{H}_z = 0.2147$ ) consists of seven stages and has a value of efficiency  $\eta_{lpc}^* = 0.88$ .

The high-pressure compressor with  $D_{tip} = \text{const}$ , high – loaded ( $\bar{H}_z = 0.273$ ) consists of seven stages and has a value of efficiency  $\eta_{hpc}^* = 0.8753$ .

The hub relative diameter at the discharge from the last stage of the HPC  $d_h = 0.9194$  does not exceed the permissible value  $\bar{d}_h = 0.92$ .

The single-stage high-pressure turbine with  $D_{hub} = \text{const}$ , high – loaded ( $\mu_t = 1.7791$ ) has a value of efficiency  $\eta_{hpt}^* = 0.8565$ .

The single-stage low-pressure turbine with  $D_{hub} = \text{const}$ , high – loaded ( $\mu_t = 1.7727$ ) has a value of efficiency  $\eta_{lpt}^* = 0.8916$ .

The four-stage fan turbine with  $D_{mid} = \text{const}$ , high – loaded ( $\mu_t = 1.8546$  per stage)

has a value of efficiency  $\eta_{ft}^* = 0.92$ .

The factor which characterize relative blades height of the turbine stages  $h/D$  should be in the range 0.065...0.32. For the high-pressure turbine it equals to 0.0618 and for the fan turbine – 0.3176.

As a result of the gas-dynamic calculation the compressor parameters were obtained that meet allthe requirements ofmodernaviationcompressors designing. Distribution of the main parameters ( $C$ ,  $T^*$ ,  $T$ ,  $P^*$  and  $P$ ) along the flow path corresponds to the typical patterns of the axial multistage compressors. Workandpressure ratioof each stage were obtained as well.

Fromthe calculation results it can be seenthat the resultingaxial compressor provides the initial pressure ratioand has a good value ofefficiency.

Seven-stage low-pressure compressor has  $M_{w1}=0.7668$  at the inlet to the first stage rotor. It has low-loaded the first, second, seventh stages and middle-loaded other stages. Efficiencies of low-pressure compressor stages are in the range 0.8849...0.9026.

Seven-stage high-pressure compressor has high-loaded all stages. The values of  $M_{w1}$  at the inlet to the all HPC stage rotors do not exceed  $M_{w1} < 0.796$ . The relative hub diameter of the HPC last stage  $\bar{d}_h=0.9212$  exceeds slightly the permissible values  $\bar{d}_h= 0.92$ . Efficiencies of high-pressure compressor stages are in the range 0.8857...0.9038.

After completing of compressor blade profiling the results obtained and the designed rotor blades cascade of the first stage of the high-pressure compressor satisfy the established requirements and can provide the required parameters.

By comparison with the prototype, the better specific parameters that reduce the metal content and the complexity of manufacture are obtained. Engine parameters are in line with modern requirements shown to modern turbofan engines.

## **2. DESIGNING PART**

## 2.1 General information about prototype

Turbofan engine D-18T is designed to be installed on heavy cargo aircrafts.

The engine is designed with the three-shaft scheme with a front located fan and shortened bypass; It consists of an axial 14-stage compressor, the intermediate casing, an annular combustion chamber, a 6-stage turbine and fixed nozzles (primary and secondary). Instead of the bypass nozzle the thrust reverser can be applied on the engine.

The feature of three-shaft scheme is the split of the compressor rotor into three independent rotors, each of which is driven by its own turbine. In this case all rotors have a different optimal rotational speeds and are interconnected only gas-dynamically.

Using of three-shaft design:

- made compressor stages very efficient;
- provide the necessary compressor stability;
- use at a lower-power starter, as it must accelerate only the high pressure rotor.

The high bypass ratio ( $m=5.6$ ) and high parameters of the gas-dynamic cycle ensure engine high efficiency.

The basic accessory units are beneath the engine, which makes it easy to access each of them.

**Single-stage fan (Fan)** has no inlet guide vanes, and consists of the impeller, a stator followed by straightening vanes, shaft bearing assembly and a rotating spinner which is heated by air.

The fan disk connections to the drive shaft and to a spinner bybolts, the blades are connected to the disk by the "dovetail" locks.

Fan blades have shroud anti-vibration shelves disposed in the bypass. Straightening vanes assembly is a non-detachable construction, with sound absorbing panels.

The shaft of fan is connected to the fan turbine shaft with splines. Both fan rotor bearings are mounted on the oil dampers.

**The low pressure compressor (LPC)** consists of a front compartment with fixed and adjustable inlet guide vanes, LPC rotor, stators, air bypass valves and the bearing assembly.

The compressor rotor of drum-disk structure is connected to the shaft by means of bolts. Both the low-pressure rotor bearings are mounted on the oil dampers.

Low pressure compressor stator with its fairing separates airflow downstream the fan impeller on the two flows - primary and secondary.

**The high pressure compressor (HPC)** is composed of inlet guide vanes, rotor, stator, air bypass valves and bearing assembly.

The high pressure compressor rotor is of drum-disk structure. Welded drum, discs of the last stages, spacers and shafts are interconnected by precise bolts.

HPC rear shaft connection with high-pressure turbine - also bolted.

Front ball bearing is mounted in the elastic support with hard stroke limiter. Rear roller bearing of high pressure rotor is installed on the oil damper.

**The intermediate casing** is used for the formation of a transition channel from the LPC to HPC and to the bypass, the attachment of accessory units and their drives, as well as attachment of the HPC front rotor support and front engine mounting belt.

## 2.2 Compressor blade strength analysis

### Strength calculation of first stage HPC

Axial compressor rotor blades are very critical parts of a gas turbine engine, reliable operation of which depends on the reliability of the engine as a whole.

#### The aim of calculating

The purpose of the calculation of the strength of the blades of the seventh compressor stage is to define the level of stress and margins in different sections along the length of the blade.

As the design mode is selected mode the maximum speed of the rotor and maximum air flow through the engine. To meet these conditions take-off mode of the engine, that is, with a rotational speed of 9382.8 rpm.

### Calculation

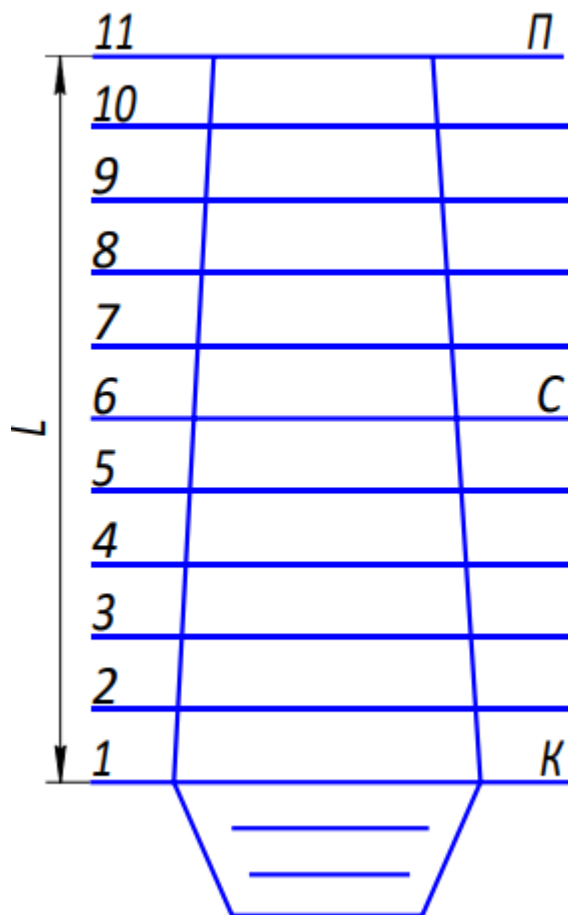


**Figure 2.1**– Design scheme used for analysis

#### 2.2.2 Data for analysis

For strength analysis of compressor blade the initial data is taken from gas dynamic calculations, blade profiling.

### 2.2.3 Blade geometric parameters

1. Material blades: VT-3

2. The length of the blade  $L = 0.08$  m;

3. The radius of the root section  $R_c = 0.342$  m;

4. The radius of the peripheral section of  $R_p = 0.422$  m; L 9

5. The amount of the binding shelves = 0 m;

6. Chord Profile section of the blade:

- In the root section of  $b_k = 0.02413$  m;
- In the middle section of  $b_{cp} = 0.02413$  m;
- In the peripheral section of  $b_p = 0.02413$  m;

7. The maximum thickness of the profile in the sections:

- In the root section = 0.002044 m;
- In the middle section = 0.001533 m;
- In the peripheral section = 0.001022 m;

8. The maximum deflection in the middle line profile sections:

- In the root cross section = 0.002044m;
- In the middle section = 0.001533 m;
- In the peripheral section = 0.001022 m;

9. The installation angle profile sections:

- In the root cross section = 1.0222 rad;
- In the middle section = 0.9283 rad;
- In the peripheral section 0.7727 rad;

The intensity of the gas forces on the average radius in the plane of rotation:

- Axial plane

$$P_a = \frac{2 \cdot \pi \cdot r}{z} (p_2 - p_1 + C_{2a}^2 \cdot \rho_2 - C_{1a}^2 \cdot \rho_1) \quad (2.1)$$

- In the plane of rotation

$$P_u = \frac{2 \cdot \pi \cdot r}{z} (C_{2a} \cdot \rho_2 \cdot W_{2u} + C_{1a} \cdot \rho_1 \cdot W_{1u}) \quad (2.2)$$

**Table 2.2– Gas force intensities**

Axial direction (Peripheral section)	N/m	1767
Axial direction (Root section)	N/m	2180.27
Circumferential direction (Mean section)	N/m	2472.27

11. The frequency of rotation of the impeller  $n = 9382.8 \text{ rev / min}$ ;

12. Density of vanes  $\rho = 4530 \text{ kg / m}^3$ ;

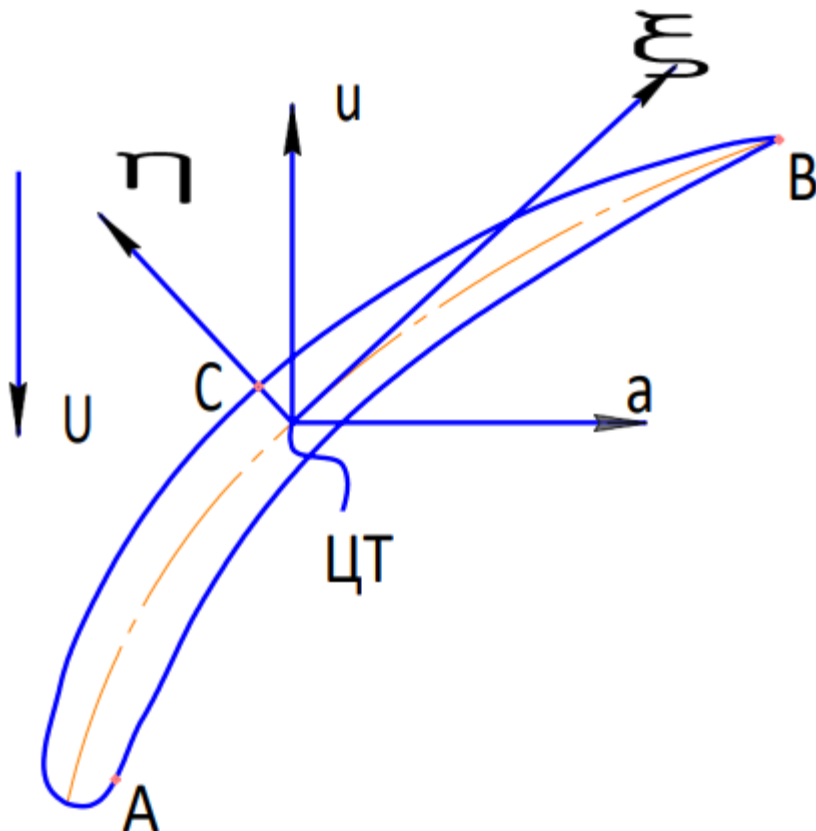
13. Limit of long-term strength  $\sigma = 950 \text{ MPa}$

According to the standards of strength and safety, the minimum margin of static strength profile of the rotor blade of the compressor should be at least 1.5.

### 2.2.3 Computer Calculation

Calculations are performed using Statlop.exe.

The results of the calculation are given in Table 2.3.



## STRENGTH ANALYSIS OF ROTOR BLADE BODY

**Table 2.3 initial data for calculation:**

## 2.2.4 Results of the calculation

Table - 2.4

N	X, m	F, m <sup>2</sup>	J <sub>min</sub> , m <sup>4</sup>	$\sigma_t$ , MPa	Bending stresses, MPa		
					$\sigma_{bA}$	$\sigma_{bB}$	$\sigma_{bC}$
1	0	3.418E-05	1.69E-11	99.5466	230.2741	239.2831	-216.3138
2	0.00803	3.247E-05	1.317E-11	92.308	230.6242	238.3829	-216.1422
3	0.01607	3.076E-05	1.125E-11	84.6504	218.6536	224.8664	-204.4706
4	0.0241	2.905E-05	9.7E-12	76.5332	199.8869	204.505	-186.501
5	0.03214	2.734E-05	8.35E-12	67.9053	175.3209	178.4398	-163.2112
6	0.04017	2.563E-05	7.13E-12	58.7024	145.78	147.61	-135.4084
7	0.04821	2.393E-05	6E-12	48.8415	112.3728	113.2133	-104.1523
8	0.0562	2.222E-05	4.952E-12	38.2142	76.84	77.0449	-71.0724
9	0.0643	2.051E-05	3.959E-12	26.6761	42.0859	42.0116	-38.8531
10	0.0723	0.0000188	3.015E-12	14.03	13.2275	13.1525	-12.191
11	0.0803	1.709E-05	2.112E-12	0	0	0	0

Table – 2.5

N	Total stresses, MPa			Safety limits		
	$\sigma_{\Sigma A}$	$\sigma_{\Sigma B}$	$\sigma_{\Sigma C}$	K <sub>A</sub>	K <sub>B</sub>	K <sub>C</sub>
1	329.8208	338.8297	-116.7672	2.8804	2.8038	-8.1358
2	322.9322	330.6909	-123.8342	2.9418	2.8728	-7.6716
3	303.304	309.5169	-119.8202	3.1322	3.0693	-7.9285
4	276.4201	281.0382	-109.9678	3.4368	3.3803	-8.6389
5	243.2262	246.3451	-95.3059	3.9058	3.8564	-9.9679
6	204.4823	206.3124	-76.7061	4.6459	4.6047	-12.3849
7	161.2143	162.0548	-55.3108	5.8928	5.8622	-17.1757
8	115.0542	115.2591	-32.8582	8.257	8.2423	-28.9121
9	68.762	68.6877	-12.177	13.8158	13.8307	-78.0159
10	27.2575	27.1825	1.839	34.8528	34.9489	516.5823
11	0	0	0	$\pm\infty$	$\pm\infty$	$\pm\infty$

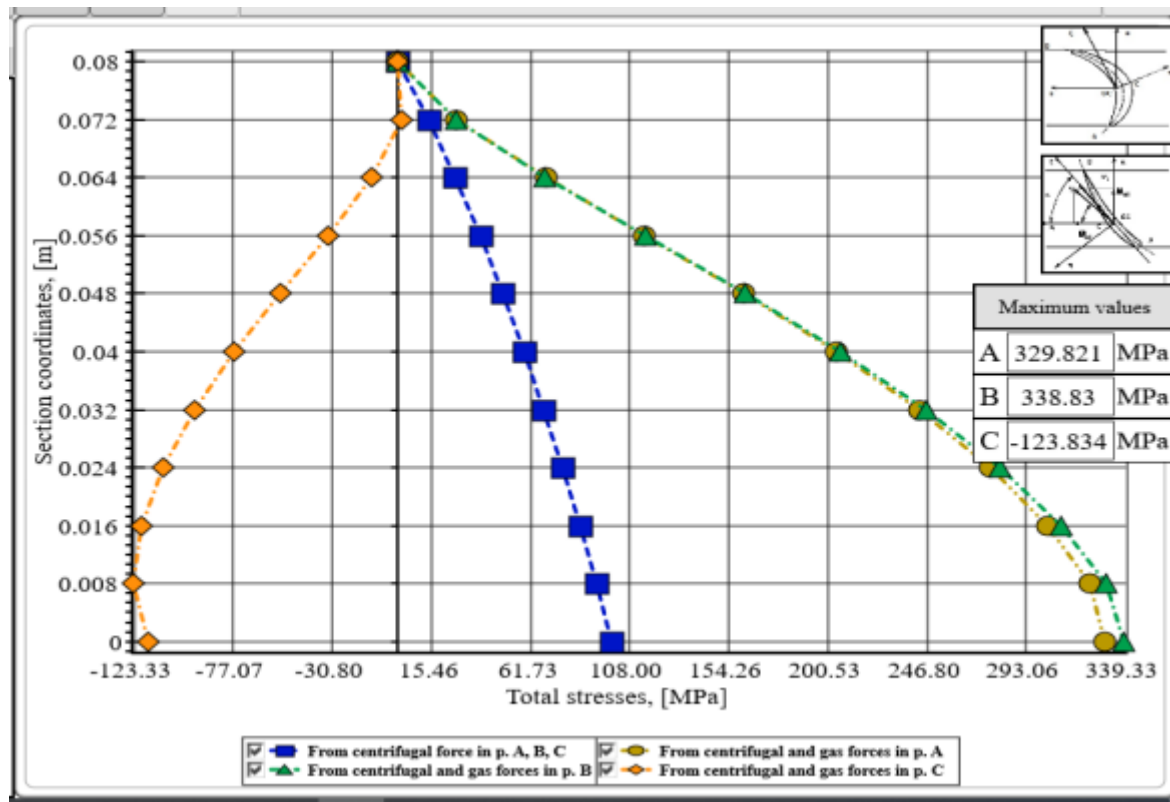


Fig 2.2–Total stresses dependent on section coordinates

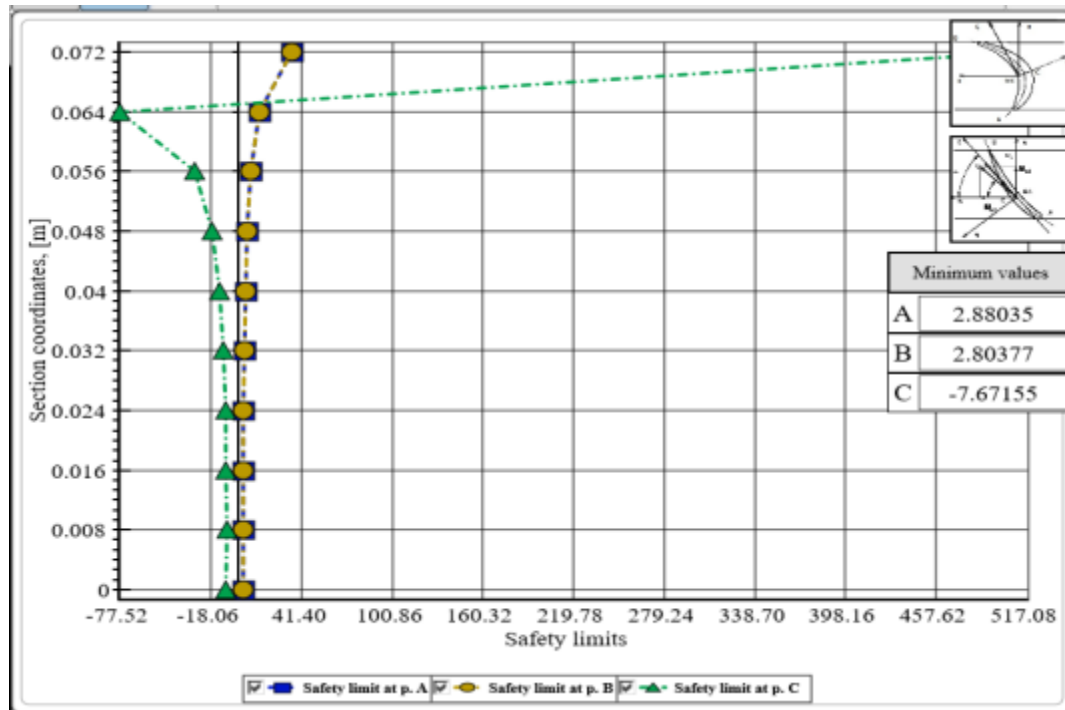


Fig 2.3 – Safety factors' functions dependent on section coordinates

## 2.2.5 Conclusion

In the blade section, the tensile stresses caused by the centrifugal forces and bending stresses caused by the gas forces are determined. The maximum stresses at each cross section

are determined by summing up tensile and bending stresses. Then the safety factors along the blade length are determined.

The analysis was done to check the static strength of the first stage high pressure compressor blade. And it can be concluded from the obtained result that the blade is strong in terms of static strength because the safety factors are well above 1.3.

At the points A and B, tensile stress is produced and at these points these stresses are approximately the same. As a result, the safety factors at these points are also approximately the same. At the point C, compressive stresses are produced, as a result of which, the total stress is much lower compared to the stresses at the points A and B.

We will be using the root area and the tensile stress of the root part of the blade for the static strength analysis of the blade locking part

## **2.3 Strength analysis of the compressor blade lock**

### **“Dovetail” General Information**

Blade joint transfers all the loads acting on the impeller blade to the disk. It also loads the disk with the centrifugal force of its own mass. Dovetail root has simple structure and is easy to manufacture. These features differ this root among the other roots. Big contact area of blade root and slot in the disk provides good heat withdrawal from the blade.

The main requirements of the blade roots are: - the provision of placing the needed number of blades in the disk; - the provision of required strength of blade root at its minimum mass; - ensuring the rigidity of each blade to get the self-oscillations being within the range specified by the designer; - the accurate attachment of blades in the disk and securing their position during operation; - the blades must be easy to produce, assemble and replace in maintenance

#### **2.3.1 Assumptions**

Simplified analysis usually considers blade to be loaded by the centrifugal forces of the blade (the air foil and the root component). Loads that appear due to the gas flow are usually neglected.

The simplified blade root strength analysis is based on the following assumptions:

- The centrifugal forces of the air foil Pcentr air foil and the root Pcentr root act in the same plane, which passes through the gravity centre of the root;
- The centrifugal forces of the air foil and the root are directed at one point and at the same radius which goes through the gravity centre of the root;
- The diameter of the disk is large enough so that it is possible to consider that the locks are situated in one plane;
- The centrifugal force of the air foil is distributed between the contact surfaces of the root proportionally to their areas.

### 2.3.2 Initial data

The purpose of the calculation is the determination of the stresses and safety factors in different sections of the radial disk. Design scheme is shown in Fig. 6.1.

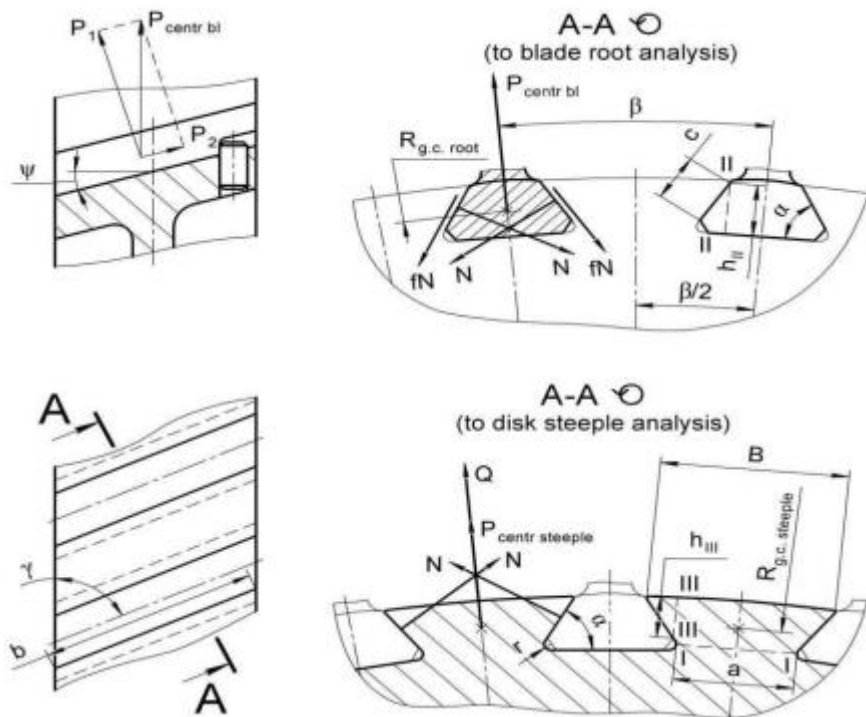


Fig. 2.3.1 -Design scheme

The geometrical parameters needed for calculation are obtained from the designed model. All other parameters are obtained from previously obtained results of strength analysis of blade and disk.

**Table 2.8–** Initial data for fir-tree lock strength analysis

Parameter	Designation	Units	Magnitude
Root radius of the blade	R <sub>r</sub>	mm	342
Number of blades	z	-	93
Material density	ρ	kg /m <sup>3</sup>	4530
Sliding friction coefficient	f	-	0.3
Rotational speed	n	rpm	9382.8
Tensile stress at the air-foil root	σ <sub>(tens root)</sub>	MPa	99.5466
Area of the root section	F <sub>(root)</sub>	m <sup>2</sup>	3.418e-5
Flank angle of the root	α	°	60
Angle between the slot floor and the axis of rotation	ψ	°	0
Slot length	b	mm	24.13
Radius of the root gravity centre	R <sub>g.c. root</sub>	mm	337.5
Radius of the steeple gravity centre	R <sub>g.c. steeple</sub>	mm	337.5
The width of the contact spot	c	mm	8.65
The width of shear area of the root	h <sub>II</sub>	mm	9
The width of shear area of the steeple	h <sub>III</sub>	mm	7.19
Neck width of the steeple	a	mm	10.54
Steeple width at the outer radius of the disk	B	mm	19.76
Radius of the rounding arc	r	mm	1
Yield Strength	[σ] <sub>0.2</sub>	MPa	1150

### 2.3.2 Calculations

The initial data is input into the program DoveTailAnalysis.exe. The results of the analysis are represented in the Fig 2.3.2

The tensile, bearing and shearing stresses are found to be:

	units	Bearing	Tensile	Shear
Acting stress	MPa	11.8577	137.83	13.31
Safety factor	-	97	8.34	86.4

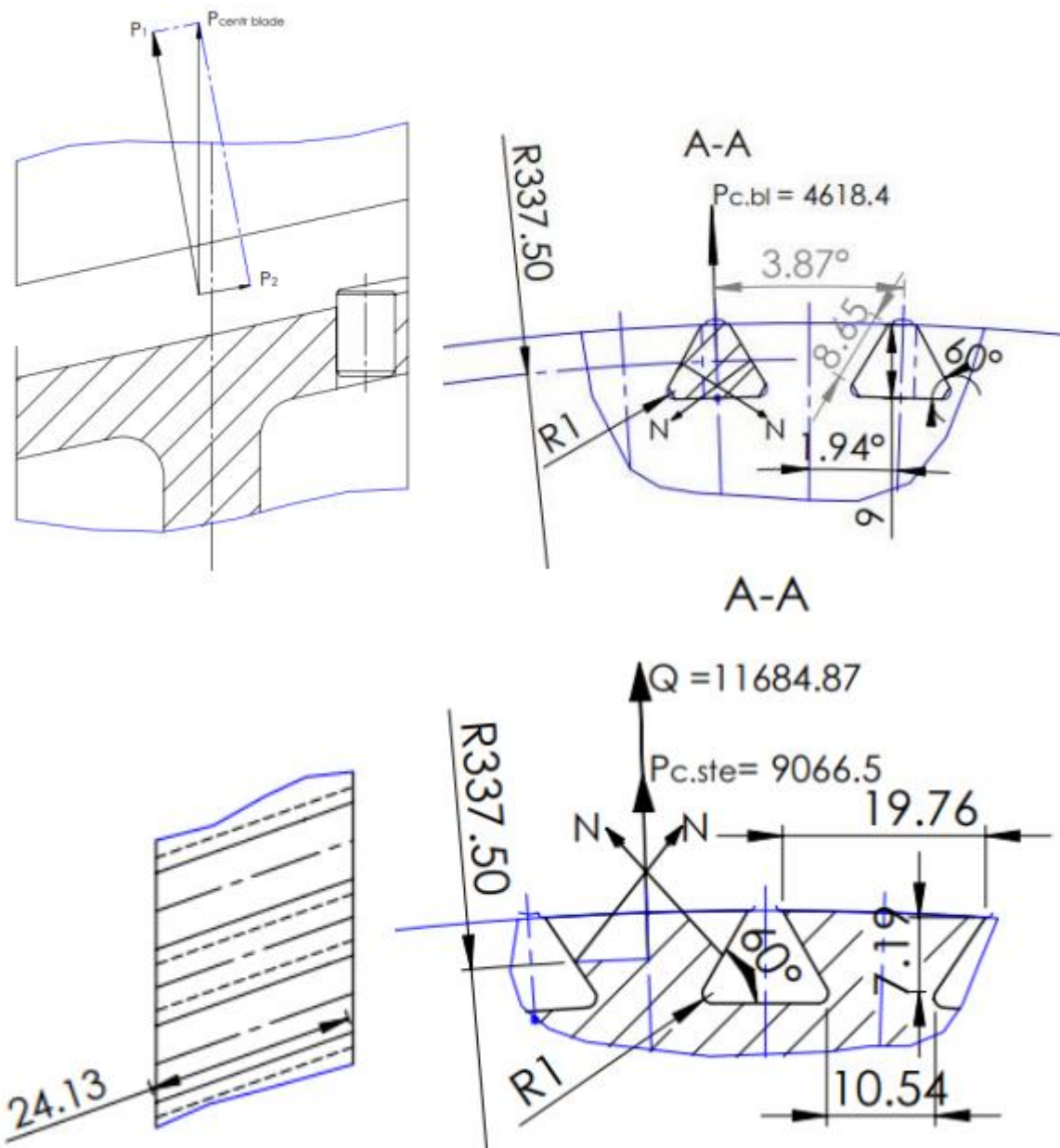


Fig 2.3.2 - Results of the calculation

#### 2.3.4 Conclusion

The analysis of the calculated safety factors reveals the following: - all the safety factors are more than 3, which means that the designed dovetail joint meets the Norms of Strength; - the most dangerous stress is the tensile stress acting the steeple neck because  $K_{tension}$  is the least among all the safety factors calculated.

## **2.4 Strength analysis of the compressor disc**

Compressor disk is the most critical elements of the designs of gas turbine engines. It is necessary for the design to be safe and reliable, easy and economical design of aircraft engines in general

### **Loads acting on the disk**

Discs are influenced by inertia centrifugal forces generated by the rotating blades of the masses of workers and the self-weight discs. These forces cause tensile stresses in the discs. Uneven heating of turbine discs having thermal stresses that can cause both tensile and compressive elements disc.

In addition to tensile and compressive stresses in the drive voltage can occur torsion and bending. Torsional stress when the disk is transmitted torque and bending - is caused by the difference in pressure and temperature on the side surface of the disc from the axial gas-dynamic forces acting on the blades, and blades of vibration of these discs, under the action of the gyroscopic moments resulting in the evolution of plane.

Of these, the most significant stresses are stresses from centrifugal forces and its own weight disc blade row, as well as the temperature (in the case of uneven heating of the disk). Bending stress depends on the thickness of the disc and the connecting method between a disc and the shaft can be significant and only thin discs. Torsional stresses are usually small and in the calculations in most cases not taken into account.

### **2.4.1 Assumptions**

In the calculation of the disk the following assumptions were made:

- The disc considered is symmetrical about a median plane perpendicular to the axis of rotation;
- The disc condition; - Disk temperature varies only by its radius and uniform thickness;
- Voltage at any radius does not change in thickness;
- The presence of holes and bosses on the canvas disk, separate projections and grooves on his part not taken into account.

### **The purpose of calculation**

The purpose of the calculation is the determination of the stresses and safety margins in different sections of the radial disk. Design scheme is shown in Fig. 2.4.2 and Fig 2.4.3.

## 2.4.2 Initial data

1. The frequency of rotation of the disk = 9382.8 rev / min;
2. The geometrical dimensions of the disc in the calculated cross sections (indicated in the figure);
3. Characteristics of the material of construction of VT-3: density = 4530 kg / m, Poisson's ratio= 0.3, modulus of elasticity= 1.2e5; 22
4. Tension in the root section of the blade tension from the centrifugal forces on the current mode = 99.5466 MPa;
5. The area of the root section of the blade = 0.00003148m;
6. The number of vanes on the impeller z = 93; 8. Limit of long-term strength of = 950MPa.

## 2.4.3 Calculations

The main design equations to determine the elastic stresses in the disk by centrifugal force and uneven heating

To calculate the disk ,we use the strength of two differential equations:

$$\begin{aligned} d\sigma_r &= \sigma_r \left( \frac{db}{R} + \frac{dR}{E} \right) + \sigma_\tau \frac{dR}{E} - \rho \omega^2 R^2 \frac{dR}{E} \\ d\sigma_\tau &= \sigma_\tau \left( \frac{dR}{R} + \frac{dE}{E} \right) + \sigma_r \left( \frac{b}{R} \frac{dR}{E} - \mu \frac{db}{b} - \mu \frac{R/E}{b} \right) - \mu \rho \omega^2 R^2 \frac{dR}{E} - E \alpha t \end{aligned}$$

where  $\sigma_r$  &  $\sigma_\tau$  - radial and circumferential normal stress; b, R - The current values of the thickness and the radius of the disk;  $\omega$  - The angular velocity of rotation of the disk;  $\rho$  - The density of the disc material; E - Modulus of elasticity of the disc material;  $\mu$  - Poisson's ratio;  $\alpha$  - Coefficient of linear expansion of the disc material; t - The temperature of the element on the disk radius.

Exact solutions of differential equations can be obtained only for a limited number of profiles. We use an approximate method of determining stresses in the disc - the finite difference method. Calculation of the disc using this method is based on the approximate solution of a system of differential equations by replacing differentials within them finite differences. To calculate the drive is divided into section. When selecting the calculated cross sections will comply with the following conditions:

$$\frac{R_n}{R_{n-1}} \leq 1.4 \dots 1.5; 0.8 \leq \frac{b_n}{b_{n-1}} \leq 1.2$$

Voltage σrl from the centrifugal forces of the blades and the joint part of the rim can be determined for the case where the blade and the disc are made of a material having the same density according to the formula:

$$\sigma_{Rl} = \frac{z \cdot \sigma_{PK} \cdot F + \rho \cdot f \cdot 2\pi \cdot R^2 \cdot \omega^2}{2\pi \cdot R \cdot b} \approx 22.76 MPa$$

Where R1 - a continuous outer radius of the disk rim; b1 - The width of the rim on the disc radius R1.

$h_r$ -height of blade root;  
 $R_{f2}$ - Gravity center of blade root;

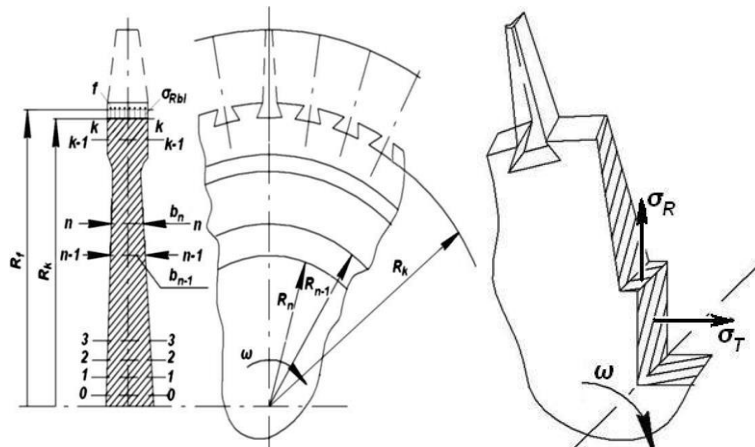


**Figure 2.4.1 – Scheme of disk analytical model**

### Computer calculation

The calculations were performed on a computer, as described in [4]. Calculations are performed in the program Disk exe.

## 2.4.4 Results of the analysis

**Table 2.4.1**—Initial data of computer calculation

Name of executor:	Mudassir Saiyed.. 240f gr.
Engine unit:	Compressor
Material:	VT-3
DISK PARAMETERS:	
Type of disc	
Sign of temperature variation on radius	not varied
Sign of corrected density variation on radius	not varied
Number of steps in width	
Numbers of radiiuses with steps in width	
LOADINGS	
Rotor rotation speed. rpm:	9382.8
Radial stress on a disc rim. MPa	22.76
PROPERTIES OF MATERIAL	
Density. kg/m <sup>3</sup>	4530

**Table 2.4.2**—Disk geometry and properties distribution

Section	Radius. m	Width. m	t. °C	E. MPa	α. 1/K	σ <sub>rr</sub> . Pa	ρ kg/m <sup>3</sup>
1	0.005	0.036	150	120000	0.0001	950000000	4530
2	0.0055	0.034	150	120000	0.0001	950000000	4530
3	0.006	0.032	150	120000	0.0001	950000000	4530
4	0.0065	0.03	150	120000	0.0001	950000000	4530
5	0.0075	0.028	150	120000	0.0001	950000000	4530
6	0.009	0.026	150	120000	0.0001	950000000	4530
7	0.01	0.024	150	120000	0.0001	950000000	4530
8	0.012	0.022	150	120000	0.0001	950000000	4530
9	0.018	0.02	150	120000	0.0001	950000000	4530
10	0.02	0.018	150	120000	0.0001	950000000	4530
11	0.025	0.016	150	120000	0.0001	950000000	4530
12	0.03	0.013	150	120000	0.0001	950000000	4530
13	0.04	0.011	150	120000	0.0001	950000000	4530
14	0.044	0.011	150	120000	0.0001	950000000	4530
15	0.05	0.011	150	120000	0.0001	950000000	4530
16	0.06	0.011	150	120000	0.0001	950000000	4530
17	0.072	0.011	150	120000	0.0001	950000000	4530
18	0.096	0.011	150	120000	0.0001	950000000	4530
19	0.132	0.011	150	120000	0.0001	950000000	4530
20	0.165	0.011	150	120000	0.0001	950000000	4530
21	0.2	0.0126	150	120000	0.0001	950000000	4530
22	0.22	0.0136	150	120000	0.0001	950000000	4530
23	0.245	0.01624	150	120000	0.0001	950000000	4530
24	0.27	0.01624	150	120000	0.0001	950000000	4530
25	0.333	0.01624	150	120000	0.0001	950000000	4530

**Table 2.4.3** –Results of disk strength calculation

Section	$\sigma_R$ , MPa	$\sigma_T$ , MPa	$\sigma_{eq}$ , MPa	K
1	0	319.293	319.293	2.9753
2	31.9178	287.3602	272.8053	3.4823
3	57.0048	264.6977	241.2993	3.937
4	77.8617	248.4546	220.1069	4.3161
5	109.2669	223.7576	193.7974	4.902
6	139.9157	203.1847	180.088	5.2752
7	157.6668	199.3712	182.1358	5.2159
8	179.0504	194.9431	187.5026	5.0666
9	202.8804	191.7618	197.5559	4.8088
10	221.7669	199.0338	211.3194	4.4956
11	240.2324	211.9617	227.4187	4.1773
12	279.0205	230.9485	258.3607	3.677
13	304.392	259.3911	284.5727	3.3383
14	299.1572	263.6708	283.0871	3.3559
15	293.0848	268.1399	281.4427	3.3755
16	285.6904	272.4072	279.2859	3.4015
17	279.57	274.0248	276.8391	3.4316
18	268.9048	273.2281	271.0923	3.5043
19	252.5775	266.2223	259.6689	3.6585
20	234.5567	256.3815	246.1957	3.8587
21	177.1336	233.1362	210.7903	4.5068
22	150.3072	217.808	193.1177	4.9193
23	103.3798	193.758	167.9253	5.6573
24	84.4481	176.0896	152.5405	6.2279
25	22.76	129.7852	120.0346	7.9144

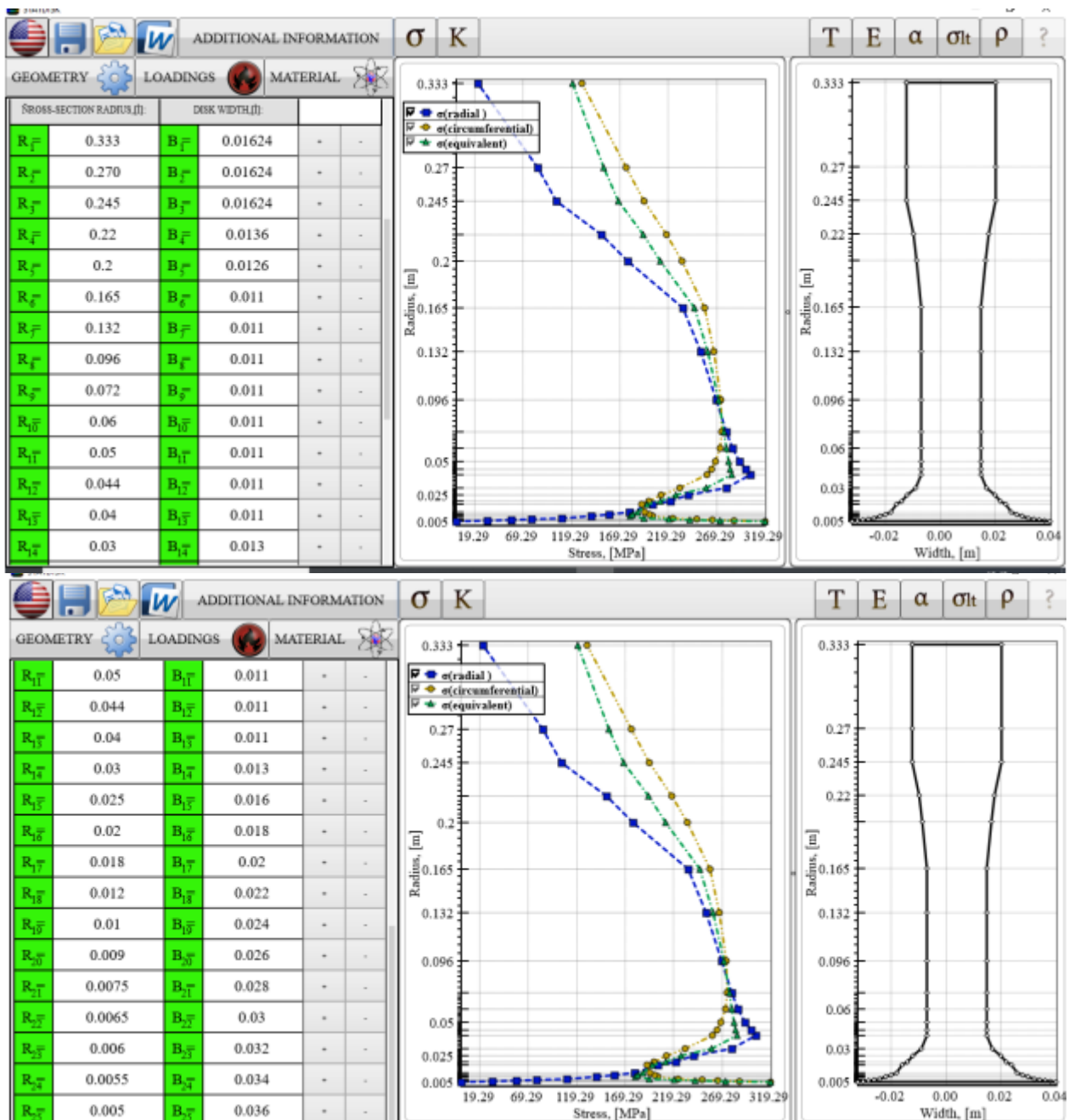


**Figure 2.4.2**—Total stresses dependent on section radius

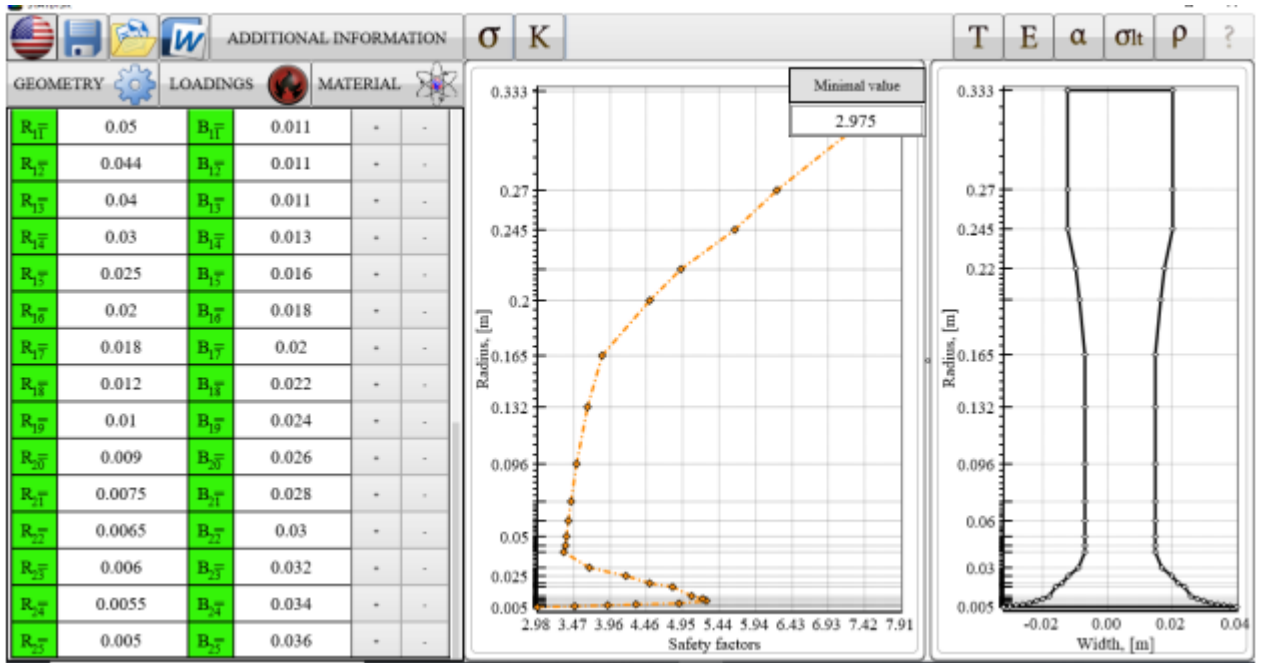


**Figure 2.4.3– Safety factors' dependent on section radius**

#### 2.4.5 Result

The calculation of the static strength of the disk of the seventh stage of the compressor. The results indicate that the values of safety margins in all sections conform to standards of safety. Shows the change in safety factor adjustment disk. The consequence of such very large values of the safety factors, as well as load balancing is an oversimplification of the true shape of the disc.

## **2.5 compressor blade oscillation analysis**

Calculation of dynamic oscillation frequency of compressor blades and building of frequency chart

When the engine operates, the air flow becomes non-uniform in the circumferential direction. The reason for this non-uniformity is the flow disturbance by the stationary vanes and struts when we consider the compressor blades.

Therefore, parameters of flow that streamlines rotor blades are periodical, thus causing periodical gas forces acting on the blades. This variation of gas forces generates blade bending oscillations. If the frequency of acting forces coincides with the blade natural frequency (Eigen frequency), then resonance condition will take place and the oscillation amplitude will increase that could breakdown the blade.

To avoid dangerous resonant conditions, it is necessary to change the blade natural frequency or to change the frequency of acting forces. Danger of resonance may be decreased by reducing the amplitude of oscillations. It can be done by lowering the acting forces or using special damping elements in the blade construction.

The preliminary analysis usually includes:

- The natural frequencies determination for the first blade shape mode;
- The dangerous harmonic estimation that initiate oscillation forces;
- The resonant modes determination.

### **The aim of the calculation**

The tasks of this analysis are to determine the blade natural frequency of the first bending mode (the first bending mode is the most dangerous), to plot the frequency diagram and to find the engine resonant operational mode.

### **Assumptions adopted in the calculation**

Assumption adopted in the calculation are;

- Blade is assumed to be fixed as a cantilever in the disk.
- Friction damping forces are neglected.

- Bending oscillations of the first shape mode are assumed to be the most dangerous.

### **Initial data**

To determine the frequency of the blade at different rotational speeds a 3D model of the blade is developed using the data from the previous calculations of blade profile. The developed model is shown in Fig.2.5.1.

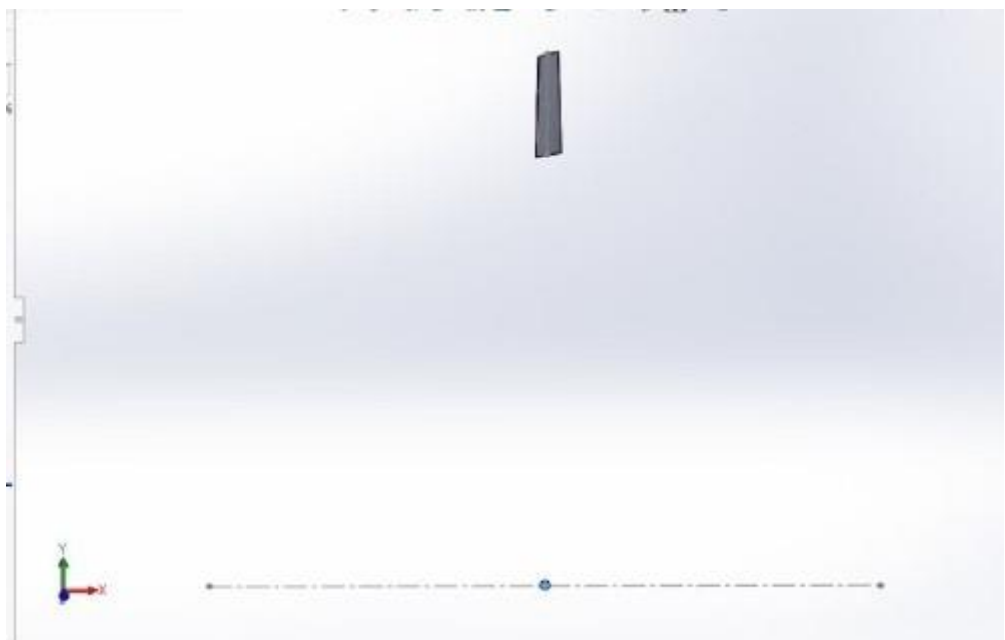


## Fig2.5.1.-Designmodeloftheblade

The following data is used to develop the frequency diagram:

- Maximum rotational speed of the rotor  $n_{max} = 9382.8 \text{ rpm} \approx 156.38 \text{ rps}$
- Idler rotational speed of the rotor  $n_{idle} = 0.6 \times n_{max} = 0.6 \times 156.38 \approx 93.828 \text{ rps}$

The rotational speeds are incremented through a range of ten values from 0 to  $n_{max}$ . These rotational speeds are then applied to the blade to calculate the dynamic frequency of the blade. The rotational speeds  $n_s$  are represented in the following section in Table 4.1.

-Exciting factors:

-Guide Vanes:

-Number of guide vanes  $K_2 = 92$

-Exciting frequency  $f_{e,IGV} = 92 * n_s \text{ rps}$

-Struts:

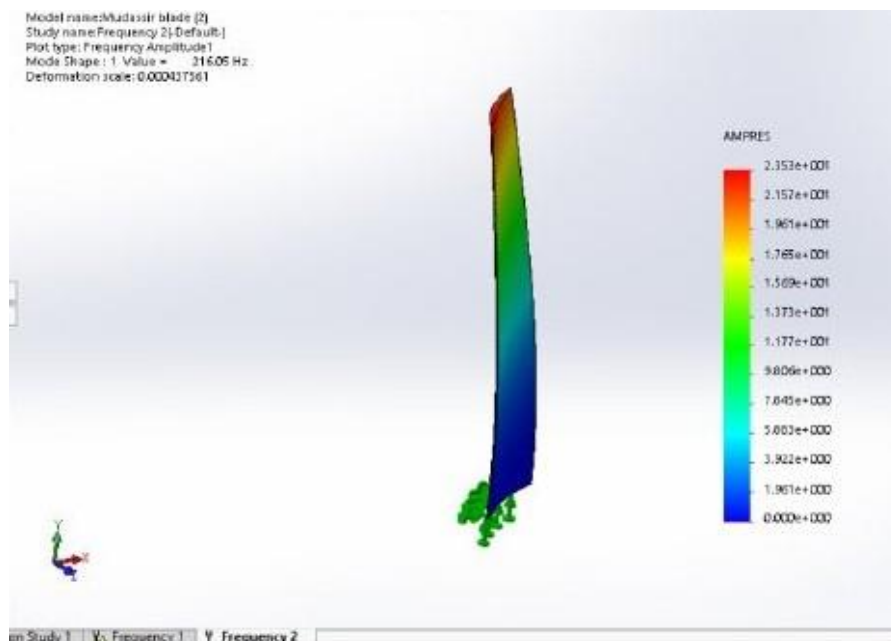
-Number of struts  $K_1 = 8$

-Exciting frequency  $f_{e,struts} = 8 * n_s \text{ rps}$

## Calculation

The 3D model is subjected to frequency analysis under the action of the varied range of rotational speeds. The analysis for natural frequency and dynamic frequency of the first value of  $n_s$  is shown in Fig. 2.5.2.

The obtained results are presented in Table 2.5.1. and the frequency diagram is created from the given data and presented in Fig. 4.3



Model name: Multisair blade (2)  
Study name: Frequency 21-Default  
Plot type: Frequency Amplitude  
Mode Shape : 1 Value = 216.05 Hz  
Deformation scale: 0.000407561

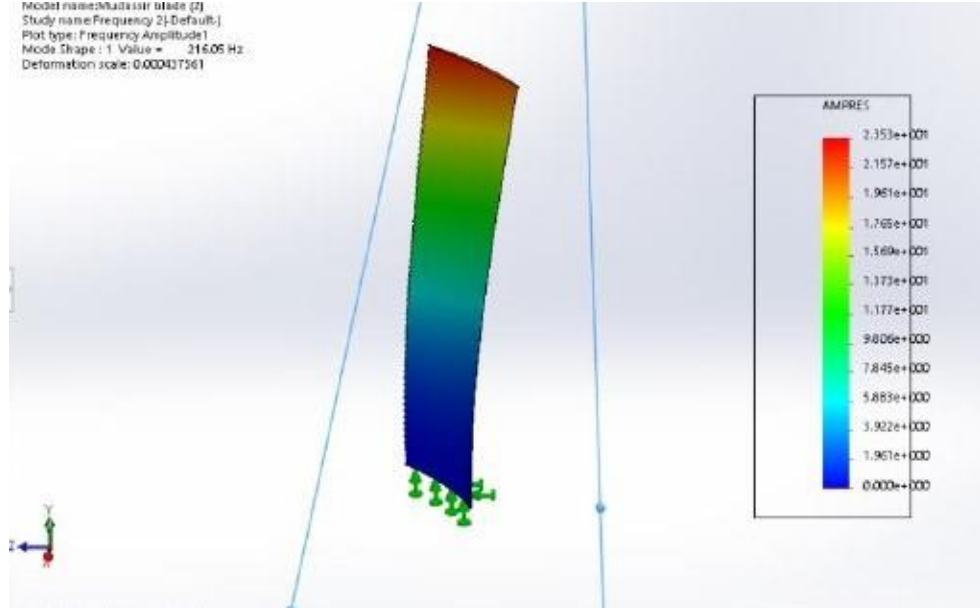


Fig 2.5.2.-Analysis of natural frequency

Calculated value of natural frequency is 338.6446 Hz. The dynamic frequencies are calculated and tabulated as follows;

Table 4.1

Q	ns(1/s)	fd(Hz)	fe2(Hz)	fe1(Hz )
1.868963 48	0	338.64 46	0	0
1.868387 22	15.6	341.66 58	1435.2	124.8
1.866328 24	31.3	350.57 05	2879.6	250.4
1.863116 74	46.9	364.92 08	4314.8	375.2
1.858724 59	62.6	384.09 55	5759.2	500.8
1.853152 04	78.2	407.39 97	7194.4	625.6
1.846920 73	93.8	434.15 31	8629.6	750.4
1.839893 34	109.5	463.74 22	10074	876
1.832111 12	125.1	495.64 27	11509.2	1000. 8
1.824081 9	140.7	529.42 09	12944.4	1125. 6
1.815682 17	156.4	564.72 48	14388.8	1251. 2

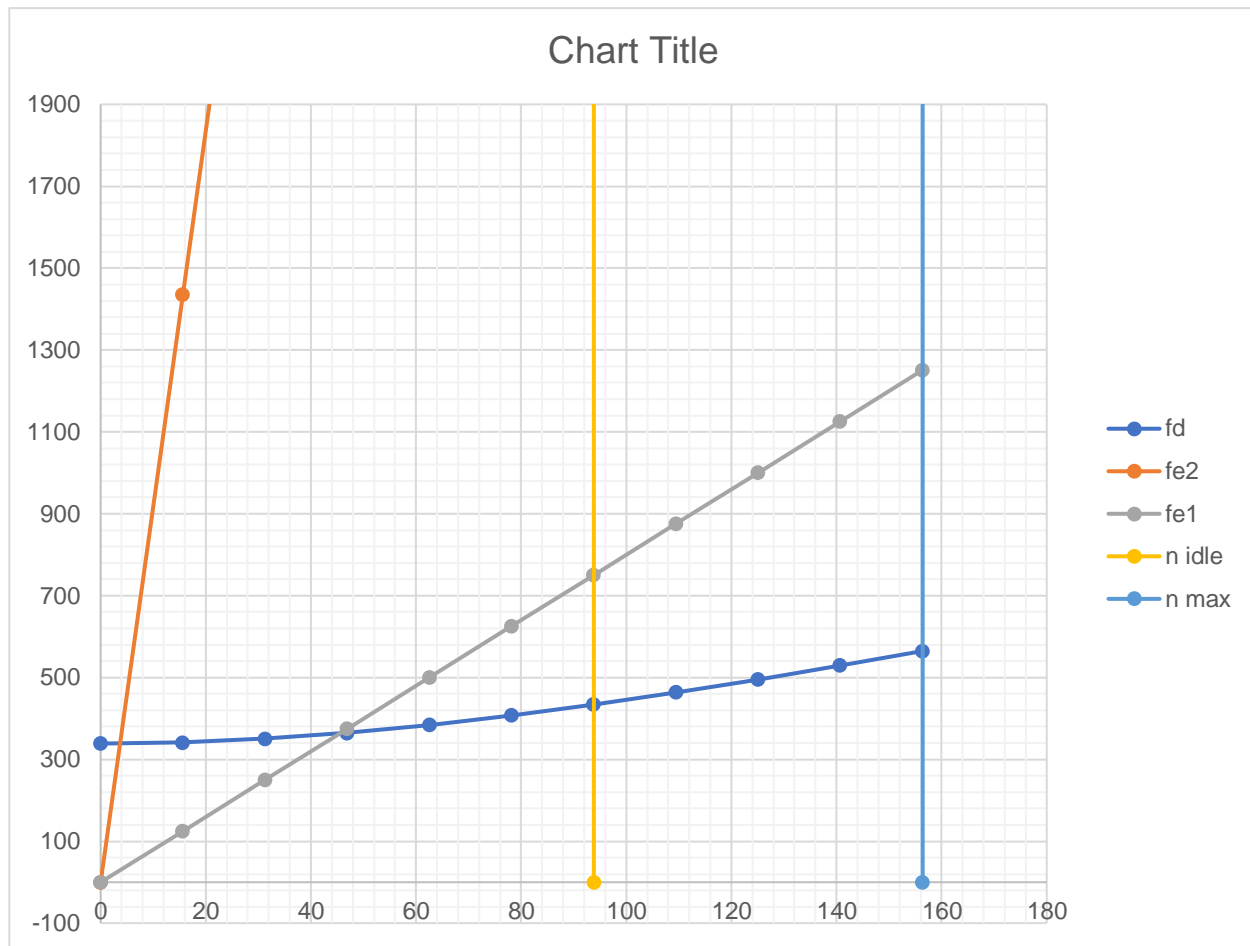


Fig.2.5.3.-Frequency diagram

### Conclusion

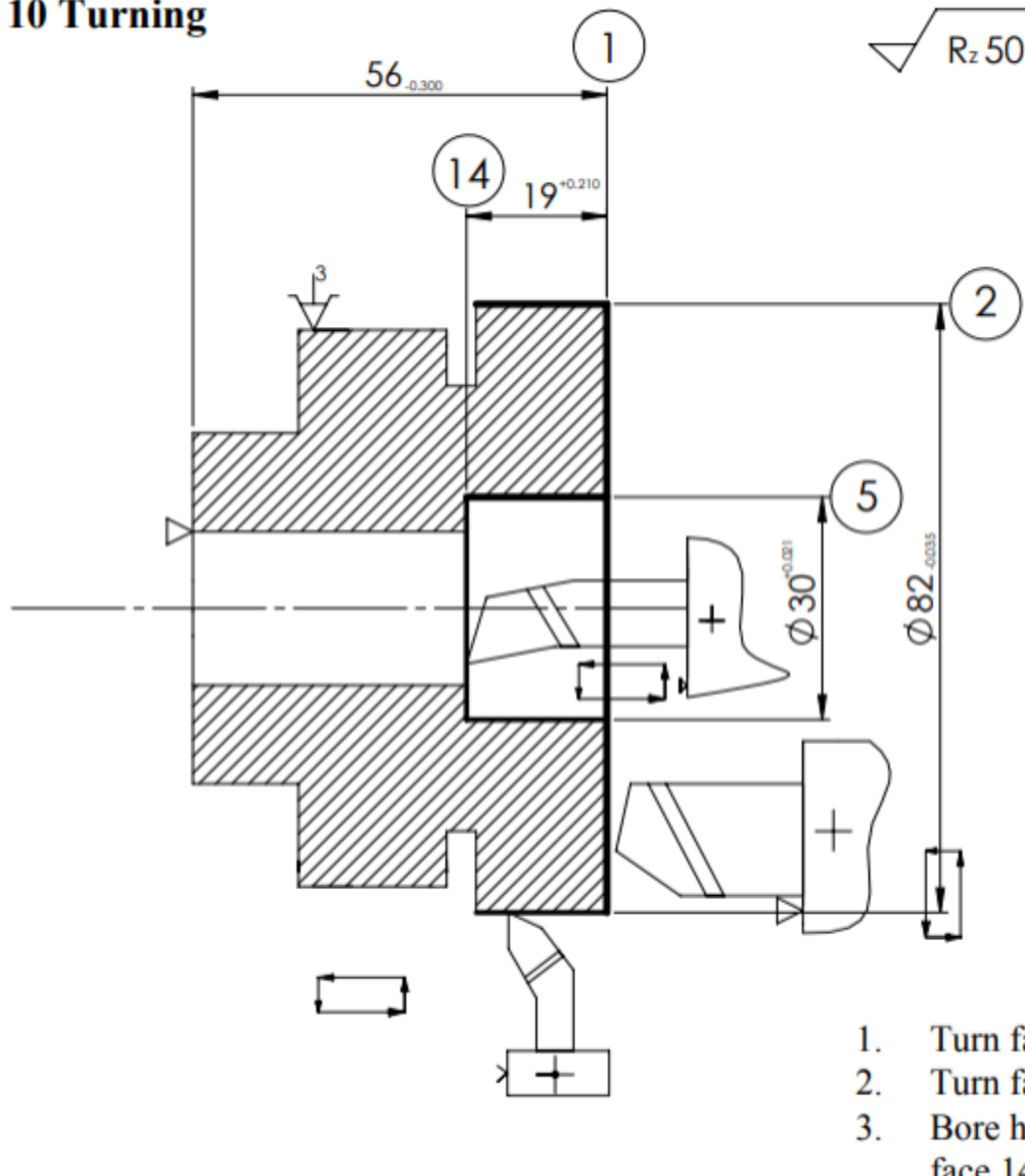
The natural frequency of the blade is 338.65Hz.

Resonances occur outside the operational range as seen in the frequency diagram presented in Fig.4.3. The resonance due to the presence of guide vanes occurs at  $n = 3.5$  rps and the resonance due to the presence of struts occurs at  $n = 45$  rps. Both of these lie outside the operational range of the engine

### **3. TECHNOLOGICAL PART**

### 3.1 Calculations of cutting conditions for turning operation

#### 10 Turning



Sketch of turning operation is shown in Fig. 3.1.1

##### 3.1.1. Identification of work material

The steel 38XH3MA (38XN3MA) according to the chemical composition is identified as belonging to the Group I (Heat-resistant chromium, chromium-nickel, chromium-molybdenum steels of perlitic, martensitic-ferritic and martensitic classes) according to the Appendix 1 [2].

### 3.1.2. Selection of design and geometric parameters of cutting tools

**Step 1 and Step 2** (surface 1 and surface 2):

According to the surface shape the selected tool is straight tuning tool GOST 18878-73: side cutting-edge angle  $\varphi = 45^\circ$  and end cutting-edge angle  $\varphi_1 = 15^\circ$  (Fig. 1.2) [3]. Other geometric parameters of cutting edge are selected from the recommendations in the book [2]. Parameters of the tool are submitted in the Table 1.1

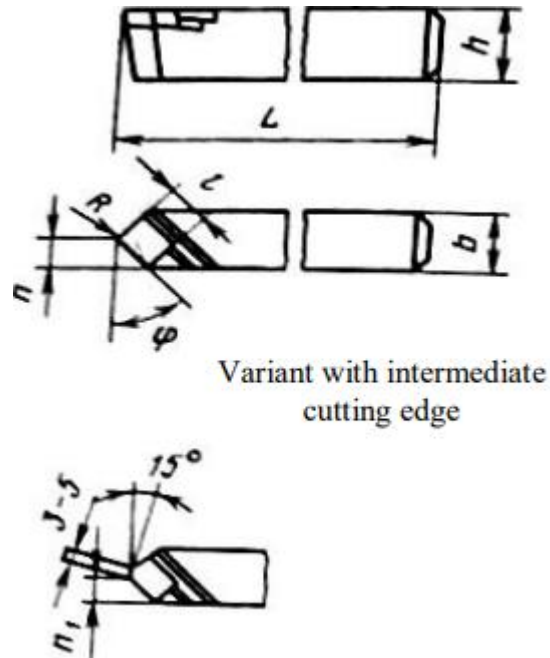


Figure 3.1.2 – Design of straight turning tool with cemented carbide tip  
 Table 3.1.1 – Parameters of the straight tuning tool (ref. Fig. 1.2 and Fig. 1.3)  
 for machining of face 2

<b><i>h</i></b>	<b><i>b</i></b>	<b><i>L</i></b>	<b><i>t</i></b>	<b><i>n</i></b>	<b><i>φ</i></b>	<b><i>φ<sub>1</sub></i></b>	<b><i>γ</i></b>	<b><i>α</i></b>	<b><i>γ<sub>1</sub></i></b>	<b><i>m*</i></b>	<b><i>r</i></b>
mm					degree					mm	
25	16	140	12	8	45	15	16	8	-2	0.3	1.0

**Step 2 (surface 2):**

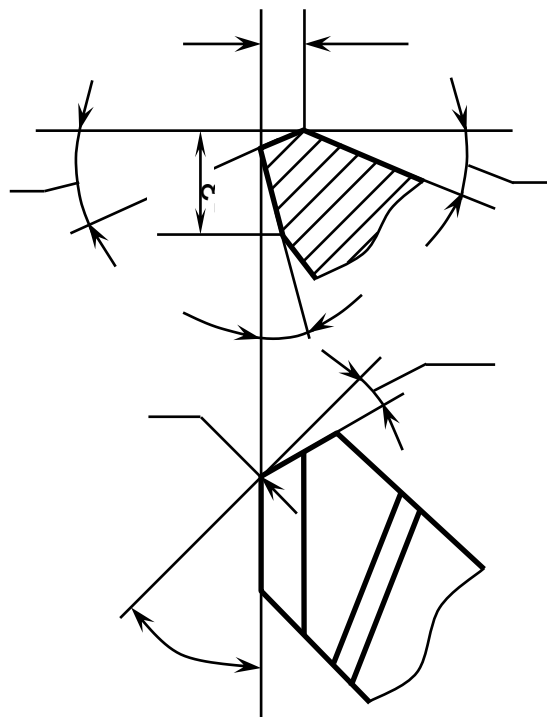


Figure 3.1.3. Geometric parameters of tool cutting point:  $\varphi$  – side cutting-edge angle;  $\varphi_1$  – end cutting-edge angle;  $\alpha$  – side relief angle;  $\gamma$  and  $\gamma_1$  – rake angles;  $r$  – nose radius;  $m^*$  – corrective margin

Turning and facing tool with cemented carbide tip is selected (Fig. 3.1.3) according to the configuration of surfaces 9 and 6 by GOST 1880-73 [3]:

- for surface 2:  $\varphi = 100^\circ$ ,  $\varphi_1 = 10^\circ$ ;

Geometric parameters are submitted in Table 3.1.2.

Table 3.1.2 – Parameters of the turning and facing tool (ref. Fig. 3.1.3)

Surface No.	<b>H</b>	<b>B</b>	<b>L</b>	<b>m</b>	<b>a</b>	<b>φ</b>	<b>φ<sub>1</sub></b>	<b>γ</b>	<b>α</b>	<b>γ<sub>1</sub></b>	<b>m<sup>*</sup></b>	<b>r</b>
	mm					degree					mm	
2	25	16	140	12	8	100	10	16	8	-2	0.3	1.0

### Step 3 (hole 5 and face 14):

Selected boring tool Design 1 (Fig. 1.5) is according to the GOST 1888-73 [3]:

- for hole 5:  $\varphi = 95^\circ$ ,  $\varphi_1 = 15^\circ$ ;
- for face 14:  $\varphi = 5^\circ$ ,  $\varphi_1 = 105^\circ$ .

Geometric parameters are submitted in Table 1.3.

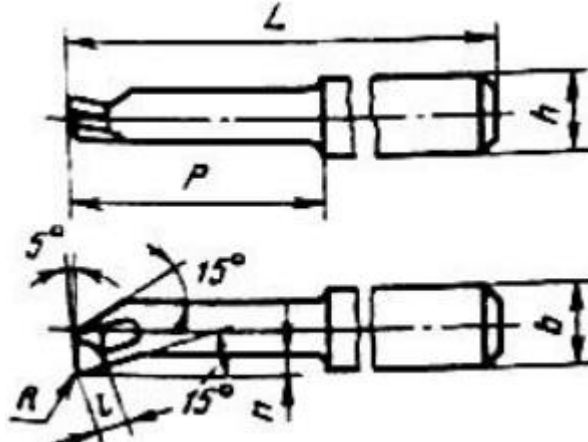


Figure 3.1.4 – Design of turning and facing tool with cemented carbide tip

Table 3.1.3 – Parameters of the boring tool (ref. Fig. 3.1.4 and Fig. 3.1.3)

Surface No.	<i>h</i>	<i>b</i>	<i>L</i>	<i>P</i>	<i>n</i>	<i>l</i>	$\varphi$	$\varphi_1$	$\gamma$	$\alpha$	$\gamma_1$	<i>m*</i>	<i>r</i>
	mm						degree				mm		
5	16	16	170	60	4.5	8	95	15	16	8	-2	0.3	1.0
14	16	16	170	60	4.5	8	5	105	16	8	-2	0.3	1.0

### 3.1.3. Selection of cutting tool material and cutting fluid

According to the recommendations cemented carbide T5K10 is selected for the cutting points of all tools applied in this rough-machining operation (see Table 1.2 in [2]).

According to the recommendations for the materials of Group I the 5-% emulsion from Укринол-1 (Ukrinol-1) emulsol is selected as a cutting fluid for all manufacturing steps.

### 3.1.4. Specifying the depth of cut

The depths of cut *t* for each surface are determined from previous calculations results [1]:

- for faces 1 and 14:  $t = Z_{max}$ ;
- for round surfaces 2 and 5:  $t = 2Z_{max} / 2$ .

Here the  $Z_{max}$  values are selected from the Table 4.5 of book [1] and the  $2Z_{max}$  values – from the Table 4.6. The *t* values are submitted in the Table 1.4.

Table 3.1.4 – Depths of cut in manufacturing steps

Step No.	1	2	3	
Surface No.	1	2	5	
$t$ , mm	1.960	1.925	1.725	
Reference [1]	$Z_{2max}$ , Fig. 4.7, Table 4.5	$2Z_{max}$ , Table 4.6	$Z_{max}$ , Table 4.6	$Z_{10max}$ , Table 4.6

### 3.1.5. Calculation of feed value

Calculated values of feed are determined from the formula

$$f_c = \frac{\sqrt{R_{zi} \cdot 8r}}{k_R}, \text{ mm/rev},$$

where  $r$  – tool nose radius, mm;  $k_R$  – total correction coefficient (for the most of operations could be adopted as  $k_R = 2$ );  $R_z$  – roughness to be obtained after the operation ( $R_z \approx 4 \cdot R_a$ ), mm.

Results of calculations and correction coefficient  $k_s$  [2] for boring steps are submitted in the Table 3.1.5.

Table 3.1.5 – Results of feed calculations

Step No.	1	2	3
Surface No.	1	2	5
$f_c$ , mm/rev	0.316	0.316	0.316
$k_s$	–	–	0.4
Corrected $f_c$ , mm/rev	0.316	0.316	0.126

### 3.1.6. Express calculations of cutting velocity, tangential constituent of cutting force and machine power

Express calculations are performed according to the following formulas:

- 1) Values of cutting velocity  $V_c$ , m/min, are calculated from two formulas for variant A (material group I):

$$V_c = \frac{C'_V}{T^{0.35} t^{0.15} f^{0.15}} k_V \text{ at feed value } 0.07 \leq f \leq 0.20 \text{ mm/rev}$$

$$\text{and } V_c = \frac{C''_V}{T^{0.35} t^{0.15} f^{0.45}} k_V, \text{ when } f > 0.20 \text{ mm/rev.}$$

Correction coefficients  $k_V$  are selected from the Paragraph 1.9 [2] and submitted in

the Table 3.1.6.

Table 3.1.6 – Correction coefficients values

Step/Surface No.	$k_{TV}$	$k_{MV}$	$k_{IV}$	$k_{rV}$	$k_{\phi V}$	$k_{\phi IV}$	$k_{cfV}$	$k_{bV}$	$k_{crV}$	$k_{gpV}$	$k_{gfV}$	$k_V$
1/1	1.00	0.75	0.60	1.00	1.00	1.00	1.00	1.00	1.20	1.00	1.00	0.54
2/2	1.00	0.75	0.60	1.00	0.80	1.00	1.00	1.00	1.00	1.00	1.00	0.360
3/5	1.00	0.75	0.60	1.00	0.81	1.00	1.00	0.80	1.00	1.00	1.00	0.292
3/14	1.00	0.75	0.60	1.00	1.61	0.80	1.00	0.80	1.00	1.00	1.00	0.461

Selected value of tool life  $T = 60$  min. (ref. Paragraph 1.9.3 [2]).

Coefficients  $C'_V$  and  $C''_V$  are selected from the Table 3.1.5 [2].

2) Tangential constituent of cutting force  $P_z$  for variant A (groups I–IV):

$$P_z = C_p V_c^{-0.15} t^{0.95} f_c^{0.75}.$$

Coefficient  $C_p$  is selected from the Table 1.5 [2].

3) Machine power  $N_{emc}$ :

Effective power for cutting process, kW

$$N_e = \frac{P_z V_c}{60 \cdot 1000};$$

Power of electric motor, kW

$$N_{emc} = \frac{N_e}{\eta_m},$$

where  $\eta_m = 0.8$  – efficiency index of turning machine.

Initial data and results of calculations for all steps of manufacturing operation are written into the Table 3.1.7.

Table 3.1.7 – Initial data and results of calculations for  $V_c$ ,  $P_z$  and  $N_{emc}$

Step/ Sur- face No.	$C'_V$	$C''_V$	$C_P$	$t_c$ , mm	$f_c$ , mm/rev	$T$ , min	$V_c$ , m/min	$P_z$ , N	$N_e$ , kW	$N_{emc}$ , kW
1/1	700	430	3750	1.650	0.316	60	86.30	1303.17	1.87	2.34
2/2				1.925	0.316	60	56.22	1608.87	1.5	1.87
3/5				1.725	0.126	60	70.12	703.70	0.8	1.0
3/14				3.850	0.126	60	52.72	1574.73	1.38	1.73

### 3.1.7. Selection of turning machine

The lathe is selected according to the power of electric motor, accuracy of machine and its geometric parameters (Table 3.1.8).

Table 3.1.8 – Technical data of the selected turning machine **16K20** (16K20)

Parameter	Units	Value
1. Sizes of work zone		
Maximal diameter of workpiece: over bed	mm	
over carriage		400
Maximal diameter of round bar fits to spindle hole		220
Maximal length of workpiece		53
Maximal travel of carriage: lengthwise / crosswise		710; 1000
		645–1935 / 300
2. Carriage feed, longitudinal (min – max)	mm/rev	0.05–2.8
2.1. Series of longitudinal feeds	mm/rev	0.050; 0.060; 0.071; 0.085; 0.101; 0.120; 0.143; 0.170; 0.203; 0.242; 0.288; 0.343; 0.408; 0.486; 0.580; 0.690; 0.822; 0.980; 1.167; 1.390; 1.656; 1.973; 2.350; 2.800
3. Carriage feed, cross-feed	mm/rev	0.025–1.4

(min – max)		
3.1 Series of cross-feeds	mm/rev	0.025; 0.030; 0.035; 0.042; 0.050; 0.060; 0.071; 0.085; 0.101; 0.121; 0.144; 0.171; 0.204; 0.243; 0.290; 0.345; 0.411; 0.490; 0.584; 0.695; 0.828; 0.987; 1.175; 1.400
4. Number of feeds' steps	–	24
5. Rotation speed of spindle (min – max)	rev/min	12.5–1600
5.1 Series of spindle speeds	rev/min	12.5; 15.7; 19.8; 25; 31.5; 40; 50; 63; 80; 100; 126; 159; 200; 252; 317; 400; 504; 635; 800; 1008; 1270; 1600
6. Number of spindle speeds	–	22
7. Power of main electric motor	kW	11

### 3.1.8. Agreement of feed value with technical data of turning machine

Machine's feed  $f_m$  are selected from machine's reference data for all manufacturing steps in relation to the calculated feeds with smaller, equal or exceeding value not more than 5 %. Results are submitted in Table 3.1.9.

Table 3.1.9 – Selected feed values according to the machine's data

Step/surf. No.	1/1	2/2	3/5	3/14
Type of feed	Cross	Traverse	Cross	Traverse
$f_c$ , mm/rev	0.316	0.316	0.126	0.126
$f_m$ , mm/rev	0.290	0.288	0.120	0.121

### 3.1.9. Calculation of cutting velocity

For turning the workpieces from heat-resistant, rust-resisting and high-temperature steels with tools with tips of cemented carbides T5K10 cutting velocity is calculated from the formulas with selected values of feed:

$$V_c = \frac{C'_V}{T^{0.35} t^{0.15} f^{0.15}} k_V \text{ m/min at feed value } 0.07 \leq f \leq 0.20 \text{ mm/rev}$$

$$\text{and } V_c = \frac{C''_V}{T^{0.35} t^{0.15} f^{0.45}} k_V \text{ m/min, when } f > 0.20 \text{ mm/rev.}$$

Results are submitted in the Table 3.1.10.

Table 3.1.10– Cutting speed values calculated with selected machine's feeds

Step/surf. No.	1/1	2/2	3/5	3/14
$V_c$ , m/min	86.30	56.22	70.12	52.72

### 3.1.10. Calculation of rotational speed of workpiece

Calculated rotational speed of workpiece (of machine's spindle) is derived from

$$n_c = \frac{1000 \cdot V_c}{\pi \cdot D}, \text{ rev/min,}$$

where  $D$  – diameter of work surface, mm (external diameter for straight turning; hole diameter for straight boring; maximum diameter of face for turning with cross feed).

Calculations results are submitted in the Table 1.10.

### 3.1.11. Agreement of rotational speed value with technical data of turning machine

Machine's values  $n_m$  are selected from machine's reference data for all manufacturing steps in relation to the calculated speeds with smaller, equal or exceeding value not more than 5 %. Results are submitted in the Table 1.10.

Table 3.1.11 – Calculated an selected rotational speed values according to the machine's data

Step/surf. No.	1/1	2/2	3/5	3/14
$D$ , mm	30	30	82	82
$n_c$ , rev/min	916.14	596.8	272.33	204.75
$n_m$ , rev/min	1008	504	252	200

### **3.1.12. Determination of actual cutting velocity**

Actual cutting velocity is derived from formula

$$V_a = \frac{\pi \cdot D \cdot n_m}{1000}, \text{ m/min.}$$

Results of calculations are written in the Table 3.1.12.

### **3.1.13. Calculations of constituents of cutting forces**

For turning the workpieces from rust-resisting and high-temperature steels of group I the tangential force is calculated from:

$$P_z = C_p V_a^{-0.15} t^{0.95} f_m^{0.75}, \text{ N.}$$

Results of calculations are written in the Table 3.1.12.

### **3.1.14. Calculation of torque**

Cutting moment is calculated from the formula

$$M_c = \frac{P_z D}{2000}, \text{ Nm.}$$

Results of calculations are written in the Table 3.1.12.

### **3.1.15. Calculation of machine drive power**

Power consumed by cutting

$$N_e = \frac{P_z V_a}{60 \cdot 1000}, \text{ kW.}$$

Power of electric motor necessary for cutting with a machine's efficiency coefficient ( $\eta_m = 0.7 \dots 0.8$ )

$$N_{emc} = \frac{N_e}{\eta_m}, \text{ kW.}$$

Results of calculations are written in the Table 3.1.12.

Table 3.1.12 – Calculated and actual cutting conditions of all manufacturing steps

Step/ Surface No.	$t$ , mm	$f_m$ , mm/rev	$V_c$ , m/min	$n_c$ , rev/min	$n_m$ , rev/min	$V_a$ , m/min	$P_z$ , N	$M_c$ , Nm	$N_{emc}$ , kW
1/1	1.650	0.290	86.30	916.14	1008	95.0	1204	18.06	2.4
2/2	1.925	0.288	56.22	596.8	504	47.5	1539	23.08	1.5
3/5	1.725	0.120	70.12	272.33	252	64.9	686	28.13	0.92
3/14	3.850	0.121	52.72	204.75	200	51.5	1533	62.85	1.64

## Conclusion

The calculated and assigned parameters for turning operation will ensure reliable and effective cutting process during 1 hour and producing the quality products.

### 3.2 Calculations of cutting conditions for drilling operation

Drilling operation 35 (ref. [1], Fig. 4.10, Tables 4.3 and 4.6) includes two manufacturing steps (Fig. 2.1). Drilling step is performed in solid material with 14-th accuracy grade and roughness no more than  $Rz50$  at the depth 10.4 mm:  $[A_{3max}] ++ [Z_{8max}] = 10.0 + 0.407 \approx 10.4$  mm (ref. [1], Fig. 4.7 and Table 4.6)

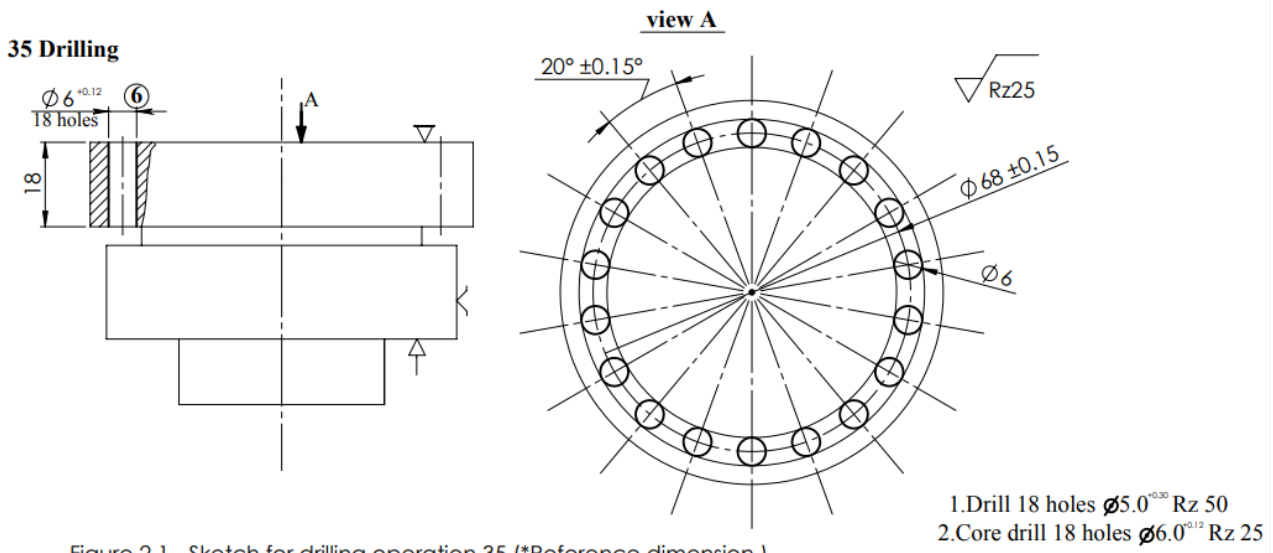


Figure 2.1 - Sketch for drilling operation 35 (\*Reference dimension.)

**Figure 3.2.1-** Sketch for drilling operation 35

#### 3.2.1 Selection of geometric parameters and tool material of drill

Drilling of solid workpieces from heat-resistant steel **38XH3MA (38HN3MA)** (group I) is recommended to perform with standard drill from high-speed steel P6M5K5 (ref. [2], Table 1.2) with shortened body (up to 10 diameters) according to the geometric configuration of the workpiece.

Geometric parameters of selected standard drill [3] with taper shank are submitted in Fig. 2.2, Fig. 2.3 and Table 2.1. Work end angles are selected according to the

recommendations [2, 3].

**Table 3.2.1** – Geometric parameters of twist drill according to GOST 10903-77

<b>d</b>	<b>L</b>	<b>l</b>	Web		<b>2φ</b>	<b>γ</b>	<b>α</b>	<b>ψ</b>
			<b>w</b>	<b>l</b>				
mm								
5	138	57	1.5	2.5	118 ° ± 2°	–	12	40–60
6	138	57	1.5	2.5	118 ° ± 2°	–	12	40–60

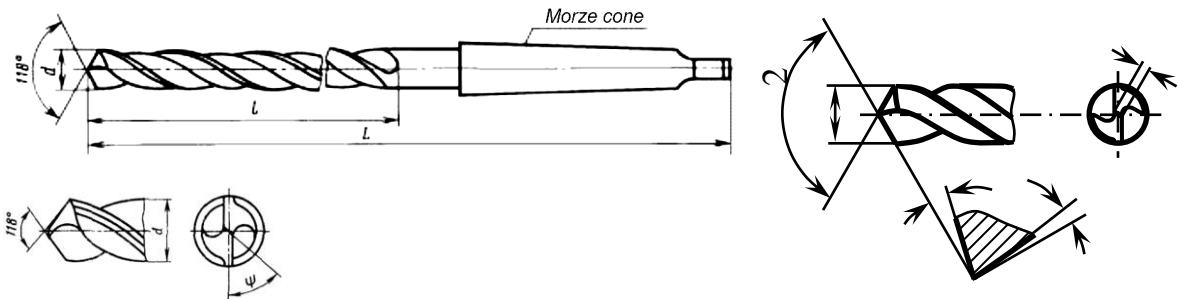


**Figure 3.2.2** – Sketch of the twist drill with taper shank according to GOST 10903-77

At drilling of diameters larger than 3 mm water emulsions are applied as cutting fluids: 1–5-% emulsion from Ukrinol-1 emulsol.

### 3.2.2 Calculation of cut depth

For a diameter of a drill 5mm

$$t = D/2 = 5 / 2 = 2.5 \text{ mm.}$$

For a diameter of a core drill 6mm

$$t = D/2 = 6 / 2 = 3 \text{ mm.}$$

### 3.2.3 Specifying the feed

Recommended feed for machining of hole in solid material with drill from high-speed steels is selected from Table 2.2 [2]  $f_c' = 0.15 \text{ mm/rev}$  (average value accepted).

The ratio of depth **l** to diameter **D** is  $l / D = 18 / 5 \approx 3.6$  (ref. Fig. 2.1).

Correction coefficient for deep drilling according to  $l / D > 3$  is  $k_{ls} = 0.9$ , therefore

$$f_c = f_c' \times k_{ls} = 0.135 \text{ mm/rev.}$$

The ratio of depth **l** to diameter **D** is  $l / D = 18 / 6 = 3$  (ref. Fig. 2.1).

Correction coefficient for deep drilling according to  $l / D = 3$  is  $k_{ls} = 1$ , therefore

$$f_c = f_c' \times k_{ls} = 0.15 \text{ mm/rev.}$$

### 3.2.4 Express calculation of cutting velocity, torque and machine power

1) Cutting velocity  $V_c$  is calculated from the formula from technological recommendation for the given drilling diameter  $D$  according to the selected feed  $f_c$ , recommended drill life  $T$ , coefficients  $C_V$  and  $k_V$

- $T = 12 \text{ min.}$
- $C_V = 1.07.$
- Total cutting-velocity correction coefficient  $k_V$  (shown in Table 3.20).

**Table 3.20 – Particular correction coefficients**

Coefficient	$k_{TV}$	$k_{MV}$	$k_{IV}$	$k_{cfV}$	$k_V$
Value	0.9	1.0	1.0	1.0	0.9

Calculated cutting velocity from formula (3.57)

$$V_c = \frac{C_V D^{0.75}}{T^{0.25} f^{0.85}} k_V = 9.49 \text{ m/min. } (D=5\text{mm})$$

$$V_c = \frac{C_V D^{0.75}}{T^{0.25} f^{0.85}} k_V = 9.95 \text{ m/min. } (D=6\text{mm}) \quad (3.57)$$

2) Torque  $M_c$  from Para 2.12 with the same  $D$  and  $f_c$  values and obtained  $V_c$  from formula (3.58)

$$M_c = C_M V_c^{-0.15} D^{1.9} f_c^{0.8} = 244.8 \text{ N}\cdot\text{cm} \quad (D=5\text{mm}) \quad (3.58)$$

$$M_c = C_M V_c^{-0.15} D^{1.9} f_c^{0.8} = 373.92 \text{ N}\cdot\text{cm} \quad (D=6\text{mm})$$

Where  $C_M = 80$ ;

3) Machine's power  $N_{emc}$  from Para 2.13 with the  $D$  value and obtained  $V_c$  and  $M_c$  from formula (3.59)

$$N_e = \frac{M_c V_c}{3000 D} = 0.155 \text{ kW. } (D=5\text{mm}) \quad (3.59)$$

$$N_e = \frac{M_c V_c}{3000 D} = 0.2067 \text{ Kw. } (D=6\text{mm})$$

Power of electric motor necessary for cutting is determined with a machine's efficiency coefficient ( $\eta_m = 0.75$  accepted) from formula (3.60)

$$N_{emn} = \frac{N_e}{\eta_m} = 0.207 \text{ kW. } (D=5\text{mm})$$

$$N_{emn} = \frac{N_e}{\eta_m} = 0.276 \text{ kW. } (D=6\text{mm}) \quad (3.60)$$

### 3.2.5 Selection of machine

Selection of machine is performed in similar manner to turning. First of all power of machine, geometric sizes of work zone and range of feeds are taken into account. Series of rotational speeds and feeds are calculated and submitted in Table 3.21.

**Table 3.21** – Technical data of selected machine

Name and type of machine <b>2H125 (2N125)</b>	Unit	Value
Sizes of work zone: - Work surface of table - Maximal distance between spindle face and work surface of table - Maximal stroke of spindle - Maximal vertical stroke of: - Spindle - Table	mm	400×450 700 200 170 270
Minimal and maximal values of spindle rotational speed	rev/min	45–2000
Number of rotational speed steps	–	12
Series (row) of spindle speeds	rev/min	45, 63, 90, 126, 178, 252, 356, 503, 710, 1003, 1416, 2000
Minimal and maximal values of feed	mm/rev	0.1–1.6
Number of feeds' steps	–	9
Sequence (row) of feeds	mm/rev	0.1, 0.14, 0.2, 0.28, 0.4, 0.56, 0.8, 1.13, 1.6
Power of drive $N_{ems}$	kW	2.2

### 3.2.6 Agreement of feed value with technical data of drilling machine

According to the selected value  $f_c = 0.135$  mm/rev and recommendation, the machine's value  $f_m$  is selected.

$$f_m = 0.14 \text{ mm/rev} \quad (\text{D}=5\text{mm and D}=6) \quad (3.61)$$

### 3.2.7 Calculation of cutting velocity

Calculations are performed with the selected machine value of feed and the same other parameters:

- $T = 12 \text{ min.}$
- $C_V = 1.07;$
- Total cutting-velocity correction coefficient  $k_V = 0.9.$

Cutting velocity is calculated by formula (3.62)

$$V_c = \frac{C_V D^{0.75}}{T^{0.25} f_m^{0.85}} k_V = 9.2 \text{ m/min.} \quad (D=5\text{mm}) \quad (3.62)$$

$$V_c = \frac{C_V D^{0.75}}{T^{0.25} f_m^{0.85}} k_V = 10.55 \text{ m/min} \quad (D=6\text{mm})$$

### 3.2.8 Calculation of drill rotational speed

Drill machine rotational speed is calculated by formula (3.63)

$$n_c = \frac{1000 V_c}{\pi \cdot D} = 585.99 \text{ rev/min} \quad (D=5\text{mm}) \quad (3.63)$$

$$n_c = \frac{1000 V_c}{\pi \cdot D} = 559.98 \text{ rev/min} \quad (D=6\text{mm})$$

### 3.2.9 Agreement of rotational speed value with technical data of drilling machine

According to the calculated value  $n_c$  and recommendations, the machine's value  $n_m$  is selected from formula (3.64)

$$n_m = 503 \text{ rev/min.} \quad (D=5\text{mm and } D=6) \quad (3.64)$$

### 3.2.10 Determination of actual cutting velocity

from formula (3.65)

$$V_a = \frac{\pi D n_m}{1000} = 7.9 \text{ m/min.} \quad (D=5\text{mm}) \quad (3.65)$$

$$V_a = \frac{\pi D n_m}{1000} = 9.5 \text{ m/min} \quad (D=6\text{mm})$$

### 3.2.11 Calculation of axial cutting force

For all groups of hard-to-machine materials, when machining with drills from high-speed steels, the axial cutting force is derived from formula (3.66)

$$P_o = C_P \times D \times f_m^{0.7} = 1388.84 \text{ N.} \quad (D=5\text{mm}) \quad (3.66)$$

$$P_o = C_P \times D \times f_m^{0.7} = 1666.61 \text{ N} \quad (D=6\text{mm})$$

Value of coefficient  $C_P = 1100$  for workpiece material of group I.

### 3.2.12 Calculation of torque

For all groups of hard-to-machine materials, when machining with drills from high-speed steels, the torque is calculated by formula (3.67)

$$M_c = C_M V_a^{-0.15} D^{1.9} f_m^{0.8} = 259.05 \text{ N}\cdot\text{cm.} \quad (D=5\text{mm})$$

$$M_c = C_M V_a^{-0.15} D^{1.9} f_m^{0.8} = 356.3 \text{ N}\cdot\text{cm} \quad (D=6\text{mm}) \quad (3.67)$$

Values of coefficient  $C_M = 80$  for workpiece materials of group I.

### 3.2.13 Calculation of required machine's drive power

Power consumed by cutting process (effective power) from formula (3.68)

$$N_e = \frac{M_c V_a}{3000 D} = 0.136 \text{ kW.} \quad (D=5\text{mm}) \quad (3.68)$$

$$N_e = \frac{M_c V_a}{3000 D} = 0.188 \text{ kW} \quad (\text{D}=6\text{mm})$$

Power of electric motor necessary for cutting is determined with machine's efficiency coefficient ( $\eta_m = 0.75$ ) from formula (3.69)

$$N_{em\tilde{n}} = \frac{N_e}{\eta_m} = 0.181 \text{ kW} \quad (\text{D}=5\text{mm}) \quad (3.69)$$

$$N_{em\tilde{n}} = \frac{N_e}{\eta_m} = 0.251 \text{ kW} \quad (\text{D}=6\text{mm})$$

Final results of calculations are submitted in Table 3.22.

**Table 3.22 – Final parameters of cutting conditions for drilling operation**

No. of	$t_c$ ,	$f_m$ ,	$V_c$ ,	$n_c$ ,	$n_m$ ,	$V_a$ ,	$P_o$ ,	$M_c$ ,	$N_{emc}$ ,
manufacturing step	mm	mm/rev	m/min	rev/min	rev/min	m/min	N	N·cm	kW
1 – drilling	2.5	0.14	9.2	585.99	503	7.9	1388.8 4	259.05	0.181
1 – core drilling	3	0.14	10.55	559.98	503	9.5	1666.6 1	356.3	0.251

### 3.2.14 Check of selected parameters of cutting conditions

Machine's torque: from formula (3.70)

$$M_m = 955000 \frac{N_{ems} \cdot \eta_m}{n_m} = 3132.7 \text{ N}\cdot\text{cm}, \quad (3.70)$$

where  $N_{ems} = 2.2 \text{ kW}$ .

$$N_{ems} \geq N_{emc}: \quad 2.2 \text{ kW} > 0.251 \text{ kW} > 0.181 \text{ kW}$$

$$M_m \geq M_c: \quad 4426.26 \text{ N}\cdot\text{cm} > 356.3 \text{ N}\cdot\text{cm} > 259.05 \text{ N}\cdot\text{cm}.$$

Thus, the above conditions are observed.

### 3.3 Calculations of cutting conditions for milling operation

Sketch of milling operation is shown in Figure 3.1 (see book [1], Fig. 4.10, page 116). Workpiece material is high-quality steel **38XH3MA** (38HN3MA) in normalised condition with HB 269 and  $\sigma_u = 930$  MPa.

#### 40 Milling

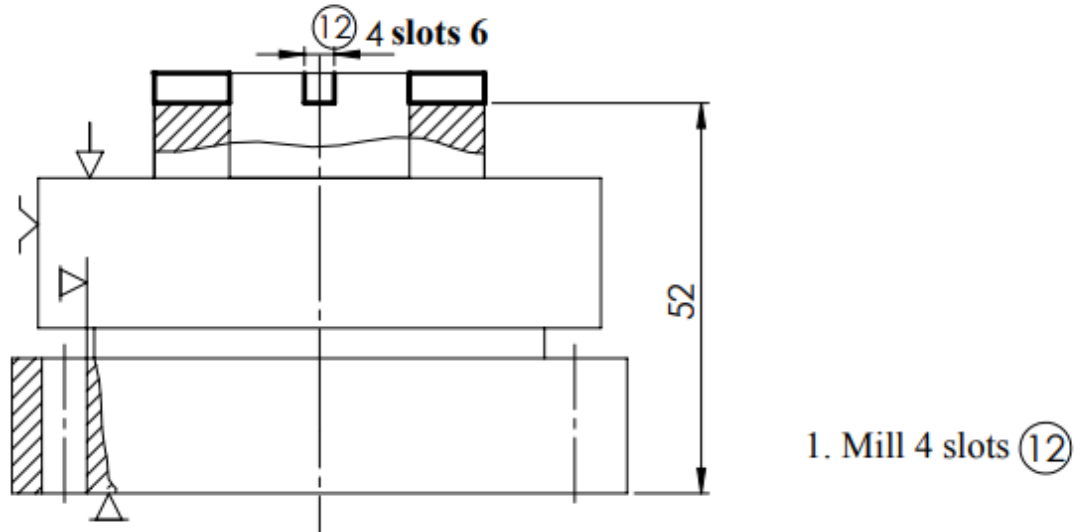
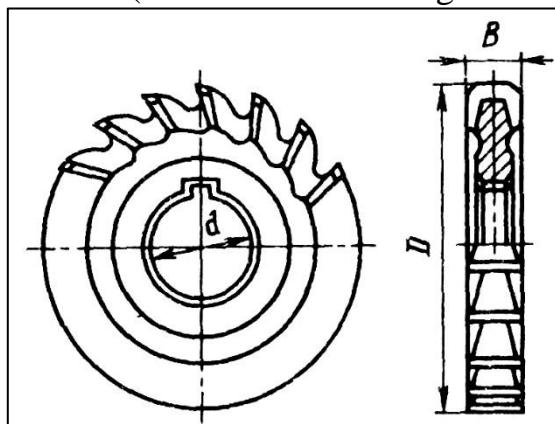


Figure 3.1 – Sketch for milling operation

*Figure 3.15* – Sketch for milling operation

#### 3.3.1 Selection of diagram and cutter for milling operation

Diagram for machining in the milling operation 40 is selected from Figure 3.15 with application of slotting mill. Geometric configuration of machined piece allows application of disk-type slotting cutter (GOST 3755-78) of the larger diameter  $D$  for the specified width of slot  $B = 7$  mm (the Sketch of milling cutter is shown in Figure 3.16).



*Figure 3.16* – Sketch of disk-type slotting milling cutter

Parameters of the selected milling cutter are:

- External diameter  $D = 50$  mm by j<sub>s</sub>16;
- Internal diameter  $d = 16$  mm by H7;
- Width  $B = 4$  mm by H9 selected;
- Number of teeth  $z = 14$ ;
  - Milling cutter material is P6M5(R6M5) selected according to the type of milling operation and selected configuration of milling cutter for structural carbon steel as the nearest to the workpiece material.

### 3.3.2 Depth and width of milling

According to the diagram and Figure 3.15 the parameters are:

- depth of milling  $t = 4$  mm;
- width of milling  $B = 4$  mm.

### 3.3.3 Feed

Feed per tooth  $f_z$  is selected according to the material and configuration of milling cutter, for smaller power of machine (up to 5 kW) due to small element to be produced, structural steel to be machined, mills with coarse teeth and middle stiffness of system workpiece–fixture from formula (3.71)

$$f_z = 0.06 \text{ mm/tooth} \quad (3.71)$$

Cutting fluid 5% emulsion from Укринол-1 (Ukrinol-1) emulsol

### 3.3.4 Cutting velocity

The cutting velocity is considered to be equal to peripheral velocity of milling cutter from formula (3.72)

$$V_c = \frac{C_V D^q}{T^m t^x f_z^y B^u z^p} k_V = 34.32 \text{ m/min.} \quad (3.72)$$

Values of coefficient  $C_V$  and indexes of power and values of tool life  $T$  are given in Table 3.23.

**Table 3.23 – Values of coefficient CV and indexes of power**

Para-parameter	$C_V$	$q$	$x$	$y$	$u$	$p$	$m$	$T, \text{min}$	$k_{MV}$	$k_{SV}$	$k_{TV}$	$k_{cfV}$	$k_V$
Value	68.5	0.25	0.3	0.2	0.1	0.1	0.2	90	0.59 84	1.0	1.0	1.0	0.59 84

Total correction coefficient for cutting velocity that takes into account actual cutting conditions from formula (3.73)

$$k_V = k_{MV} \times k_{SV} \times k_{TV} \times k_{cfV} \quad (3.73)$$

where  $k_{MV}$  – coefficient describing the quality of workpiece material;  
 $k_{SV}$  – coefficient describing condition of workpiece surface;  
 $k_{TV}$  – coefficient describing the milling cutter material;  
 $k_{cfV}$  – coefficient taking into account the application of cutting fluid (if the fluid is applied,  $k_{cfV} = 1.0$ ).

Coefficient of workpiece material from formula (3.74)

$$k_{MV} = k_{SV} = k_G \left( \frac{750}{\sigma_u} \right)^{nV} \approx 0.565 \quad (3.74)$$

where  $nV = 1.00$ ,  $k_G = 0.7$ ,  $\sigma_u = 930$  MPa for chromium-nickel-molybdenum steel 38XH3MA.

Rotational speed is calculated from formula (3.75)

$$n_c = \frac{1000 \cdot V_c}{\pi \cdot D} = 218.6 \text{ rev/min.} \quad (3.75)$$

where  $D$  – diameter of milling cutter, mm.

### 3.3.5 Cutting force

Main constituent of cutting force at milling is peripheral force from formula (3.76)

$$P_z = \frac{10C_P t^x f_z^y B^u z}{D^q n_c^w} k_{MP} = 612.25 \text{ N} \quad (3.76)$$

Where  $z$  – number of milling cutter teeth;  
 $n_c$  – calculated rotational speed of milling cutter, mm/rev.

Values of coefficient  $C_P$  and indexes of power are given in Table 3.23. Correction coefficient for quality of workpiece material  $k_{MP}$  for steel and cast iron is shown in the Table 3.24:

**Table 3.24** – Correction coefficient for quality of workpiece material

Parameter	$C_p$	$x$	$y$	$u$	$q$	$w$	$k_{MP}$
-----------	-------	-----	-----	-----	-----	-----	----------

Value	68.2	0.86	0.72	1.0	0.86	0	1.067
-------	------	------	------	-----	------	---	-------

Coefficient for quality of workpiece material:from formula (3.77)

$$k_{MP} = \left( \frac{\sigma_u}{750} \right)^n = 1.067 \quad (3.77)$$

Where  $n = 0.3$  for cutting with high-speed steel tool.

### 3.3.6 Torque

Torque of spindle for drive of milling cutter is calculated from formula (3.78)

$$M = \frac{P_z \cdot D}{2 \cdot 1000} = 15.3 \text{ N}\cdot\text{m}, \quad (3.78)$$

### 3.3.7 Power of cutting

Effective power of cutting is calculated formula (3.79)

$$N_e = \frac{P_z V}{1020 \cdot 60} = 0.343 \text{ kW.} \quad (3.79)$$

Power of electric motor necessary for cutting is determined with a machine efficiency coefficient ( $\eta_m = 0.75$ )from formula (3.80)

$$N_{emc} = \frac{N_e}{\eta_m} = 0.458 \text{ kW.}$$

(3.80)

### 3.3.8 Selection of machine

Milling machine is selected according to the recommendations, and its technical data is shown in Table 3.25

**Table 3.25** – Technical data of the selected horizontal milling machine **6P80 (6R80)**

Parameter	Unit	Value
Sizes of work zone: - Dimensions of work surface of table (width×length) - Distance from axis of horizontal spindle to table surface	mm	200×800 20–320
Minimal and maximal values of traverse feed	mm/min	25–1120
Number of feeds' steps		12
Series (row) of feeds	mm/min	25, 35.3, 49.9, 70.5, 99.6, 140.8, 198.9, 281, 397, 561, 792.7, 1120
Minimal and maximal values of spindle rotational speed	rev/min	50–2240
Number of rotational speed steps		12
Series (row) of spindle speeds	rev/min	50, 70, 99, 141, 199, 281, 397, 562, 794, 1122, 1585, 2240
Power of drive electric motor $N_{ems}$	kW	3

### 3.3.9 Agreement of rotational speed with technical data of milling machine

Adopted value is  $n_m = 199$  rev/min ( $n_m \leq n_c = 218.6$  rev/min).

### 3.3.10 Agreement of feed with technical data of milling machine

The calculated minute feed value is from formula (3.81)

$$f_{mc} = f_z z n_m = 161.16 \text{ mm/min} \quad (3.81)$$

The selected minute feed value is from formula (3.82)

$$f_{mm} = 140.8 \text{ mm/min} \quad (11.45 \% \text{ lesser than } f_{mc}) \quad (3.82)$$

### 3.3.11 Actual parameters of cutting process

Actual cutting velocity from formula (3.83)

$$V_a = \frac{\pi \cdot D \cdot n_m}{1000} = 31.24 \text{ m/min.} \quad (3.83)$$

Actual feed per tooth  $f_{za}$  is calculated with application of the minute feed agreed with machine's data from formula (3.84)

$$f_{za} = f_{mm} / (z n_m) = 0.05 \text{ mm/tooth} \quad (3.84)$$

Main constituent of cutting force at milling is peripheral force in formula (3.85)

$$P_{za} = \frac{10C_P t^x f_{za}^y B^u z}{D^q n_m^w} k_{MP} = 541.1 \text{ N.} \quad (3.85)$$

Actual torque of spindle for drive of milling cutter is calculated from formula (3.86)

$$M_a = \frac{P_{za} \cdot D}{2 \cdot 1000} = 13.53 \text{ N}\cdot\text{m} \quad (3.86)$$

Actual effective power of cutting from formula (3.87)

$$N_{ea} = \frac{P_{za} V_a}{1020 \cdot 60} = 0.276 \text{ kW} \quad (3.87)$$

Actual power of electric motor necessary for cutting is determined with a machine efficiency coefficient ( $\eta_m = 0.75$ ) from formula (3.88)

$$N_{ema} = \frac{N_{ea}}{\eta_m} = 0.368 \text{ kW} \quad (3.88)$$

The results of calculations and selections are written down into Table 3.26.

Table 3.26 – The results of calculation

No. of step	$t$ , mm	$B$ , mm	$f_{mm}$ , mm/min	$f_{za}$ , mm/tooth	$n_m$ , rev/min	$V_a$ , m/min	$P_{za}$ , N	$M_a$ , Nm	$N_{ema}$ , kW	$N_{ems}$ , kW
1	4	4	140.8	0.05	199	31.24	541.1	13.53	0.368	3

## **Conclusion**

The calculated and assigned parameters for milling operation, technical data of selected machine will ensure reliable and effective cutting process ( $N_{ems} \geq N_{ema}$ ) for producing the quality products.

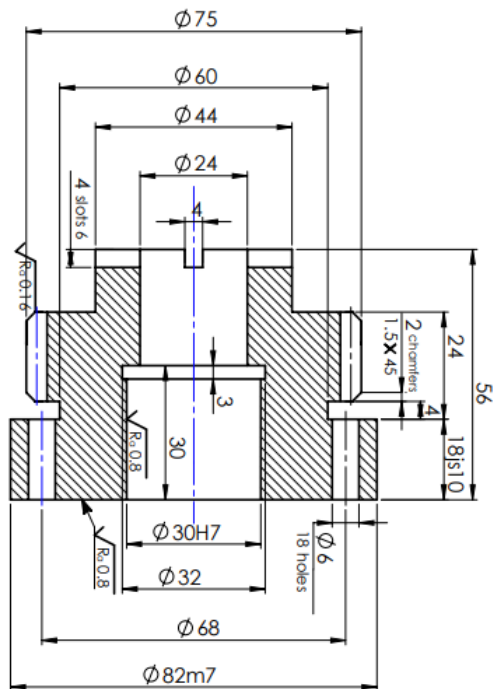
### **3.4 Drawing of part**

2022.Mudassir.240F

$\sqrt{R225} (V)$

Module	m	1.5
Number of teeth	z	48
Basic rack	-	GOST13755-81
Addendum modification coefficient	x	0
Accuracy degree by GOST 1643-81	-	8-7-6-B
Base tangent length	W	25.364
Tolerance for radial variation of toothings	F <sub>r</sub>	0.045
Tolerance for variation of base tangent length	F <sub>MW</sub>	0.028
Limit deviation base pitch	$\pm f_{pb}$	$\pm 0.013$
Tolerance for tooth flank	f <sub>t</sub>	0.011
Tolerance error of tooth distortion	F <sub>b</sub>	0.012
Pitch circle diameter	d	72
Base pitch	P <sub>b</sub>	4.71

A



1. Unspecified tolerances: H12, h12,  $\pm \frac{\text{IT12}}{2}$ ,  $\pm \frac{\text{AT13}}{2}$
2. Unspecified radii 0.3.....0.5
3. HRC 38.....42, KCU = 70....78 J/cm<sup>2</sup>

## 2022.Mudassir.240F

Изм.	Лист	№ докум.	Подп.	Дата	Лит.	Масса	Масштаб
Разраб.	Mudassir						
Пров.	Prof. Baghmet						
Т. контр.					Лист		
Н. контр.					Листов		
Утв.							

**Gear shaft**

Лист	Масса	Масштаб
		1:1

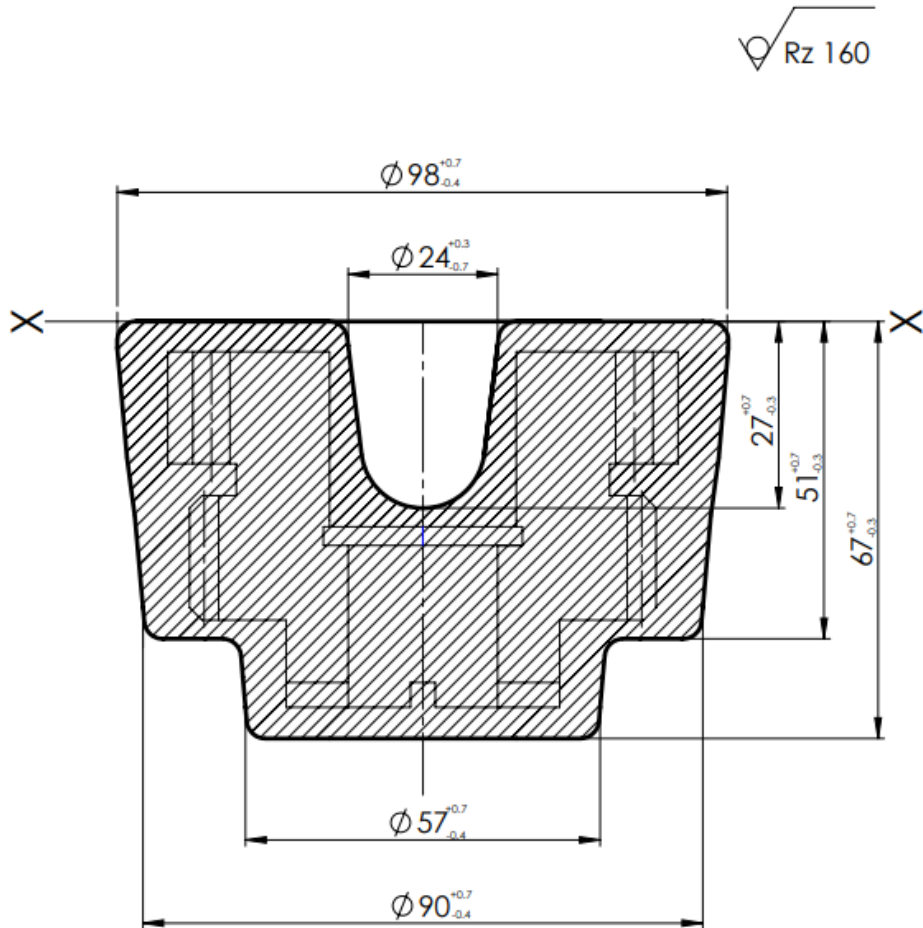
Steel 38Х3МА  
GOST 8479-70  
RUSSIA

формат А3

### **3.5 Drawing of blank**

Перв. примен.	
Справ. №	
Подп. и дата	
Взам. инв. №	Инв. № дубл.
Инв. № подп.	Подп. и дата

2022.Mudassir.240F



1. Blank is forging
2. Draft angles 5-7 degrees
3. Radiiuses 3mm

2022.Mudassir.240F

Blank

Лит.	Масса	Масштаб
		1:1
Лист		Листов
SolidWorks		RUSSIA

Копировал

Формат А4



## **CONCLUSION**

In this project regarding the research and development of turbine stages based on prototype engine: turbofan engine D-18T, a systematic method of progress was adopted. The method of progression of the design of turbine included theoretical part which dealt with the profiling coordination and virtual estimation of the parameters of the newly developed turbine. Further it includes design and strength analysis of the major components, such as blade body, fir-tree lock, discs and also included the frequency analysis of the turbine blade.

Following, that the technological part of manufacturing an aviation part was considered, In which manufacturing of a gear shaft was considered. The technological part considers all the basic problems involved in the planning of the manufacturing process and the machining process. All the steps involving determination of production type, selection of method of production of blank, quantity of manufacturing steps, machining methods, plan of manufacturing processes, selection of datums were made. Allowances and operation dimensions for round and face surfaces, dimensions of blank were made. The technological part also includes calculation of cutting parameters of various operation including turning, drilling and milling operation. The calculated parameters ensures safe and economically profitable.

## **REFERENCE**

1. Strength analysis of rotor blade [Text] : Tutorial / S. Yepifanov, Y. Shoshin, R. Zelenskyi. — Kharkov: National Aerospace University «Kharkov Aviation Institute», 2013. — 32 p.
2. Blade bending oscillations analysis [Text] : Tutorial / S. Yepifanov, Y. Shoshin, R. Zelenskyi. — Kharkiv: National Aerospace University «Kharkiv Aviation Institute», 2014. — 24 p.
3. Strength analysis of disc [Text]: Tutorial / S. Yepifanov, Y. Shoshin, R. Zelenskyi. — Kharkiv: National Aerospace University «Kharkiv Aviation Institute», 2014. — 28 p.
4. The strength analysis of blade roots [Text] : Manual / E. Martsenyuk. — Kharkiv: National aerospace university «Kharkiv aviation institute», 2016. — 52 p.
5. Planning of Manufacturing Metal-Cutting Processes. Calculations of OperationDimensions: Manual to Term Projects / A.I. Dolmatov, B.S. Bilokon, M.E. Markovych, M.K. Knyazyev. — Kharkiv: National Aerospace University named after M. Ye. Zhukovsky “Kharkiv Aviation Institute”, 2015. — 143 p.
6. Білоконь Б.С. Розрахунки режимів різання токарної, свердлильної фрезерної операцій: навч. посібник (англ. мовою) / Б.С. Білоконь, М.К. Князєв. — Х.: Нац. аерокосм. ун-т «Харк. авіац. ін-т», 2009. — 83 с.
7. Справочник технолога-машиностроителя в 2-хт. Т.2/ Подред. А. Г. Косиловой Р. К. Мещерякова. — 4-е изд. перераб. и доп. — М.: Машиностроение, 1985, 496 с.

